ALMA MATER STUDIORUM – UNIVERSITY OF BOLOGNA

SCHOOL OF ENGINEERING AND ARCHITECTURE

Department of
Electrical, Electronic, and Information Engineering
"Guglielmo Marconi"
DEI

INGEGNERIA DELL'ENERGIA ELETTRICA

curriculum:

ELECTRICAL ENGINEERING

MASTER THESIS
in

Advanced Electromagnetics and Circuit Modeling M

Analysis of the impact of stationary energy storage systems in trolleybus grids using Simulink-based modelling

CANDIDATE:
Giulia Bonora

SUPERVISOR:
Prof. Mattia Ricco

CO-SUPERVISOR:
Prof. Vincenzo Cirimele
Ing. Riccardo Mandrioli
Ing. Rudolf Francesco Peternost

Academic Year 2020/2021

Period V

A tutti coloro che mi vogliono bene

Outline

Sommario

Per via dell'attuale tendenza globale verso tecnologie più ecologiche al fine di raggiungere la neutralità climatica entro il 2050, la mobilità elettrica sta diventando sempre più importante nel contesto del trasporto pubblico. Il settore dei trasporti è infatti responsabile di circa un quarto delle emissioni europee di gas serra. L'introduzione di reti filoviarie a corrente continua al posto degli attuali autobus alimentati a diesel consente di ridurre l'inquinamento derivante dal trasporto pubblico nelle città.

Uno dei problemi principali dell'utilizzo di una rete filoviaria è legato al profilo di tensione delle linee aeree di contatto (catenaria) tra le sottostazioni di trazione. Il profilo di tensione della catenaria è influenzato dalla corrente assorbita dal filobus e dalla sua posizione rispetto alle sottostazioni: maggiore è la corrente richiesta dal bus e maggiore è la distanza del bus dalle sottostazioni, maggiore è la caduta di tensione. Se più filobus sono collegati alla stessa sezione di alimentazione (zona elettrica), la catenaria può sovraccaricarsi portando la tensione ai terminali del filobus al di sotto del valore minimo consentito dalla norma (500 V). Qualora si verificasse questa condizione, i relè di minima tensione dei filobus interverrebbero e i filobus sarebbero costretti a diminuire i propri consumi diminuendo la propria velocità (quindi la corrente richiesta alla rete) entrando in stand-by. Per evitare che ciò accada si possono attuare le seguenti azioni:

1. Limitare il numero di filobus collegati alla zona elettrica;
2. Installare sistemi stazionari di accumulo di energia nei punti deboli della catenaria (punti lungo la catenaria caratterizzati da cadute di tensione più profonde).

Questa tesi si occupa dell'analisi dei miglioramenti apportati dall'installazione di una batteria stazionaria al normale esercizio di una zona elettrica particolarmente sovraccaricata della rete filoviaria di Bologna.

L' elevata densità di energia e il basso tasso di auto-scarica caratteristici delle batterie agli ioni di Litio rendono il loro utilizzo in una rete filoviaria ideale quando l'obiettivo è quello di migliorare il profilo di tensione della catenaria. Il sistema di accumulo stazionario a batterie può essere infatti caricato dalle sottostazioni durante le ore non di punta (di notte e quando la frequenza degli autobus è bassa) ed erogare l'energia immagazzinata quando la catenaria è sovraccaricata. La scarica del sistema di accumulo permette di alleggerire il carico sulle sottostazioni nelle ore di punta e di ridurre le cadute di tensione causate dall'assorbimento di corrente dei filobus.

L'attuale flotta filoviaria della città di Bologna è composta da due tipologie di filobus articolati da 18 m (TPL e TPGV). A breve, si prevede che verranno aggiunti veicoli equipaggiati con batterie

che si caricano durante il moto (IMC), che consentiranno loro di viaggiare al di fuori della rete filoviaria senza utilizzare motori a diesel. Tuttavia, questi nuovi filobus hanno un impatto maggiore sul profilo di tensione della catenaria a causa della loro maggiore assunzione di corrente. I filobus IMC, infatti, assorbono dalla rete sufficiente corrente per la trazione e per ricaricare la batteria di bordo per il funzionamento senza catenaria. In questa tesi si considera che tutti i filobus della rete di Bologna siano di tipo IMC nella prospettiva di una futura dismissione di tutti i veicoli con motore a combustione interna.

In questo elaborato viene presentata una strategia di controllo per il sistema di accumulo stazionario a batterie che non solo mira a mantenere la tensione della catenaria all'interno dell'intervallo di tensione stabilito dalle normative ([500 1000] V), ma assicura anche che tutte le limitazioni fisiche dei componenti della rete (corrente massime dei cavi e C-rate della batteria) siano rispettate. Un modello della zona elettrica Marconi-Trento Trieste è stato implementato su Simulink per simularne il funzionamento quotidiano e confrontare il comportamento della rete filoviaria con e senza batteria. Dalla simulazione senza batteria si deduce quale è il migliore posizionamento del sistema di accumulo e il suo controllo. Inoltre, dalla conoscenza della curva di carico, derivata dal circuito equivalente di Thevenin della zona elettrica vista dal punto di connessione della batteria, e della transcaratteristica del controllo della batteria, si formula una previsione della distribuzione di tensione al punto di connessione della batteria. La previsione viene quindi confrontata con i risultati della simulazione per validare il modello Simulink.

I risultati della simulazione con la batteria mostrano una diminuzione delle cadute di tensione lungo la catenaria e della corrente erogata dalle sottostazioni, indicando che il sistema di accumulo stazionario può essere una soluzione per migliorare il funzionamento della rete filoviaria. Viene inoltre dimostrato il corretto funzionamento del controllo della batteria mostrando come la sua corrente di uscita sia sempre nei limiti per evitare sollecitazioni sulla batteria stessa. Inoltre, l'installazione del sistema di accumulo permette di diminuire le perdite Joule.

Grazie al miglioramento del profilo di tensione, in futuro la frequenza degli autobus nella zona elettrica potrebbe essere aumentata senza compromettere il funzionamento dei filobus. Inoltre, l'installazione di un sistema di accumulo potrebbe consentire di integrare le fonti di energia rinnovabile nella produzione di energia (pannelli fotovoltaici), diminuendo ulteriormente l'inquinamento dovuto al trasporto. A causa della natura intermittente delle fonti di energia rinnovabile, il loro uso sarebbe inefficace senza un sistema di accumulo che immagazzini l'energia prodotta per successive necessità. Infine, l'utilizzo di fonti rinnovabili per produrre l'energia sarebbe il primo passo verso lo sviluppo di comunità energetiche locali.

Abstract

Due to the current global trend towards greener technologies to reach climate neutrality by 2050, electric mobility has become increasingly important in the context of public transport. The transport sector is indeed responsible for around one quarter of Europe's greenhouse gas (GHG) emissions. The introduction of DC trolleybus networks in place of diesel-driven bus systems allows to reduce the pollution derived from public transport in cities.

One of the main problems of the operation of a trolleybus DC network is related to the voltage profile of the overhead contact lines (OCLs) between traction substations (TSSs). The OCL voltage profile is affected by the trolleybus current intake and by its position with respect to the TSSs: the higher the current requested by the bus and the further the bus from the TSSs, the deeper the OCL voltage drop. If multiple trolleybuses are connected to the same feeding section (FS), the OCL can become overloaded leading to the drop of the trolleybuses' operating voltages below the minimum value allowed by the standard (500 V). When this condition occurs, the minimum voltage relays of the trolleybuses intervene, and the trolleybuses are forced to decrease their consumption by decreasing their speed (thus their input current) entering a stand-by condition. To avoid this occurrence two actions could be undertaken:

1. Limit the number of trolleybuses connected to the FS;
2. Install stationary energy storage systems (ESS) at weak points (points along the OCL characterized by deepest voltage drops).

This thesis deals with the analysis of the improvements that the installation of a stationary battery ESS (BESS) produces in the operation of a particularly loaded FS of the DC trolleybus network of the city of Bologna.

The characteristic high-energy density and low self-discharge rate of Lithium-ion batteries make their installation in a trolleybus network ideal when the goal is to improve the OCL voltage profile of the catenary. The stationary BESS can indeed be charged by the TSSs during off-peak times (at night and when the bus frequency is low) and deliver the stored energy when the catenary is overloaded. The discharge of the ESS allows to alleviate the load on the TSSs during peak hours and reduce the deep voltage drops caused by the trolleybuses' current absorption.

The current trolleybus fleet in the city of Bologna consists of two types of 18-meter articulated trolleybuses (TPL and TPGV). Soon, vehicles suitable for In-Motion Charging (IMC) operation are expected to be added to the fleet allowing catenary-free operation without diesel engines. However, these new trolleybuses have a greater impact on the DC catenary voltage profile because of their

higher current intake. The IMC trolleybuses, indeed, absorb enough current to power their traction motor and recharge the on-board battery for catenary-free operation while connected to the catenary. In this thesis, it is considered that all trolleybuses in the trolleybus network of the city of Bologna are of the IMC type in the prospect of a future disposal of all internal combustion engine vehicles.

This thesis presents a control strategy for the stationary BESS that not only aims at keeping the catenary voltage within the admissible voltage range set by regulations ([500 1000] V), but also makes sure that all physical limitations of the network components (cable maximum currents and battery C-rate) are met. A model of FS Marconi-Trento Trieste is implemented in Simulink environment to simulate its daily operation and compare the behavior of the trolleybus network with and without BESS. From the simulation without BESS, the best location of the energy storage system is deduced, and the battery control is tuned. Furthermore, from the knowledge of the load curve, derived from the equivalent Thevenin circuit of the FS seen from BESS connection point, and the battery control trans-characteristic, it is formulated a prediction of the voltage distribution at BESS connection point. The prediction is then compared with the simulation results to validate the Simulink model.

The simulation results with the BESS show a decrease of the voltage drops along the catenary and of the current delivered by the TSSs, indicating that the BESS can be a solution to improve the operation of the trolleybus network. The correct operation of the battery control is also demonstrated showing how the battery output current is always within the admissible limits to avoid stress on the battery itself. Furthermore, the installation of the BESS allows to decrease the Joule losses.

Thanks to the improvement of the voltage profile, the bus frequency in the FS could be increased in the future without compromising the trolleybus operation. Furthermore, the installation of a BESS could allow to integrate renewable energy sources (RESs) in the energy generation (PV panels), decreasing ulteriorly the pollution due to public transportation. Due to the intermittent nature of RESs, their use would be ineffective without an ESS that stores the produced energy for later use. Lastly, the use of RES would be the first step toward the development of local energy communities.

Keywords*: DC Trolleybus network, Stationary Energy Storage System, Battery Energy Storage System (BESS), Lithium-ion battery, In-Motion Charging (IMC), Control Strategy, Transportation Electrification, Dynamic Modelling, Feeding Section (FS), Traction Substation (TSS), Overhead Contact Line (OCL); Smart City.*

1 Introduction

The European Commission (EC) has set through the European Climate Law (ECL) the goal to reduce the net greenhouse gas emissions by at least 55 % by 2030 compared to 1990 levels and to reach climate-neutrality by 2050 [33]. Considering that in 2018 passenger road vehicles (cars and buses) accounted for 10.8 % of total CO_2 emissions [35] and that the International Energy Agency (IEA) estimated in 2005 that the total global passenger travel using motorized vehicles would increase by around 35 % by 2050 [34], the amount of CO_2 produced is bound to increase in the next years unless some actions are undertaken. Therefore, reduction of pollution has become a key issue in the transport sector.

The implementation of a trolleybus network allows to substitute the diesel-driven buses with electric powered trolleybuses, thus reducing the CO_2 emissions in urban areas. Unfortunately, in 2018 Statista estimated that only 39.8 % of the energy produced in Italy comes from renewable sources (Hydroelectric, Biomass, Solar and Wind), while the remaining 60.2 % comes from natural gas, coal, and other fossil fuels, which are sources of pollution [36]. One way to limit pollution generated by electrical transportation is to reduce the energy consumption from the AC distribution grid for the trolleybuses' operation installing energy storage systems (ESSs) [3].

The electric drive of the trolleybus powertrain is indeed able to work in reverse mode as generator and convert the kinetic energy of the braking vehicle into electric energy. If ESSs are not installed, this energy is used in one of the following ways:

- It is provided to nearby accelerating trolleybuses connected to the same electric section, thus reducing the energy requested from the AC distribution grid;
- It is fed back to the AC distribution grid in the case the DC trolleybus network is equipped with bidirectional substations when there are no accelerating trolleybuses;
- It is dissipated to heat in braking resistors mounted on board the trolleybus in case neither of the two previous conditions are guaranteed to avoid the increase of the pantograph voltage above the normal range established by the standards (regeneration cancellation).

Installing ESSs allows to store the surplus energy recuperated during the regenerative braking of the trolleybus and to provide it back during its subsequent acceleration, effectively reducing the energy demand of the transport system, and with it the pollution that it would have produced [1]-[6], [8], [12], [13], [15], [18], [23], [25], [27], [28], [31].

The ESSs can be installed either on-board of the trolleybuses, like in the case of In-Motion Charging (IMC) trolleybuses or e-buses, or off-board. In the stationary case, the ESS can be placed either inside a traction substation or at a weak point along the overhead contact line (OCL). The former configuration is referred to as substation-inside ESS, while the latter as wayside energy storage system (WESS). Substation-inside ESSs are preferred when recovery of the regenerative braking energy (RBE) is the sole purpose of the ESS installation, while WESSs are installed to improve the OCL voltage profile as well [6],[13]. On-board ESSs are preferred when a reduction of the current peaks drawn by the vehicles is required [17] or when the catenary-free operation of the trolleybus is needed [12], but their sizing is limited by the vehicle weight and available space [13]. Contrary, stationary ESSs are not limited by weight and required space, but they are characterized by lower efficiencies in storing and releasing surplus energy [13]. As a matter of fact, the stationary ESSs store a lower amount of RBE with respect to on-board ESSs in the same working conditions because of the OCL losses, whose amount increases the further the trolleybus is from the ESS [10]. For this reason, choosing the optimal location and sizing of the stationary ESS is fundamental to recover the maximum RBE and obtain the best possible voltage profile of the catenary. In the following dissertation, the design of on-board ESS is not treated.

ESSs not only allow to store the RBE and therefore reduce the total energy consumption, but they also allow to achieve voltage regulation. Trolleybuses are powered through OCLs from the traction substations (TSSs). The OCL voltage profile is affected by the trolleybus current intake: the higher the current requested by the bus, the higher the OCL voltage drop. If multiple trolleybuses are connected to the same feeding section (FS), the OCL can become overloaded leading to the drop of the trolleybuses' operating voltages below the minimum allowed value by the standard. When deep voltage drops, occur (i.e. voltage value drops below 500 V), the minimum voltage relays of the trolleybuses intervene and the trolleybuses are forced to decrease their consumption by decreasing their speed, thus their input current, entering a stand-by condition. As mentioned previously, the installation of ESS in critical points along the line boosts the OCL voltage improving the line performance without needing expensive modifications of the existing DC line such as repowering of the TSS or increasing the OCL cross-sectional area [7],[10],[16],[17]. Given that the capacity of the trolleybus network is limited by the power supplied by the TSS, the installation of ESS can also allow to increase the number of simultaneously operating trolleybuses on the same FS of the OCL [7],[10].

Another advantage that can be obtained from the installation of ESS is power peak shaving [1],[10], which allows to obtain significant electric energy cost savings [11]. The storage system can

be charged at low currents from the AC grid through the TSS during off-peak periods and then be discharged during peak moments to support the substations and avoid the extra charges due to the *peak load charging method* applied by the energy provider (ENEL) [4]. The ESS can also provide traction power support for a short period of time operating as a back-up source in case of fault of the TSS where it is installed [11], [21]. Lastly, the connection of a storage device with its properly controlled power converter to the DC line allows to improve the dynamic response of the overall system [15],[19],[31].

An example of an urban transport system where the installation of a stationary ESS could improve the overall performance is the trolleybus network of the city of Bologna, Italy, whose trolleybus fleet, which is currently composed of standard trolleybuses (TPL and TPGV), will soon be expanded with the addition of the so-called In-Motion Charging (IMC) trolleybuses. Unlike the traditional trolleybuses, the IMC ones are equipped with on-board batteries, which are charged while the trolleybus is connected to the OCL and are used for catenary-free operation [40]. Since the RBE recuperated during braking is stored in the on-board batteries, the voltage of the OCL never overcomes the upper voltage limit set by regulations (1000 V). Due to the global trend toward greener technologies, it is also expected that in the future all diesel-driven trolleybuses will be replaced with e-buses, IMC or similar technologies. Therefore, in this thesis the analysis of the impact of the installation of a WESS is performed considering that the bus fleet is composed only of IMC trolleybuses.

Due to the higher current intake of these new trolleybuses, it is expected that the existing trolleybus network will be greatly impacted by their presence. To compensate for the deep voltage drops the existing trolleybus network could be enhanced by increasing the power output of the traction substations, adding reinforcement feeders where needed or building reversible substations. Unfortunately, these solutions require a huge investment in terms of money and time, so they cannot be pursued. The installation of a stationary ESS in the most overloaded FSs could be the cheapest solution to improve the voltage profile.

Supercapacitors (SCs) stationary energy storage systems are commonly used to support the DC catenary of urban transportation systems [4]-[19]. The high-power density makes the SC ideal for the installation in a trolleybus network because of their frequent acceleration and braking, which requires and provides high peaks of power, respectively, due to the short running time between bus stops [13]. Furthermore, the short discharge/charge time allows the SC to quickly compensate the voltage drops

and perform voltage regulation [17]. However, using SCs to store energy for back-up purposes is meaningless due to their high self-discharge rates. Lithium-ion batteries, instead, are commonly used in railway systems to improve the voltage profile of the catenary [28], or to help provide the power for train departure through auxiliary battery substations built close to the train stations [21], [22].

The inclusion of a wayside battery energy storage systems (BESSs) represents an innovative solution for 600-750 V DC power supply networks and it requires an adequate control system to manage its charging and discharging according to the intrinsic catenary and battery limitations. In literature, storage systems are mostly used to store RBE [5],[6] or to better manage the energy flow among the vehicles and traction substations to improve energy saving and reduce voltage drops [10]. The operation of the storage system is regulated through a DC/DC converter. Paper [5] and [6] propose a storage system control strategy aimed at maximizing the recuperation of RBE to reduce energy consumption in urban rail transit systems. Paper [10] proposes a control based on the real-time management of the voltage level at the supercapacitor WESS connection point. An optimal operating point control method for Lithium-ion batteries is proposed in [31], where the charging, discharging or idle state of the battery is determined based on the voltage and SOC level.

In chapter 2 the existing trolleybus grid of the city of Bologna is described and the main information about the chosen FS is provided. Chapter 3 discusses the way to implement the catenary system in the Simulink environment. In chapter 4 the BESS model and control are analyzed in detail. Furthermore, a prediction of the voltage distribution obtained thanks to the battery installation is formulated. In chapter 5 the model of the FS with the battery ESS is run and its results are compared to the ones obtained without the battery ESS and to the predicted ones. Finally, in chapter 6 the conclusions are drawn.

2 Trolleybus network of the city of Bologna

In this chapter, the main characteristics of the trolleybus network of the city of Bologna are briefly described. In paragraph 2.1, general information about the methodology used to perform the analysis is provided. Paragraph 2.2 is dedicated to giving an overview of the existing trolleybus grid of the city of Bologna, while in paragraph 2.3 the FS chosen for the analysis of the impact of the introduction of a BESS is described in detail.

Currently, the trolleybus network is composed of 5 trolleybus lines (lines 12, 13, 14, 32 and 33) that employ only TPL (trasporto pubblico locale) and TPGV (trasporto pubblico a guida vincolata) trolleybuses. TPER, the company that manages the trolleybus network, has recently acquired 70 new IMC (in-motion charging) trolleybuses, that are equipped with on-board batteries, to expand the network. Therefore, this dissertation considers the future trolleybus system of the city of Bologna, which will be composed of the existing trolleybus lines and 3 new ones (lines 11, 19 and 25) for a total of 42 TPGV, 19 TPL and 70 IMC vehicles. For the sizing of the BESS (battery energy storage system) only IMC trolleybuses are considered to perform a more burdensome analysis of the trolleybus network behavior.

The electric power supply of the trolleybus network is performed through traction substations (TSSs) that power the trolleybuses through overhead contact lines (OCLs). The auxiliary systems of the substations (lighting, driving force, smoke detection, anti-intrusion, ventilation, and rainwater draining systems) and the line, stop, depot, and traffic light systems are not considered in the analysis.

The calculations performed in this thesis are based on codified methodologies and on data and information obtained from TPER technical reports and field surveys. Working hypotheses are introduced when necessary (however specified).

2.1 Technical feasibility project

The map of the trolleybus network of the city of Bologna is reported in Figure 2-1. In particular, the IMC trolleybuses are used for the routes of the bus lines 11, 13, 14 and 25, which are not all completely electrified. To be specific, bus lines 11 and 25 are electrified for around 45% of their route, bus lines 14B and 14C are 65% electrified, while bus lines 13 and 14A are completely electrified. To account for the additional energy that IMC trolleybuses need to charge their on-board

batteries, the bus lines 11 and 25, 14, and 13 are supposed to be 30%, 52% and 60% electrified respectively.

The TPL trolleybuses are used for the routes of bus lines 13, 32 and 33, while TPGV trolleybuses for bus lines 12 and 19. To account for the possible future use of IMC trolleybuses also for these routes, the TPL and TPGV trolleybuses are assumed to withdraw from the DC grid a higher power than in reality [37].

Legend	color
11	Purple
12	Orange
13	Yellow
14	Brown
19	Blue
25	Magenta
32/33	Light blue

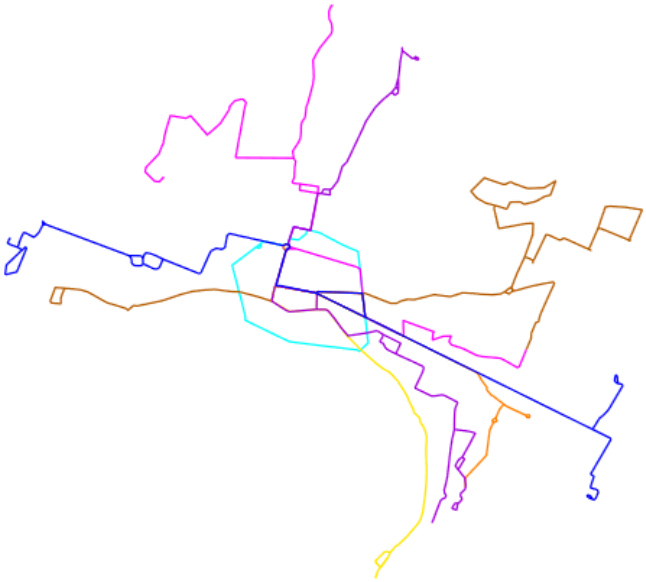

Figure 2-1 Map of trolleybus network of the city of Bologna. Legend: bus line 11 purple; bus line 12 orange; bus line 13 yellow; bus line 14 brown; bus line 19 blue; bus line 25 magenta; bus lines 32/33 light blue.

2.1.1 Bus lines in Bologna

The trolleybus network of the city of Bologna exploits 3 different types of trolleybuses, which are characterized by different absorption profiles:

- TPGV (trasporto pubblico a guida vincolata): guided public transport;
- TPL (trasporto pubblico locale): local public transport;
- IMC: trolleybuses equipped with on-board batteries and in-motion charging technology.

The latter typology is the most challenging due to the presence of on-board batteries, that absorb additional power from the DC grid to recharge during the vehicle movement.

In Table 2-1 it is reported for each trolleybus line the length of the overhead contact line in kilometers, the type and number of trolleybuses that are exploited and the total number of vehicles per kilometer.

Bus line	OCL length [km]	Vehicles/bus line	TPGV	TPL	IMC	Vehicles/km
12	14,888	15	15	-	-	1,0075
13	15,2885	19	-	7	12	1,242764
14	25,1958	18	-	-	18	0,7144
19	31,397	27	27	-	-	0,859955
11/25	49,834	40	-	-	40	0,802665
32/33	15,983	12	-	12	-	0,750798

Table 2-1 Calculation of the total number of trolleybuses per kilometer per bus line.

The mean distance between two subsequent bus stops is 340 m, while the mean bus speed is assumed to be 15 km/h.

2.1.2 Work methodology

For the sizing of the BESS the following input data and criteria have been used:

1. **Vehicle data**: the trolleybus absorption profiles of TPL, TPGV and IMC buses are considered;
2. **Frequency, number of operating vehicles and traffic characteristics**: data provided by TPER;
3. **Traction substations**: the location and sizing of the TSSs are provided by TPER;
4. **Subdivision of the trolleybus network into feeding sections (FSs)**: the trolleybus network is divided into FSs, which are completely isolated from each other and not meant to work in parallel. The sizing of the BESS is performed on the basis of the traffic conditions of the chosen FS;
5. **Power supply of feeding sections**: most of the FSs are bi-frontally powered by two different TSSs, which are powered by ENEL primary cabins. Only few FSs, which are mainly the ones that contain the terminal of the bus routes, are one-sided powered;
6. **Partial failure of a traction substation**: most of the TSSs contain two conversion groups, composed by a transformer and its associated rectifier, which are sized to guarantee the normal operation of the powered FSs in the case of failure of one conversion group;

2.1.3 Reference technical standards

The following technical standards are considered for the analysis:

- EN 50119: Railway applications - Fixed installations - Electric traction overhead contact lines;
- EN 50122-1: Railway applications - Fixed installations - Electrical safety, earthing and return circuit. Part 1: Protection against electric shock;

- EN 50122-2: Railway applications - Fixed installations - Electrical safety, earthing and return circuit. Part 2: Measures against the effects of stray currents caused by direct current traction systems;
- EN 50122-3: Railway applications - Fixed installations - Electrical safety, earthing and return circuit. Part 3: Mutual interaction of AC and DC traction systems;
- EN 50149: Railway applications - Fixed installations - Electrical traction - Copper and copper alloy shaped contact wires;
- EN 50163: Railway applications - Supply voltages of traction systems;
- EN 50328: Railway applications - Fixed installations - Power electronic converters for substations;
- EN 50329: Railway applications - Fixed installations - Traction transformers;
- IEC TC 20: Electric cables;
- IEC 60364-8-2:2018: Prosumer's low voltage electrical installations;
- IEC 0-16: Technical rules of reference for connection of active and passive users to HV and MV grids of electricity distributors;
- EN 61936: Electrical installations above 1 kV AC;
- EN 50328: Railway applications - Fixed installations - Electronic power converters for substations;
- EN 60076: Dry-type power transformers;
- EN 50522: Earthing of electrical installations at voltages above 1kV AC.

2.2 Overview of the trolleybus network

In the following 4 paragraphs an overview of the trolleybuses typologies, traction substations, feeders and overhead contact lines of the trolleybus network of the city of Bologna is given.

The trolleybus network nominal voltage is 750V, while the minimum allowed OCL voltage for the operation of a trolleybus is 500V in compliance with technical standard EN 50163: Railway applications - Supply voltages of traction systems (2006/2008).

2.2.1 Trolleybuses

As mentioned before, there are 3 different typologies of trolleybuses employed in the trolleybus network of the city of Bologna. In this section, their main characteristics are itemized.

TPL and TPGV trolleybuses are not equipped with on-board batteries and their operation is basically the same with the difference that the maneuver to approach the bus stop platform of the TPGV trolleybus is automated to ease the boarding of handicapped people. These trolleybuses can therefore operate only when connected to the catenary.

IMC trolleybuses can operate both by power supply from the OCL and catenary-free employing their on-board batteries. While travelling connected to the catenary, the IMC trolleybus takes an additional power with respect to the one required for traction to recharge the on-board batteries. The power stored in the battery is then used for the catenary-free traction of the trolleybus.

To account for the possible future replacement of the TPGV and TPL trolleybuses with IMC ones, each vehicle of these typologies is assumed to require an additional 35kW power with respect to its normal traction power, which results in an increase of their current absorptions. The power required for the charge of the on-board battery depends on various factors, such as the percentage of electrified route, the mean trolleybus speed, the instantaneous trolleybus speed, RBE, limitations of the OCL, battery capacity, and the state of charge of the battery.

The study of the current and power absorptions of the trolleybuses is out of the scope of this thesis. From the traction cycles of the 3 different trolleybus typologies and under the assumption of the future substitution of TPGV and TPL trolleybuses with IMC ones, it is possible to derive the average starting current I_s, the mean current I_m, and the RMS current I_{rms} for each typology and percentage of electrified route. These values are reported in Table 2-2.

Bus typology	I_s **[A]**	I_{rms} **[A]**	I_m **[A]**
TPL	397	220	145
TPGV	355	215	155
IMC Line 13 - 60 %	296	205	160
IMC Line 14 - 52 %	323	225	180
IMC Lines 11 and 25 – 30 %	460	340	267

Table 2-2 Average starting current, RMS current and mean current of all the trolleybus typologies when TPGV and TPL buses are assumed to absorb an additional 35kW power.

To simplify the calculations, additional hypotheses are made. TPL, TPGV and IMC Line 13 (60% electrified route) are assumed to all absorb a mean current of 160 A and an RMS current of 220 A (worst case scenario). The IMC lines 11 and 25 (30 % electrified route) are assumed to absorb 460 A mean starting current, while all the other trolleybus typologies and IMC routes absorb 400 A. These surcharges make the sizing of the BESS more conservative and allow to manage extraordinary

overload requests due to service anomalies (stop suppression, increase of mean speed, etc. etc.). Therefore, the current values used for the analysis are the ones reported in Table 2-3.

Bus typology	I_s [A]	I_{rms} [A]	I_m [A]
TPL	400	220	160
TPGV	400	220	160
IMC Line 13 – 60 %	400	220	160
IMC Line 14 – 52 %	400	225	180
IMC Lines 11 and 25 – 30 %	460	340	267

Table 2-3 Average current, RMS current and mean current of trolleybus typologies used in the sizing process.

2.2.2 Electrical traction substations

Each traction substation includes:

- MV section with 12.5 kA internal arc sealed cells on three sides of modular type equipped with Sulphur Hexafluoride (SF_6) switches;
- Three-winding MV/LV transformers (15 kV/590 V) for powering silicon dry rectifiers (Graetz double bridge connection) with the primary winding delta connected and two secondary windings magnetically coupled, one of which is delta connected and the other star connected. The primary winding is incorporated in epoxy resin, while the secondary windings are vacuum impregnated in resin to be suitable for indoor installation;
- DC section composed by a removable armored switchboard consisting of the following functional compartments, whose number and typology is determined through single-line design diagrams:
    - 12-pulse rectifier compartment consisting of 1 or 2 compartments;
    - Bipolar disconnector compartment;
    - Line feeder compartments;
    - Back-up power supply compartment;
- One or more conversion groups with rectifiers suitable for powering electric traction systems. The rectifier unit is composed of two 6-pulses Graetz bridge rectifier compartments parallel connected on the DC side through an interphase coil in order to realize a 12-pulses rectifier;
- Overhead contact line feeder section composed of circuit breakers;
- Auxiliary services section composed by:
    - Resin 15 kV/400 V transformer of 50 kVA (Auxiliary transformer);
    - LV command and control panel;

- Battery charger and auxiliary power supply 110 Vdc-230 Vac section;
- Ni-Cd batteries;

The simplified scheme of a traction substation with two conversion groups and an auxiliary transformer is shown in Figure 2-2.

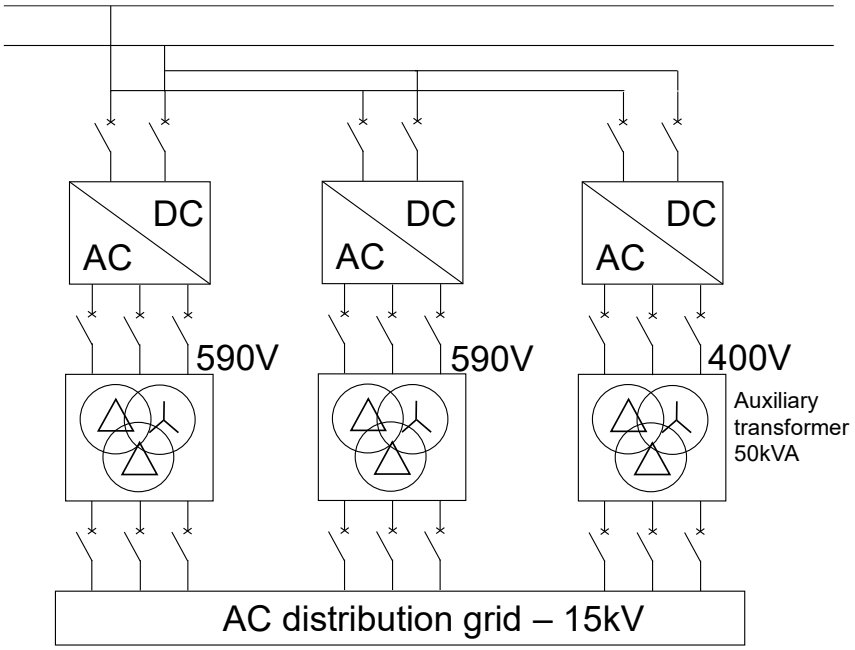

Figure 2-2 Simplified scheme of a traction substation with 2 conversion groups.

The trolleybus network of the city of Bologna is currently composed of 17 TSSs. 6 new TSSs (Togliatti, Romagnoli, Scalo, Ferrarese, Gomito, and Fossolo) will be built for the new trolleybus lines. In Table 2-4 it is possible to see the list of all TSSs, their installed power and the number of conversion groups (transformer + rectifier).

TSS	Installed power [kW]	TSS	Installed power [kW]
Marconi	2 x 1500	Sant'Isaia (2)	930
Gramsci	2 x 1000	Carducci (1)	930
Irnerio	1000	Carducci (2)	2 x 930
Trento Trieste	2 x 1500	Massarenti	2 x 930
Pontevecchio	2 x 1500	Murri	1600
Lambrakis	1500	Pavese	2 x 1000
Caselle	2 x 1000	Tanari	2 x 1000
Piave	2 x 1000	Romagnoli	2 x 1000
Deposito 2 Madonne	2 x 1000	Togliatti	2 x 1000
Longo	1000	Ferrarese	2 x 1000
Tofane	930	Gomito	2 x 1000
Barca	930	Fossolo	2 x 1000
Sant'Isaia (1)	930		

Table 2-4 List of TSSs with their relative installed power and number of conversion groups.

2.2.3 Feeders

The 15 kV power supply is ensured by the electricity distributor (ENEL) through individual supplies located nearby the TSSs. From the delivery point, the TSSs are powered directly without interposing circuit breakers. The utilities powered by the MV switchboard are the main transformers and auxiliary services. As it can be seen in Figure 2-2, the traction substations are characterized by 4 different voltage levels between different components, which require different types of cables:

- Cables type RG7H1R 18/30 kV are used for the 15 kV AC power supply between the delivery point and the transformers;
- Cables type RG7H1R 1.8/3 kV are used for the 750 V DC power supply from the traction substations to the catenary (feeders and reinforcement feeders);
- Cables type FG16OR16 0.6/1 kV are used for the 400 V AC power supply between the auxiliary services and the command-and-control panel.

The 15 kV cables have a unified section of 95 mm^2 and a current rating of 300 A when laid in a closed channel with an ambient temperature of 30 °C. Being the design current in the most severe conditions (full power of TSS Marconi) slightly above 180 A, the sizing margin is quite large.

Regarding the 750 V DC feeders, their sizing has been performed to guarantee the following conditions:

i. Overload protection;

The verification of overload protection requires that the cable current rating (I_Z) is greater than the design current (I_B):

$$I_Z > I_B \quad (1)$$

TPER evaluates the design current I_B as the sum of the rms currents of TPGV, TPL and IMC trolleybuses (2) (overestimation of the total rms current):

$$I_B = I_{rms\,TPL} + I_{rms\,TPGV} + I_{rms\,IMC\,13} + I_{rms\,IMC\,14} + I_{rms\,IMC\,11/25} \quad (2)$$

The values of the rms currents for the different trolleybus types are listed in Table 2-3.

ii. Short-circuit protection at the beginning of the line;

The verification of short-circuit protection at the beginning of the line requires to evaluate the maximum short-circuit current downstream the conversion groups. The latter can be derived from the characteristic voltage-current curve of the rectifier varying the coupling factor k. Assuming that the coupling factor k is equal to 0.9, the maximum short-circuit current is 25.6 kA.

The cable is protected against short-circuits at the beginning of the line if the short-circuit current at the beginning of the line (I_{sc_max}) is lower than the breaking capacity of the protective device (P_{int}) (3) and if the let-through energy ($I^2_{sc\_max}\ t$) is lower than the specific let-through energy of the cable (K^2S^2) (4).

$$I_{sc\_max} \leq P_{int} \quad (3)$$

$$I^2_{sc\_max}\ t \leq K^2S^2 \quad (4)$$

t is the tripping time of the protection device against short-circuits at the beginning of the line (0.1 s), *K* is a coefficient related to the cable insulation (143 for HEPR rubber) and *S* is cable section [mm^2].

iii. Short-circuit protection at the end of the line;

The verification of short-circuit protection at the end of the line requires to evaluate the minimum short-circuit current at the end of the OCL. To do so, the fault resistance of the circuit (feeder + OCL + additional fault resistances) must be evaluated first. Therefore, the minimum short-circuit current can be obtained graphically through the voltage-current characteristic of the rectifier at different values of the coupling factor, k. TPER considers a coupling factor of 0.9.

The cable is assumed protected if the minimum shirt-circuit current (I_{sc_min}) is greater than k times the working design current (I_B) (5).

$$I_{sc\_min} > kI_B \quad (5)$$

In practice, it is assumed that if I_{sc_min} is higher than 2-3 times the design current of the cable (I_B), the circuit breaker can distinguish the fault from the operating conditions and effectively protect the cable:

$$I_{sc\_min} > 2\text{-}3\ I_B \quad (6)$$

For the feeding sections that do not satisfy equation (5) or (6), the protection against the short-circuit at the end of the line is achieved with the calibration of the relay ME-MPS13L through the function of maximum current variation according to the current gradient Δi/Δt.

iv. Voltage drop of feeder and OCL is within the admissible limits provided by regulations ([500 1000] V).

2.2.4 Overhead contact lines

The OCLs are made of raw extruded copper conductors of 100 mm^2 nominal cross-section shaped in a way to allow the attachment to the suspension clamps. Each bifilar line is composed of two OCLs placed 600 mm away from each other: the one placed on the left with respect to the direction of travel is the positive pole, while the one on the right is the negative pole. The contact lines are suspended with elastic elements on special supports or connected to walls and pillars. The OCLs are double insulated from the ground-connected metallic parts and are placed at 5.60 m from the road level.

The OCLs are divided into feeding sections (FSs), which are insulated from each other and powered by different TSSs.

Technical standard EN 50119: Railway applications - Fixed installations - Electric traction overhead contact lines (2010) states that the 100 mm^2 OCLs should not carry a continuous current higher than 451 A and that the steady-state temperature of the OCLs should be below 80 °C. The maximum temperature that the OCLs can reach during a transient is 120 °C.

2.2.5 Stationary BESS

Lithium-ion batteries and supercapacitors (SCs) are two storage technologies widely used in the transportation sector for different purposes. While batteries are mainly used to provide the average power demand of the vehicle (cruising and costing), SCs are employed when a transient high power is required or provided (acceleration or fast braking of the vehicle) [29]. The reason for their different use is to be credited to their different electric energy storage technology. In the analysis of the impact of the introduction of a stationary ESS along the catenary performed in this thesis, only BESSs are considered.

Electrochemical batteries are a mature energy storage technology that find a lot of applications in a great variety of fields that range from a few kilowatts in residential applications to megawatt systems for different grid services (energy management, back-up systems, seasonal reserves, and load levelling) [24].

In electrochemical batteries, chemical energy is transformed directly into electric energy. A Lithium-ion cell is composed of a negative electrode (made typically of Graphite), a positive electrode (made of a chemical compound that contains Lithium), a protective layer over the anode (Solid electrolyte interface, SEI) and an electrolyte and a separator in between. During its charge Lithium ions move through the electrolyte from the positive electrode (cathode) toward the negative one (anode) where they are accumulated generating energy. When all the Lithium ions reach the anode, the charging process is completed. During the discharge process, the ions reverse their motion releasing the stored energy. The cell is completely discharged when there are no more Lithium ions on the anode. The charge/discharge currents that a Lithium-ion battery can sustain (rate capability) depend on the Li-ion diffusion rate through the electrodes, so the charge/discharge time is limited by the slow movement of ions inside the electrolyte. When Li-ion batteries are subjected to high C-rates for a prolongated period, the Lithium ions intercalation into the anode and de-intercalation from the cathode is so rapid that it can cause cracks in the SEI and the formation of Lithium dendrites that can lead to internal short-circuits and uncontrolled temperature increase [26].

The Li-ion battery’s most advantageous features are its high energy density and low self-discharge rate. However, it presents relatively low power density and high recharge time, and it can be subjected to a limited number of life cycles (complete charge and discharge) [1, 6]. Lithium-ion batteries are indeed subjectable to chemical deterioration with operating time and cycle life [24, 29].

Because of the chemical reactions that occur inside batteries, they are not able to deliver high powers for a prolonged period [15] and they are sensitive to over-temperatures [24]. The actual operating life of the battery is affected by many factors, such as the rate and depth of discharge, temperature, and humidity level. Typically, the higher the depth of discharge, the lower the cycle life.

In Table 2-5 all the main Lithium- ion battery characteristics are listed.

Li-ion battery characteristics	Range	References
Gravimetric energy density	150 – 250 Wh/kg	[25]
Gravimetric power density	500 – 2000 W/kg	[25]
Volumetric energy density	400 – 650 Wh/L	[25]
Volumetric power density	1500 – 10 000 W/L	[25]
Discharge time	minutes - hours	[6],[24]
Typical storage duration	minutes-days	[25]
Voltage range	3.0 – 4.2 V	[25]
Lifetime	5 – 20 years	[24],[25]
Cycle efficiency	95 – 99 %	[24]
Daily self-discharge rate	0.1 – 0.5 %	[24],[25]
Cycle life	1000 – 10 000 cycles	[24], [25]
Operating temperature	-20 – 60 °C	[24]
Energy capital cost	273 – 1000 $/kWh	[25]
Power capital cost	900 – 1300 $/kW	[25]

Table 2-5 Lithium-ion battery characteristics.

2.3 FS Marconi-Trento Trieste

The feeding section considered for the analysis of the impact of installing a battery ESS in the DC trolleybus network of the city of Bologna is the one fed by TSSs Marconi and Trento Trieste, which is referred to as FS 17 or FS Marconi-Trento Trieste.

Its selection is dictated by 2 main factors:

1. High bus traffic during daily operation;
   Considering the bus frequency mentioned in Table 2-1 and the bus routes listed in Table 2-6, in the worst-case scenario 15 trolleybuses can be connected to this FS at the same time. The current absorption of all these buses causes very deep voltage drops that can compromise the operation

of the trolleybus network. The installation of a stationary battery ESS charged by the TSSs during off-peak times can compensate part of these voltage drops and relieve the load on the substations at peak times.

2. Feeding section topology;

   FS Marconi-Trento Trieste has a meshed configuration with reinforcement feeders and a single bifilar ring, so it is not characterized by electrical symmetry if seen from its middle point.

To simplify the notations in the following discussion the OCLs from TSS Marconi to TSS Trento Trieste and vice versa are referred to as outward and return paths respectively. Looking at the feeding points of the FS provided by TPER, it is possible to say that bus stops Ugo Bassi and Albertoni correspond to the beginning of the outward and return paths respectively.

The path of the considered feeding section is depicted in Figure 2-3, where the green and yellow dots represent the feeders' and reinforcement feeders' connection points to the catenary, respectively.

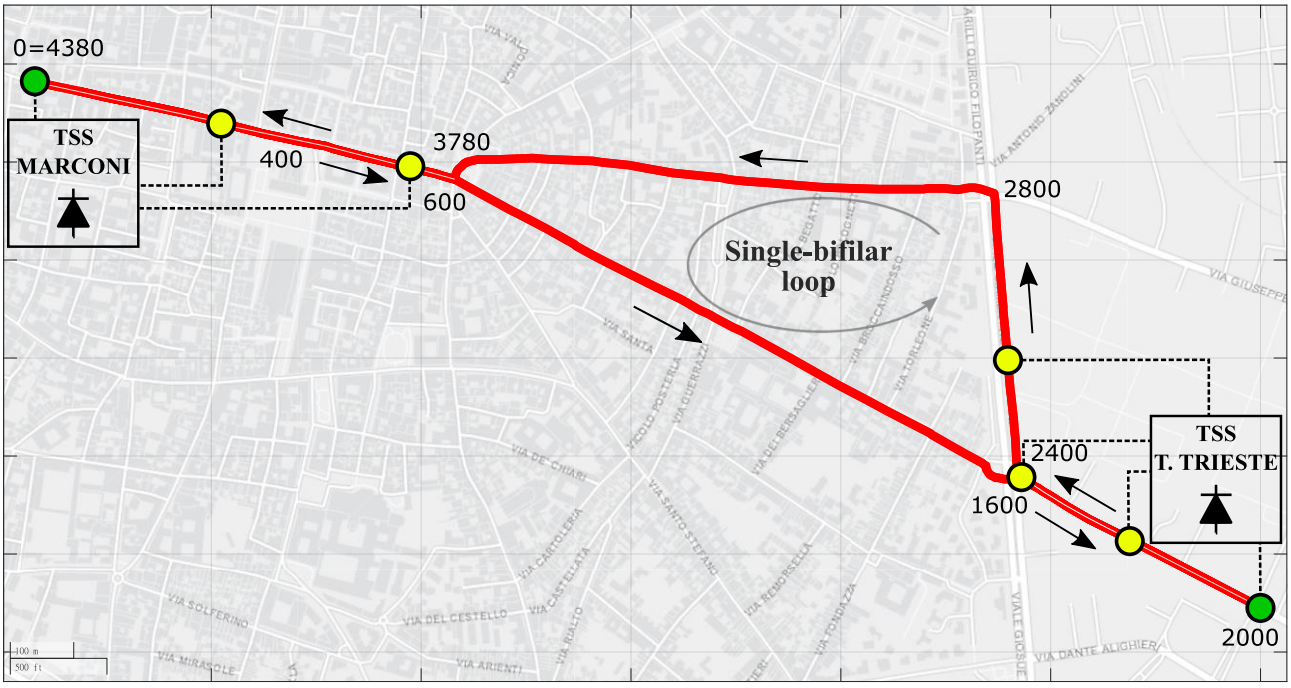

Figure 2-3 FS 17 Marconi - Trento Trieste.

2.3.1 IMC traction profile

The analysis of the catenary voltage profile requires the knowledge of the current absorptions of the trolleybuses that it powers. As has been anticipated, it is assumed that only IMC trolleybuses are used for public transportation in the considered feeding section. This assumption is acceptable in

the perspective that in the future all other trolleybus topologies will be replaced with IMC ones because of their ability to travel catenary-free without a diesel engine. Moreover, this assumption allows to perform a more burdensome analysis regarding voltage drops and energy demand because of their higher current absorptions (worst-case scenario).

Because of the impossibility to know exactly the real absorption profile of each trolleybus travelling beneath the catenary due to its dependance on unpredictable factors like traffic conditions and human behavior, the traction diagram is derived considering simplified standard operating conditions, which are listed below:

- Distance between bus stops: 340 m
- Maximum speed allowed by traffic laws: 50 km/h
- Route slope: 0 %
- Acceleration: 1.1 $\mathrm{m/s^2}$
- Deceleration: -1.2 $\mathrm{m/s^2}$
- Braking time: 12 s
- Stop time at the bus stop: 10 s
- Mass of fully loaded vehicle: 30 tons
- Nominal DC voltage: 750 V
- AC and auxiliaries: always on

The traction profile considers the electrical, mechanical, and aerodynamics characteristics of the vehicle over an average route between two bus stops. The IMC traction profile accounts both for the energy required for traction and for charging the battery for the catenary-free operation. For what concerns the power and current required to charge the battery, their values depend on multiple parameters, such as:

- Percentage of electrified trolleybus route (ratio between the length of OCL and total length of the route);
- Average speed of the vehicle;
- Instantaneous speed of the vehicle;
- State of charge of the battery;
- Limitations on the charging current due to OCL limits;
- Useful battery capacity (assumed to be 80% of nominal capacity).

It is acceptable to say that the IMC trolleybus electric characteristics are well described by the current absorptions needed (blue curve in Figure 2-4) to travel from one bus stop to the next one following the standard speed profile (red curve in Figure 2-4). It is important to reaffirm that the vehicle braking energy is stored in the on-board batteries during decelerations, resulting in no current delivery to the contact line. During stop time, the traction profile shows a constant current intake of 100 A, which is used to power the auxiliaries.

As has been previously stated, the standard traction profile does not represent the real behavior of the moving IMC trolleybus because it misses the contributions due to the random accelerations, decelerations and stop times that play an important role in the charging process. However, the use of these simplified traction profiles allows to perform meaningful comparisons between the behavior of the catenary with and without stationary ESSs. Therefore, all random factors have not been considered in the simulation model. In the simulation it is also assumed that the traction profile remains unchanged as the OCL voltage varies if the trolleybus voltage remains within the limits allowed by regulations ([500 1000] V).

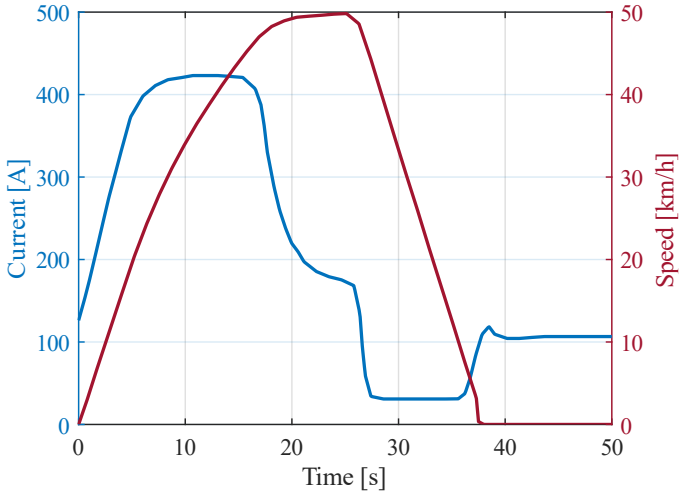

Figure 2-4 IMC trolleybus traction profile. Legend: current profile (blue curve); speed profile (red curve).

2.3.2 Traffic description of FS Marconi-Trento Trieste

This thesis aims to simulate the real movement of trolleybuses inside the feeding section to best emulate the real behaviour of the catenary. To do so, the present timetables and routes of all the trolleybuses that travel in the considered feeding section have been considered. Since the actual speed profile of all trolleybuses is affected by random variables, like traffic condition and delays, the vehicles are assumed to repeat the standard speed profile, which is constituted by periods of

acceleration, constant speed, deceleration and stop (see the red curve in Figure 2-4), for the entire duration of their route.

The bus lines that travel connected to FS Marconi-Trento Trieste are 12, 14, 19, 25, and 33. For the evaluation of the voltage profile along the catenary at every instant of the day, the schedule and route of all these buses is taken from the official website of TPER. The route and total distance covered in one round trip of each bus line in the considered FS are reported in Table 2-6, where positions 0 and 4380 m correspond to TSS Marconi, while position 2000 m correspond to TSS Trento Trieste.

Bus lines	**Outward path [m]**	**Return path [m]**	**Travelled distance (L_{bus}) [m]**
12	0-2000	2000-4380	4380
14	400-1600 and 2400-2800	2800-4380	3180
19	0-2000	2000-4380	4380
25	0-2000	2000-4380	4380
33	/	2400-2800	400

Table 2-6 Bus routes in FS 17.

While the routes of bus lines 12, 19 and 25 coincide exactly with the considered feeding section path, trolleybuses 14 and 33 are connected only to some of its parts. In the outward journey trolleybuses 12, 19 and 25 perform 5 stops (Rizzoli; Strada Maggiore; Torleone; Porta Maggiore; Albertoni), while in the return journey they perform 6 stops (Porta Maggiore; Porta San Vitale; San Vitale; Due Torri; Rizzoli; Ugo Bassi). On the contrary, during its outward journey trolleybus 14 travels from bus stop Rizzoli to bus stop Porta Maggiore, performing 3 stops, and then from Porta Maggiore to Porta San Vitale (1 stop). Instead, during its return journey, trolleybus 14 travels from bus stop Porta San Vitale to bus stop Ugo Bassi performing 4 stops. Finally, Trolleybus 33 performs only 1 stop in the considered feeding section travelling from porta Maggiore to porta San Vitale. The abovementioned routes are summarized in Table 2-7.

Bus line	Outward route [m]	Return route [m]
12, 19, 25	Ugo Bassi; Rizzoli; Strada Maggiore; Torleone; Porta Maggiore; Albertoni	Albertoni; Porta Maggiore; Porta San Vitale; San Vitale; Due Torri; Rizzoli; Ugo Bassi
14	Ugo Bassi; Rizzoli; Strada Maggiore; Torleone; Porta Maggiore; Porta San Vitale	Porta San Vitale; San Vitale; Due Torri; Rizzoli; Ugo Bassi
33	/	Porta Maggiore; Porta San Vitale

Table 2-7 Trolleybus stops in the considered FS path.

Summing up, for the evaluation of the bus traffic in the considered FS, the following assumptions are made:

1. The trolleybuses travel on time following exactly the winter working schedule provided by TPER;
2. All the trolleybuses are of the IMC type;
3. The trolleybus absorption between two bus stops is given by the IMC traction profile (see Figure 2-4);
4. The distance between bus stops is assumed to be 340 m;
5. The routes of trolleybus lines 12, 19 and 25 coincide exactly with the overhead contact line between the two substations in both directions (see Figure 2-3);
6. Bus line 14 travels 1200 m connected to the considered FS from bus stop Rizzoli (400) up to Porta Maggiore (1600) and 400 m from Porta Maggiore (2400) to Porta San Vitale (2800) during its outward journey, while it travels 1580 m from Porta San Vitale (2800) to TSS Marconi (4380) on its way back (see Figure 2-3);
7. The first bus stop of each line travelling from TSS Marconi toward TSS Trento-Trieste coincides with TSS Marconi, which will be referred to as TSS 1, with the exception of bus line 14 which starts its journey from position 400;
8. The first bus stop of bus lines 12, 19 and 25 travelling from TSS Trento-Trieste toward TSS Marconi coincides with TSS Trento-Trieste, which will be referred to as TSS 2;
9. The first bus stop of bus line 14 in its return journey coincides with Porta San Vitale (2800);
10. The first bus stop of bus line 33 coincides with Porta San Maggiore (2400).

2.3.3 General info about FS Marconi-Trento Trieste

The lengths of the overhead bifilar line in the outward and return paths are respectively 2000 m and 2380 m, for a total of 4380 m for the whole FS. Looking at Figure 2-3, one can deduce that the loop in the FS is composed of a single bifilar line because the trolleybuses travel only in one way, while the remaining segments of the FS are composed of double bifilar lines.

The traction substations feed the catenary through a bundle of cables of 240 mm^2 section, called feeders. The feeders that connect TSS Marconi and TSS Trento Trieste to the considered FS are 15 m and 100 m long, respectively, and they are constituted by six 240 mm^2 cables in parallel. As mentioned in paragraph 2.2.3, the number of cables that constitute the feeders must guarantee that the circuit breakers intervene in case of overload and, short-circuit at the beginning and at the end of the line. Remembering that it is assumed that all trolleybuses deployed in the considered FS are of the IMC type, the following three verifications are performed to check if the current feeders can withstand the new working conditions:

i. The verification of overload protection requires that the cable current rating (I_Z) is greater than the design current (I_B).

I_Z can be calculated applying equation (1) from the knowledge of the trolleybus types and their current absorptions (Table 2-3). The total number of trolleybuses per bus line connected to the feeding section is evaluated by multiplying the number of trolleybuses per kilometer per bus line by the length of the bus line route in the FS (7). The number of trolleybuses per kilometer per bus line ($N_{bus/km,i}$) are listed in Table 2-1 and they refer to an ideal condition in which the trolleybuses are evenly spaced out. The lengths of the line bus routes in the considered FS ($L_{bus,i}$) can be found in Table 2-6.

$$N_{bus,i} = N_{bus/km,i} L_{bus,i} \tag{7}$$

The number of trolleybuses per bus line and the total number of trolleybuses in the considered FS are shown in Table 2-8.

Feeding section		$N_{bus,i}$					N_{total}
ZE	**Path**	**12**	**14**	**19**	**25**	**33**	**Total**
17	Marconi-Trento Trieste	4.4	2.3	3.8	3.5	0.3	14.3

Table 2-8 Number of trolleybuses per bus line and total number of trolleybuses connected to FS 17.

The design current for each trolleybus line ($I_{B,i}$) is evaluated by multiplying the number of trolleybuses per bus line in the FS by the current absorption of the IMC trolleybuses, which can be found in Table 2-3 (8).

$$I_{B,i} = N_{bus,i} I_{rms,i} \quad (8)$$

Since bus lines 12, 19 and 33 are characterized by a bus route which is currently completely electrified, their current absorption is set equal to the one of bus line 13 (60 % electrified). The total design current is calculated by applying equation (2).

The values of the design current per bus line and the total FS design current are listed in Table 2-9.

Feeding Section		$I_{B,i}$ **[A]**					$I_{B,total}$ **[A]**
Number	**Path**	**12**	**14**	**19**	**25**	**33**	**Total**
17	Marconi - Trento Trieste	968	511	836	1190	66	3571

Table 2-9 Calculation of the total design current of FS Marconi-Trento Trieste with reference to the worst working conditions (15 trolleybuses in the FS at the same time).

Being the FS fed by two traction substations the total design current is equally divided between them, so the feeders must be sized to carry half of the total design current. The current rating of the bundle of cables used as feeders is evaluated by multiplying the number of cables by the current rating of one single cable (330 A).

FS Marconi-Trento Trieste is also characterized by the presence of two 300 mm^2 reinforcement feeders (see yellow dots in Figure 2-3):

1. The reinforcement feeder starting from TSS Marconi has a total length of 650 m and it is connected to the OCL every 300 m starting from the beginning of the catenary;
2. The reinforcement feeder starting from TSS Trento Trieste has a total length of 650 m and it is connected to the OCL approximately every 200 m starting from position 2000.

For the sake of simplicity, the reinforcement feeders are not considered in the verification of overload protection (more burdensome condition).

The verification of the overload protection for FS 17 is performed in Table 2-10. Being the verification successful when the reinforcement feeders are discarded, a fortiori it is verified in the real condition because the design current is divided between more cables.

TSS	Feeding section	$I_B = \frac{I_{B,tot}}{2}$ [A]	Number of cables in parallel	Section [mm^2]	I_Z[A]	$I_Z > I_B$
Marconi	17 Marconi - Trento Trieste	1785.5	6	240	1980	yes
Trento Trieste		1785.5	6	240	1980	yes

Table 2-10 Verification of overload protection of the feeders of FS 17.

ii. The protection from short-circuit at the beginning of the line is guaranteed when equations (3) and (4) are both satisfied.

Knowing that at the beginning of the line the maximum short-circuit current per conversion group is 25.6 kA and that the protection devices installed by TPER have a breaking capacity (P_{int}) of 70 kA in 200 ms, equation (3) is satisfied. The verification of this first condition is shown in Table 2-11.

Feeding section	Number of conversion groups	I_{sc_max} [kA]	P_{int} [kA]	$I_{sc_{max}} < P_{int}$
17 - Marconi-Trento Trieste	2	51.8	70	yes
17 - Trento Trieste-Marconi	2	51.8	70	yes

Table 2-11 Verification of breaking capacity of circuit breaker at the beginning of the line.

Knowing that the protection device tripping time (t) is 0.1 s and the maximum short-circuit current for conversion group ($I_{SC_{max}}$) is 25.6 kA, $I^2_{sc_{max}}t$ can be evaluated. From the knowledge of the coefficient related to the cable insulation (K = 143 for HEPR rubber) and the feeders' total section (S_{tot}), it is possible to evaluate $K^2S^2_{tot}$. The verification of the second condition for short-circuit protection at the beginning of the line for FS 17 is shown in Table 2-12.

Feeding section	Number of conversion groups	$I^2_{sc_{max}}t$ [kA^{2}s]	S_{tot} [mm^2]	$K^2S^2_{tot}$ [kA^{2}S]	$I^2_{sc_{max}}t < K^2S^2_{tot}$
17 - Marconi-Trento Trieste	2	262144	1440	42403046.4	Yes
17 - Trento Trieste-Marconi	2	262144	1440	42403046.4	Yes

Table 2-12 Verification of the feeders let-through energy at the beginning of the line for FS 17.

iii. The cable is considered protected from short-circuits at the end of line when the minimum short-circuit current (I_{sc_min}) is greater than 2-3 times the design current (I_B).

Because of the meshed topology of the considered FS the evaluation of the minimum short-circuit current is performed using the circuit simulation software LTspice. The results of such simulation are reported in Table 2-13 without further explanation.

Feeding section	**OCL [m]**	**Feeder [m]**	I_{min} **[A]**	I_B **[A]**	$I_{min} > 2I_B$
17 - Marconi-Trento Trieste	4380	15	1936	1785.5	No
17 - Trento Trieste-Marconi	4380	100	1922	1785.5	No

Table 2-13 Verification of short-circuit protection at the end of the line for FS 17.

As has been anticipated in paragraph 2.2.3, when the verification of short-circuit protection at the end of the line is not successful, the protection is achieved with the calibration of the relay ME-MPS13L through the function of maximum current variation according to the current gradient Δi/Δt.

3 Trolleybus grid Simulink dynamic model

In this chapter, the circuit model of the trolleybus grid implemented in Simulink environment is described in detail. Dynamic modelling is intended as simulating the trolleybus network behaviour as a function of the time variation of the vehicle position.

Figure 3-1 shows the electric circuit of one feeding section of the trolleybus grid that feeds *k* trolleybuses when a stationary wayside battery energy storage system is installed. Each element of the scheme, except the BESS which will be analyzed in chapter 4, is described in the following paragraphs. To be precise, the traction substation, trolleybus and catenary models are introduced in paragraphs 3.1, 3.2 and 3.3. The Simulink dynamic model of FS Marconi-Trento Trieste is described in Paragraph 3.4.

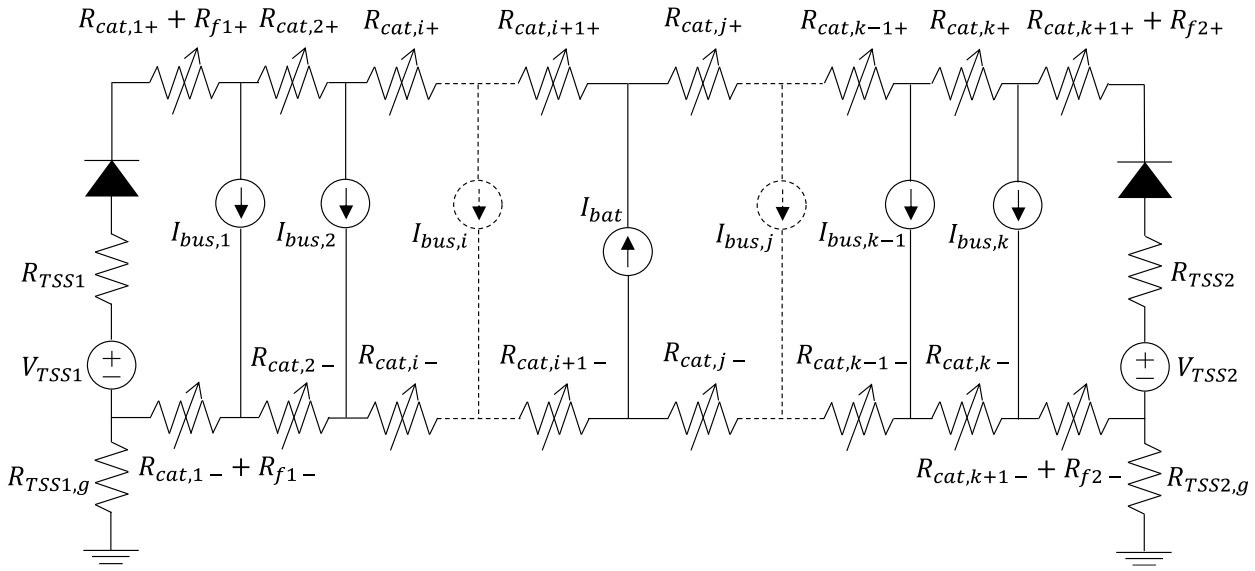

Figure 3-1 Electric circuit of a feeding section of the trolleybus grid that feeds k trolleybuses when a stationary wayside battery energy storage system is installed.

3.1 Traction substation modelling

The components of a traction substation of the trolleybus grid of the city of Bologna are listed in paragraph 2.2.2, where a simplified scheme is also illustrated (Figure 2-2). Such a detailed scheme is not necessary to analyze the voltage profile along the catenary. Assuming that the traction substations are sized accordingly to the actual power demand of the trolleybuses insisting on the feeding sections, the TSSs can be modelled using the Thevenin representation by a constant voltage generator and a series resistor that accounts for the losses inside the substation. To account for the unidirectionality of the power flow in the TSSs a series ideal diode is also added to the electrical

scheme. For safety reasons, a ground resistor in the ground connection must be added too. Therefore, the electrical model of a traction substation can be simplified as it is shown in Figure 3-4. The Simulink model of the simplified TSS scheme is illustrated in Figure 3-3.

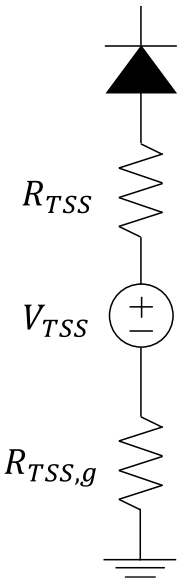

Figure 3-2 Simplified traction substation electrical scheme.

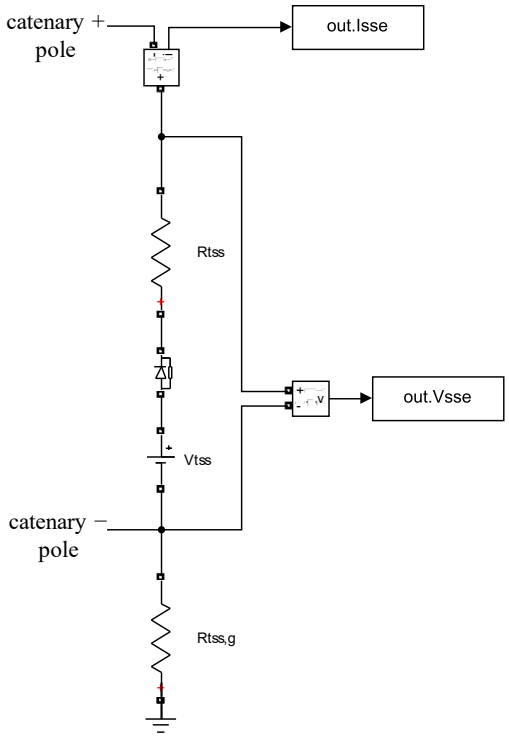

Figure 3-3 Simulink model of TSS.

Being the conversion stage of the TSS a parallel 12-pulse rectifier presenting 590 V input voltage, the voltage generator open-circuit voltage is set to 800 V (V_{TSS}), which is the mean value of the output voltage of the 12-pulse rectifier. The TSS output resistance (R_{TSS}) and its ground resistance ($R_{TSS,g}$) are assumed to be 66 mΩ and 0.5 Ω respectively.

The connection of the TSSs to the catenary is realized through feeders (one for each pole of the catenary), which are modelled by resistors whose resistance value depends on the number of cables in parallel, their section, and the length of the feeders themselves. Therefore, the resistance of the feeders can be calculated using equation (9), where *r* is the per unit length resistance of a 100 mm^2 cable [Ω/m], L_f is the feeder length [m], *A* is the ratio between the cable section and 100 mm^2, and N_{cable} is the number of cables in parallel.

$$R_{feeder} = \frac{r L_f}{A\, N_{cable}} \tag{9}$$

The feeders used by TPER for the trolleybus grid of the city of Bologna are composed of cables of 240 mm^2 section, so *A* is equal to 2.4.

3.2 Trolleybus modelling

According to the traction profile, the trolleybus absorbs (or delivers) current from (to) the trolleybus grid for its motion. Thus, the trolleybus operation can be ideally modelled as a current generator, as commonly done in literature ([5], [6], [21], [31]). The determination of the trolleybuses' current absorption profiles is out of the scope of this thesis, so the generic profiles provided by TPER are employed.

The trolleybus is modelled in Simulink with a controlled current generator, like it is shown in Figure 3-5 (circled in red). Knowing the departure time, and the start and end point of the trolleybus ride, a control is implemented to simulate its motion along the feeding section. The detailed explanation of the trolleybus motion control working principle is given in paragraph 3.3.

3.3 Catenary modelling

The power supply of a trolleybus is performed through the connection of its trolley poles to the negative and positive poles of the overhead bifilar line. The current flows from the TSSs through the positive pole to the trolleybus and then flows back through the negative one.

Since this thesis deals with long-term evolutions, electric transients are neglected, thus no dynamic component is used to model the catenary, as has been done in [5]. Therefore, the negative and positive poles of the overhead contact line between two traction substations are electrically modelled by resistors. When one trolleybus travels from one end to the other of the OCL, the trolleybus connection point with the OCL, as well as the length of the two sections of the OCL that separate the trolleybus from the TSSs, change with time accordingly to its speed profile. Therefore, the two sections of the OCL can be modelled as variable resistors whose value depends on the trolleybus position (Figure 3-4).

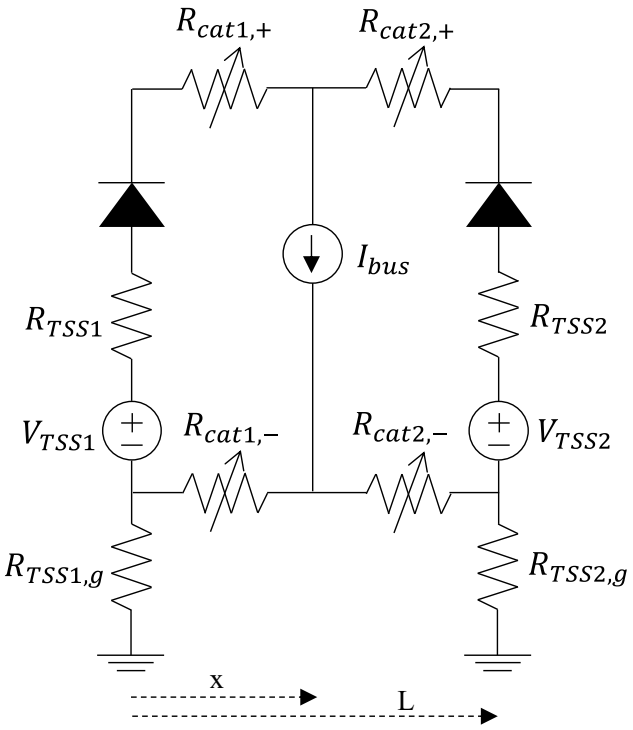

Figure 3-4 Electrical scheme of an FS with one trolleybus.

The resistance of the two sections of the catenary can thus be calculated as follows:

$$R_{cat1} = xr \tag{10}$$

$$R_{cat2} = (L - x)r \tag{11}$$

where x is the trolleybus position with respect to TSS1, L is the length of the feeding section (FS) and r is the per unit length resistance of the catenary. The per unit length resistance of the catenary of the trolleybus grid of the city of Bologna is equal to $247.5\ \mu\Omega/\mathrm{m}$.

If *k* trolleybuses are connected to the same FS, like it is shown in Figure 3-1, the catenary can be divided into *k*+1 sections, which have at their ends either two trolleybuses or one trolleybus and a TSS. Therefore, the resistance of each section at every time instant can be calculated by multiplying the length of the section by the per unit length resistance of the catenary.

However, Simscape (the SPICE engine within Simulink environment) implements variable resistors using current-controlled voltage generators or voltage-controlled current generators. If the variable resistors were to be modelled with the first type generators, the circuit would present cut-off sets made of current generators only that lead to singularities according to the circuit theory. If they were to be modelled with the second type generator, particular care should be taken in the setting of the initial conditions to avoid an un-physical representation of the circuit, such as the short-circuit of the entire contact line section if the initial voltage were to be set to 0. Furthermore, the model would

experience criticalities in the event of null resistance (for example when the trolleybus is in the proximity of the TSS). More importantly, the above-described approach fails on representing the actual morphology of the line because it does not consider equipotential connections between different segments of the overhead bifilar line. Thus, another strategy must be implemented to represent the motion of the trolleybuses in a feeding section.

Since the trolleybus length is around 20 m (18 m simply articulated trolleybus used in Bologna), only one trolleybus at a time can be connected to a 20 m segment of the OCL. Therefore, discretizing the overhead bifilar line in 20 m long segments does not introduce relevant representation artifacts. The series connection of multiple 20 m long segments allows to simulate the desired length of the feeding section (rounded to a multiple of 20 m). A control is then implemented to determine to which 20 m segment the trolleybus is connected. In Figure 3-5 it is displayed the Simulink model of a 20 m long segment of the OCL, where the controlled current generator (circled in red) represents the trolleybus current absorption. The 20 m long segment of the overhead bifilar line has an "H" configuration, which means that the resistors are placed symmetrically with respect to the current generator. The resistance value of the 4 resistors in the 20 m long span is $247.5\ \mu\Omega$, which corresponds to the resistance of a 10 m long section of the catenary.

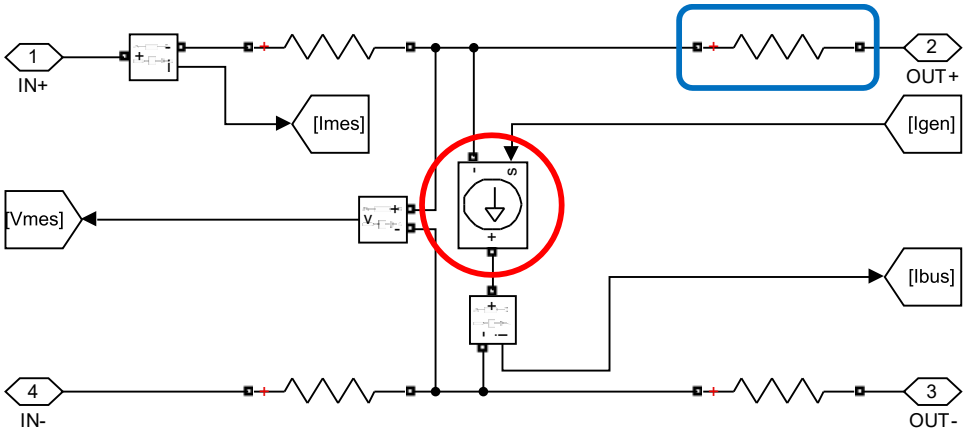

Figure 3-5 Simulink model of 20 m long OCL. Trolleybus model circled in red. Resistance of 10 m of catenary circled in blue.

The controlled current source is governed by a MATLAB function (12), that determines if the trolleybus is in the considered 20 m segment and how much current is absorbing [Igen] from the time vectors of the trolleybus positions [xin] and current absorptions [I] (Figure 3-6).

$$[I_{gen}, x_{out}] = \text{fcn}(x, d, I) \tag{12}$$

If the trolleybus is not in the considered span, the current generated by the controlled current source is null. When the trolleybus enters the considered span, [Igen] assumes the values of the current

time vector [I] until its exit. Because of the "H" configuration of the span, the trolleybus is assumed to be in the middle of the span for the time it requires to travel the 20 m segment. This means that the trolleybus is assumed to move in 20 m jumps, thus the controlled current source is turned on as soon as the trolleybus enters the considered span and stays on regardless of its actual position inside the span.

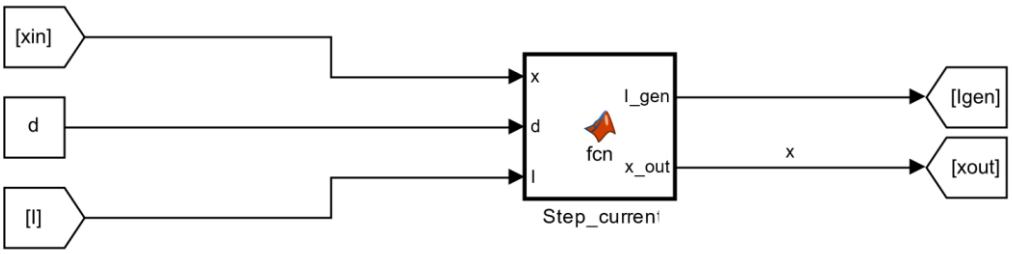

Figure 3-6 Trolleybus current control based on its location.

The inputs of the MATLAB function (12) are the time vector of the positions of all the trolleybuses in 24 hours period (x), the length of the span (d=20 m), and the time vector of the current absorptions of all the trolleybuses in 24 hours period (I), while the outputs are the time vector of the current generated by the controlled current source of the considered span (I_{gen}), and a variable that points out whether the trolleybus is in the considered span in that instant (x_{out}). To be sure that the current generator of the first span block turns on when the trolleybus is at the beginning of its journey an offset of 10 m was introduced to the original time vector of the trolleybus' positions. The code of the MATLAB function (12) can be found hereafter.

```
function [I_gen,x_out] = fcn(x,d,I)

x_out=x-d;
k=ones(size(x_out));
k(abs(x_out)>d/2 | x_out==d/2)=0;
I_gen=k'*I;

end
```

The trolleybuses positions (x) are obtained from their daily schedule provided by TPER, while their current absorptions (I) are given by the traction profile. More information about the building of these two-time vectors is given in paragraph 2.3.

To simulate a feeding section multiple "T_block" blocks are connected in series until the desired length is reached. For example, a 200 m long segment of an FS is represented in Figure 3-7.

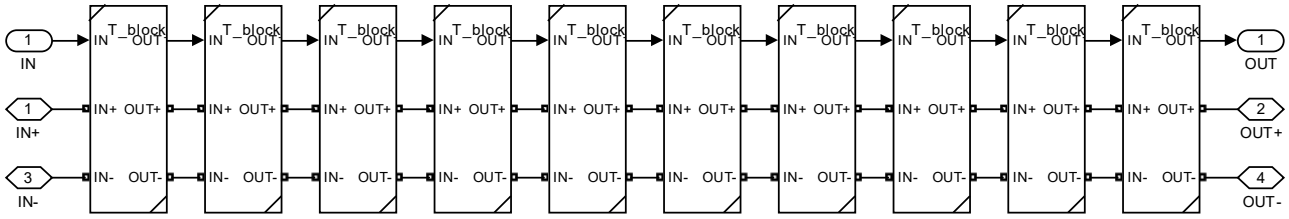

Figure 3-7 Simulink model of 200 m segment of an FS.

The inputs and outputs of each "T_block" are listed below:

- IN: information matrix entering the considered "T_block" from the previous one or from the control logic block (described later in the paragraph) if the "T_block" is the first of the chain (Figure 3-8). The IN vector contains information about the trolleybus position (xin), current absorption (I), voltage of the catenary at the trolleybus position as a function of time (Vin), measured OCL voltage (Vmes), measured OCL current (Imes) and trolleybus current as a function of time (Ibus). (Din) is an auxiliary parameter that is used to verify whether the simulated OCL length corresponds to the desired value;

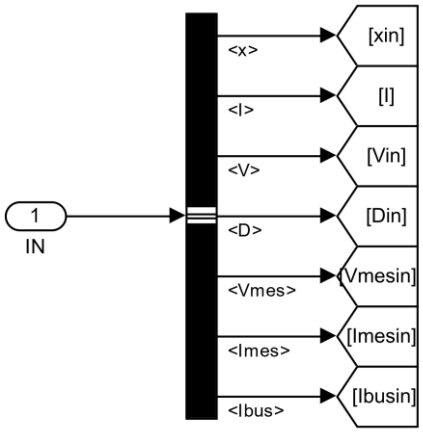

Figure 3-8 Inputs of span block.

- OUT: information matrix exiting the considered "T_block" with updated values with respect to the ones entering (Figure 3-9);

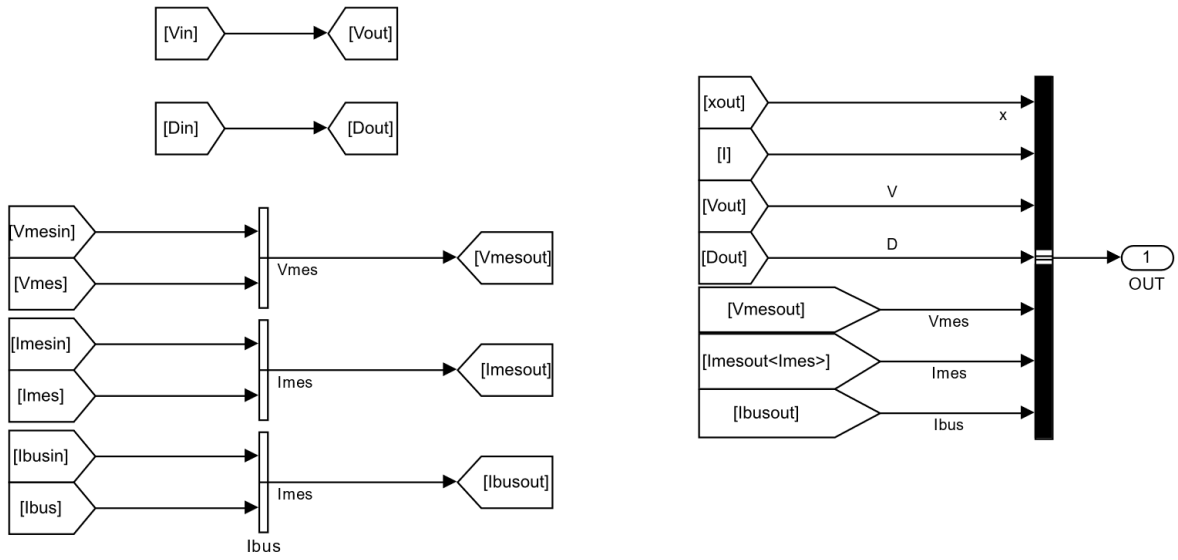

Figure 3-9 Outputs of span block.

- IN+/IN-: positive and negative input pole current;
- OUT+/OUT-: positive and negative output pole current.

The control logic block of the Simulink model of the catenary is represented in Figure 3-10, where the original input matrix is built. tsX and tsI are respectively the time vectors of the trolleybuses' position and current absorption during the 24 h simulation created in MATLAB using the trolleybus daily schedule and traction profiles. The voltage of the catenary at the trolleybus position as a function of time (Vin) and the auxiliary variable (D) are initialized as row vectors with a number of columns equal to the total number of trolleybuses that circulate in the considered FS throughout the day. The measured voltage (Vmes) and current (Imes), and the trolleybus current (Ibus) are initially grounded.

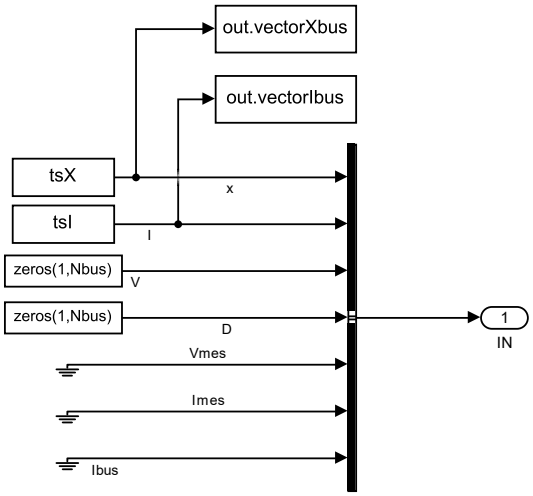

Figure 3-10 Control logic block.

3.4 Simulink model of FS Marconi-Trento Trieste without battery

In Figure 3-11 it is illustrated the Simulink model of the considered feeding section.

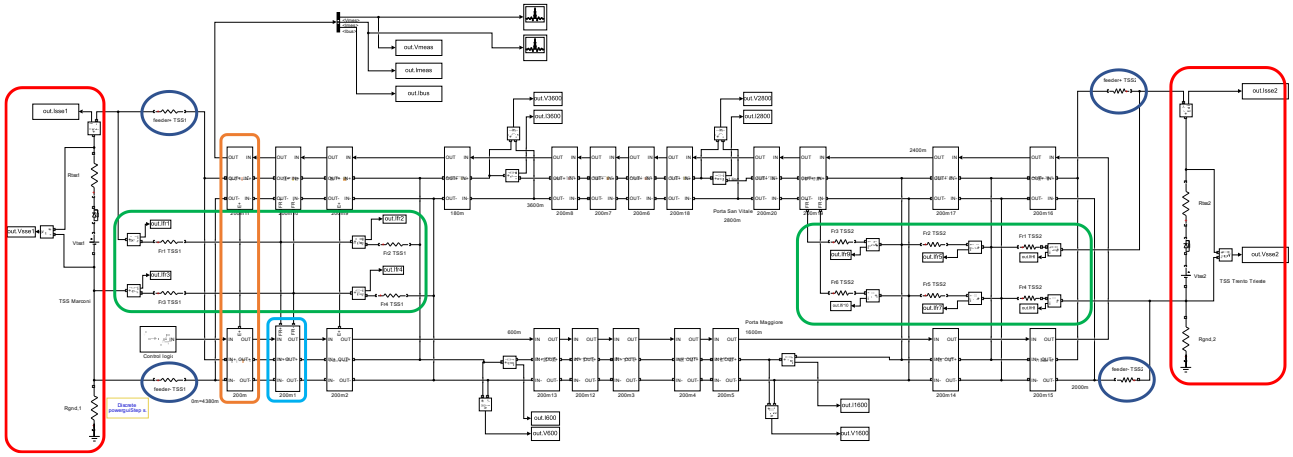

Figure 3-11 Simulink model of FS Marconi-Trento Trieste.

All components of the model are described hereafter:

1. Red rounded squares: TSS Marconi on the left, and TSS Trento Trieste on the right. A close-up image of the traction substation can be found in paragraph 3.1 (Figure 3-3).
2. Blue circles: resistance of the positive and negative feeders that connect the traction substation to the catenary. To be specific, the feeders that connect the TSSs to the catenary are composed of six 240 mm^2 cables and they are 15 m (feeders of TSS Marconi) and 100 m long (feeders of TSS Trento Trieste). The resistance values of said feeders, calculated using equation (9), are listed in Table 3-1. A close-up of the positive and negative feeders of TSS Marconi can be seen in Figure 3-14.

TSS	Number of cables	Length of feeders [m]	R_f [mΩ]
Marconi	6	15	0.258
Trento Trieste	6	100	1.72

Table 3-1 Resistance of TSS' feeders.

3. Green rounded squares: resistance of the positive and negative reinforcement feeders that connect the TSSs to intermediate points of the catenary. To be specific, the reinforcement feeders that connect the TSSs to the catenary are composed of one 300 mm^2 cables and they are both 650 m long. The resistance values of said feeders, calculated using equation (9), are listed in Table 3-2.

TSS	Number of cables	Length of RF [m]	R_{fr} [mΩ]
Marconi	1	650	53.63
Trento Trieste	1	650	53.63

Table 3-2 Resistance of TSS' reinforcement feeders.

In Figure 3-12 it is shown a close-up of the reinforcement feeders of TSS Marconi. These reinforcement feeders connect to the double bifilar line 300 m and 600 m away from the beginning of FS Marconi-Trento Trieste.

In Figure 3-13 it is shown a close-up of the reinforcement feeders of TSS Trento Trieste. These reinforcement feeders connect to the double bifilar line at a distance of 200 m and 400 m from position 2000, and to the single bifilar line in the return route at a distance of 540 m.

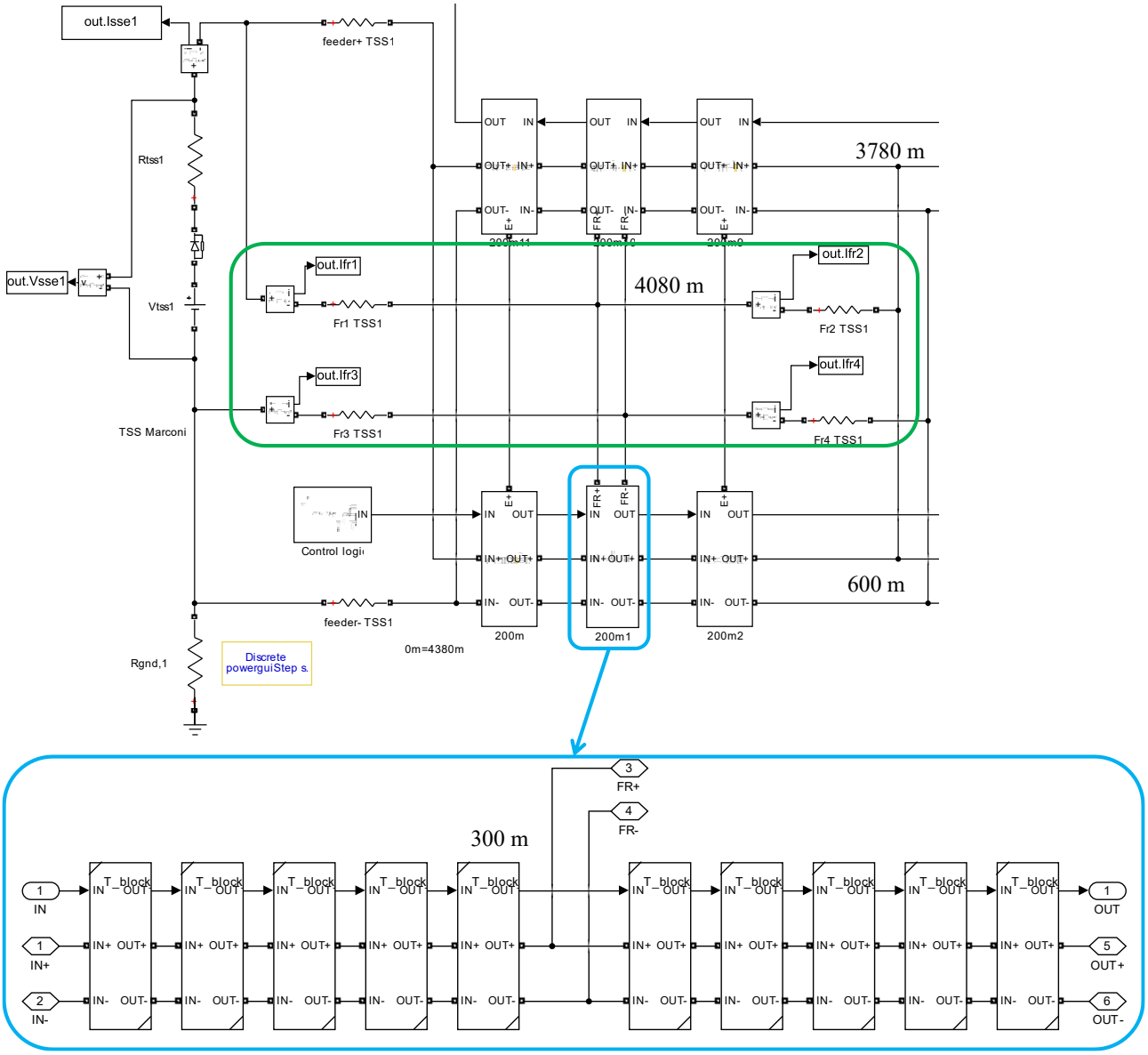

Figure 3-12 Reinforcement feeders of TSS Marconi circled in green. Close-up of connection of RF at 300 m circled in light-blue.

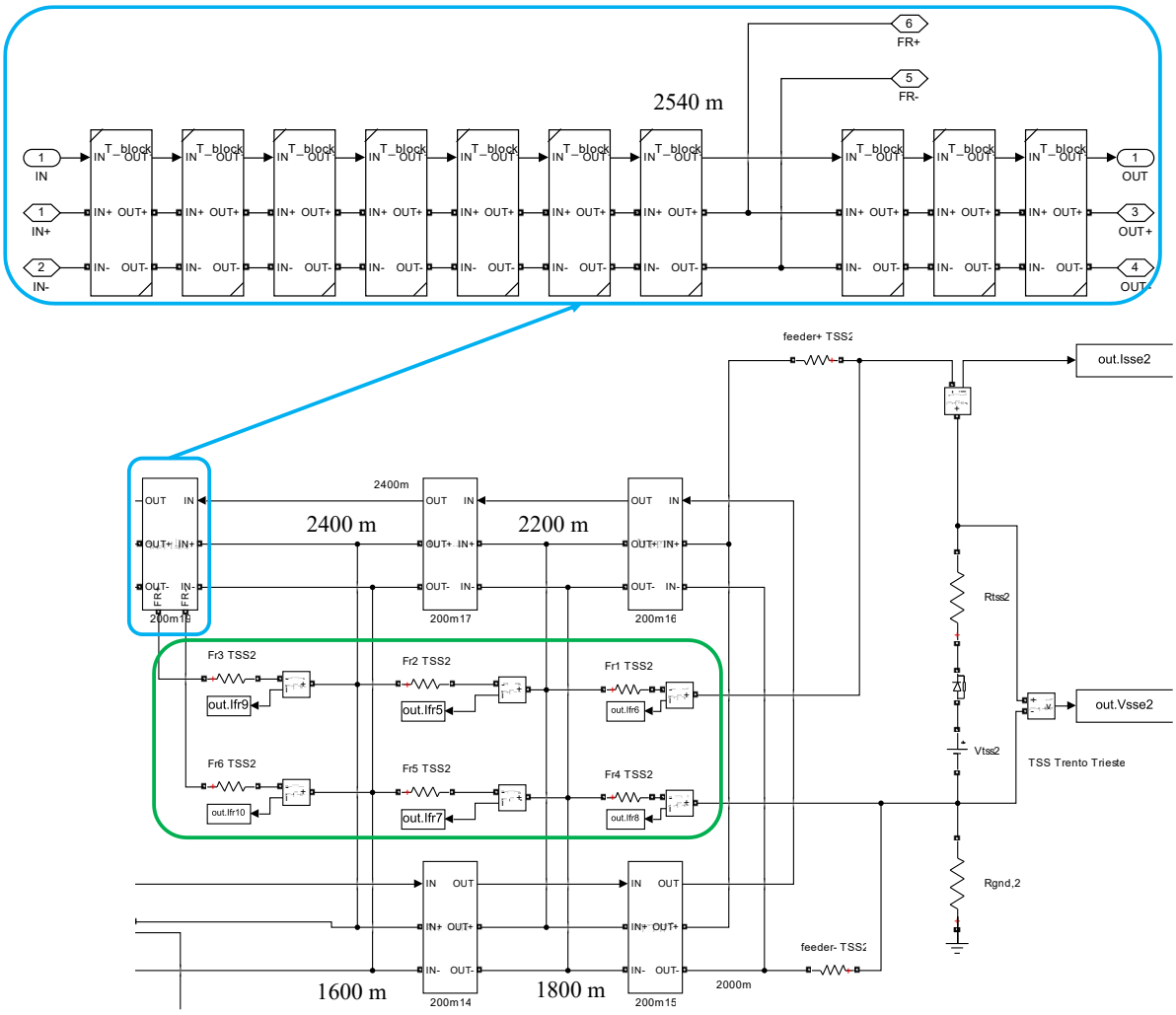

Figure 3-13 Reinforcement feeders of TSS Trento Trieste circled in green. Close-up of connection of RF at 2540 m circled in light-blue.

The resistances of all the reinforcement feeders' segments depicted in Figure 3-12 and Figure 3-13 (circled in green) are listed in Table 3-3, where the positive and negative reinforcement feeders' resistances are highlighted in yellow and green, respectively. The total resistance of each RF equals the one indicated in the last column of Table 3-2.

TSS	R_{fr1} [mΩ]	R_{fr2} [mΩ]	R_{fr3} [mΩ]	R_{fr4} [mΩ]	R_{fr5} [mΩ]	R_{fr6} [mΩ]
Marconi	28.88	24.75	28.88	24.75	/	/
Trento Trieste	25.58	16.5	11.55	25.58	16.5	11.55

Table 3-3 Resistance of reinforcement feeders of TSSs Marconi and Trento Trieste used in simulation.

4. Orange rounded square: equipotential connection between positive or negative poles of the overhead bifilar line. In FS Marconi-Trento Trieste there are only two equipotential connections between the positive poles of the overhead bifilar lines between positions 160 and 4220, and between positions 440 and 3940. The equipotential connections can be seen in Figure 3-14.

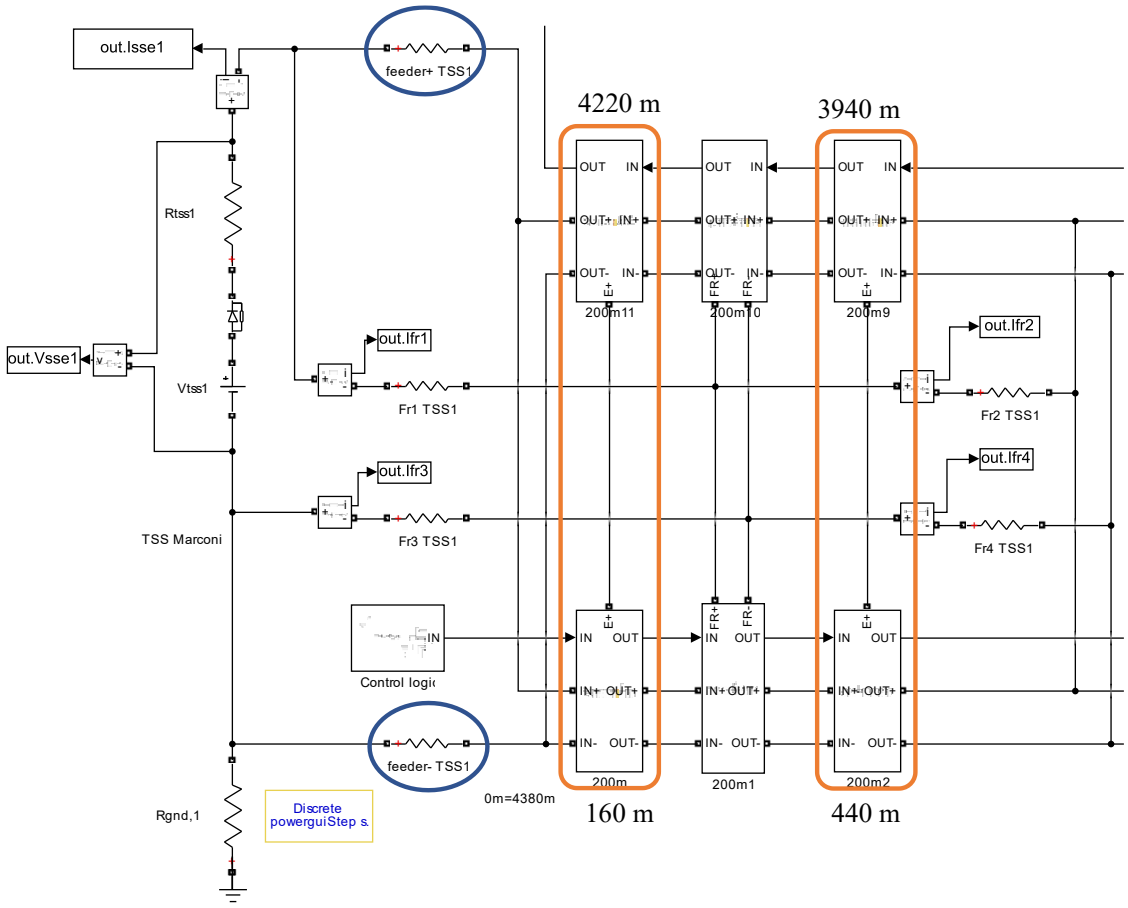

Figure 3-14 Equipotential connections of FS Marconi-Trento Trieste are circled in orange. Resistors that represent negative and positive feeders of TSS Marconi are circled in blue.

The equipotential connections and reinforcement feeders affect the voltage and current profiles of the catenary. The voltage profile of the catenary at 07:00 am is illustrated in Figure 3-15, where particular attention is given to the effects that the feeders (green dots), equipotential connections (blue dots), reinforcement feeders (red dots) and trolleybuses (black dots) have on the voltage profile. Since the trolleybuses absorb current from the catenary, their overall effect on the voltage profile is to produce voltage minima. On the contrary, reinforcement feeders and feeders provide current to the catenary, so their overall effect is to raise the voltage. The equipotential connections parallelize the catenaries for the two travel directions (outward and return journeys). Doing so the resistance of the line is reduced, thus the voltage profile is higher than it would be if no connection was made. At 07:00 am 4 trolleybuses are connected to the considered FS.

The need to install a BESS is clearly understandable looking at Figure 3-16, where it is visible that the minimum voltage profile (dashed line) is out of the admissible voltage range for the normal operation of the trolleybuses. In Figure 3-16 the central inter-percentile range (coloured area), which

is the interval of voltage values that have a 95 % cumulative probability to occur during the simulation in every position of the catenary, and the mean voltage profile are also depicted.

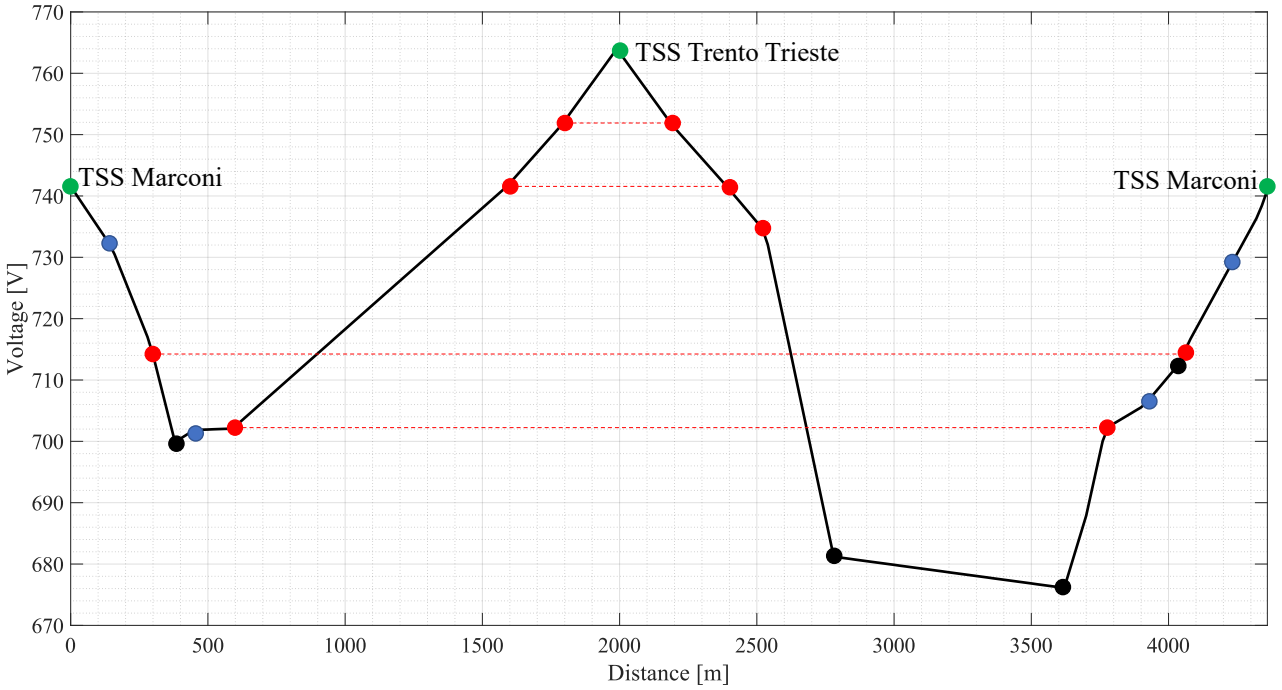

Figure 3-15 Voltage profile of FS Marconi-Trento Trieste at 07:00 am. Legend: Feeders (green dots); Reinforcement feeders (red dots); equipotential connections (blue dots); trolleybuses (black dots).

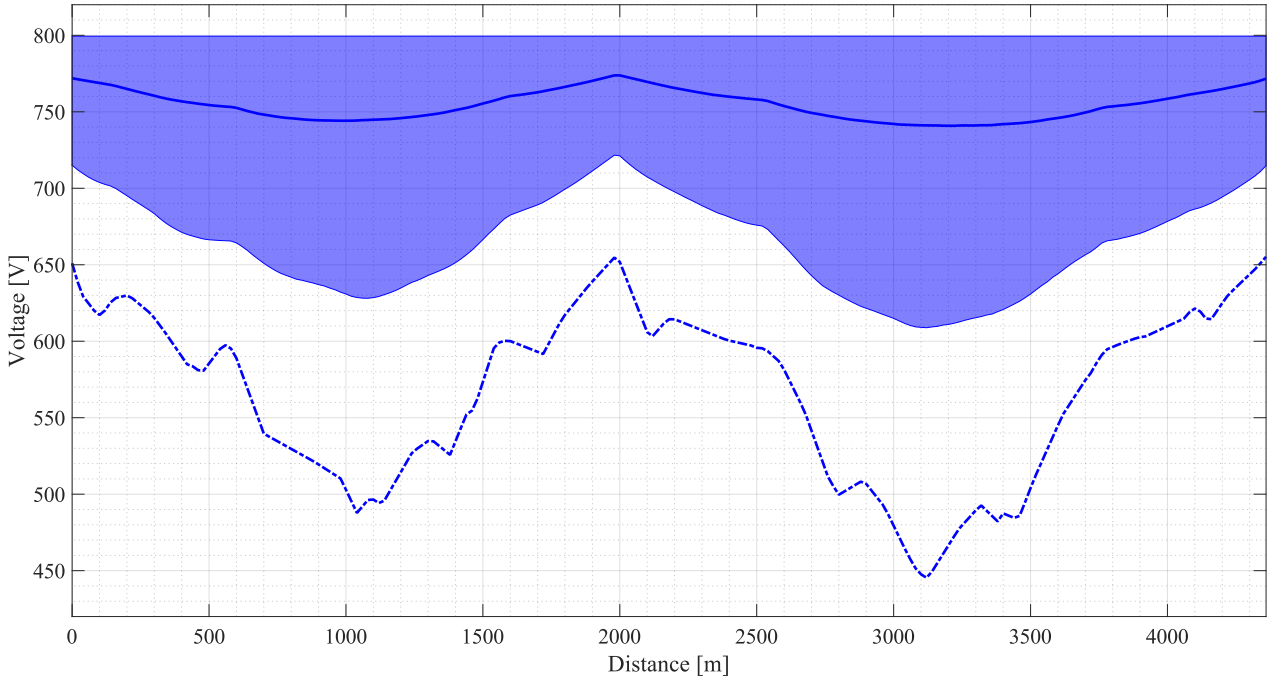

Figure 3-16 Voltage profile along the catenary during 24 h simulation. Legend: Minimum voltage profile (dashed lines); Mean voltage profile (solid line); 95 % central inter-percentile range (coloured area).

4 Battery ESS modelling and control

This chapter deals with the modelling of the BESS and the tuning of its control.
First, the battery control strategy is introduced in paragraph 4.1. The output current of the DC/DC converter is controlled in function of the line voltage and the battery SOC. The current in the output of the converter is limited by the maximum current that can flow in the bifilar line conductor, while the current in the input of the converter (battery side) is limited by the battery C-rate value. In paragraph 4.2 the results obtained from simulating the model without the BESS are discussed to determine the best location of the BESS and the BESS control idle range. Paragraph 4.3 deals with the battery control for the considered FS. In paragraph 4.4, it is formulated a prediction of the voltage distribution at the BESS connection point after its installation. Finally, in paragraph 4.5 and 4.6 the Simulink models of the BESS and of FS Marconi-Trento Trieste with the battery ESS are described, respectively.

4.1 Battery control strategy

Technical standard EN 50163: Railway applications-Supply voltages of traction systems (2006/2008) states that the admissible voltage range for traction systems is [500 1000] V and that the nominal voltage for railway and trolleybus applications is 750 V.

The control objective is to charge or discharge the battery whenever the catenary voltage at the battery connection point goes above or below a specified voltage range, called idle region. Instead, when the catenary voltage is within the idle region, the battery is inactive, and the catenary behaves following its natural evolution. The determination of the upper and lower limits of the idle region is performed analyzing the voltage distribution at the catenary location where the battery ESS will be installed. In this paragraph, the lower and upper limits of the idle region are referred as V_l and V_u respectively.

Technical standard EN 50119 states that the 100 mm^2 catenary cables should not carry a continuous current higher than 451 A. Assuming that the trolleybuses are uniformly distributed in the FS, the output (or input) current of the stationary ESS is equally divided between the right-side and left-side of the catenary. Therefore, the maximum output (or input) current of the battery ESS is 902 A, which is approximated to 900 A in the following analysis. This means that when the catenary voltage is at the limit of the admissible voltage range, the battery ESS should provide the maximum

admissible current for safe cable operation. When the catenary voltage is between V_l and V_u, the reference output current of the battery ESS is nil, and the battery is in the idle state. Outside of the idle region, the reference output current of the ESS is linearly dependent on the catenary voltage.

The battery control trans-characteristic is expressed by equation (13), where A_1 and A_2 are the slopes of the lines in the voltage ranges [500 V_l] V and [V_u 1000] V, respectively.

$$\begin{cases} I_{out,ESS} = A_1(V_{line} - V_l) & if\ V_{line} < V_l \\ I_{out,ESS} = 0 & if\ V_l \leq V_{line} \leq V_u \\ I_{out,ESS} = A_2(V_{line} - V_u) & if\ V_{line} > V_u \end{cases} \quad (13)$$

The trans-characteristic of the battery control refers to the passive sign convention, which defines as positive the electric power flowing out of the catenary into the battery. Thus, when the catenary voltage is lower than V_l, the battery discharges and its output current is negative, while when the catenary voltage is higher than V_u, the battery charges and its output current is positive. The trans-characteristic of the battery control given by equation (13) is plotted in Figure 4-1.

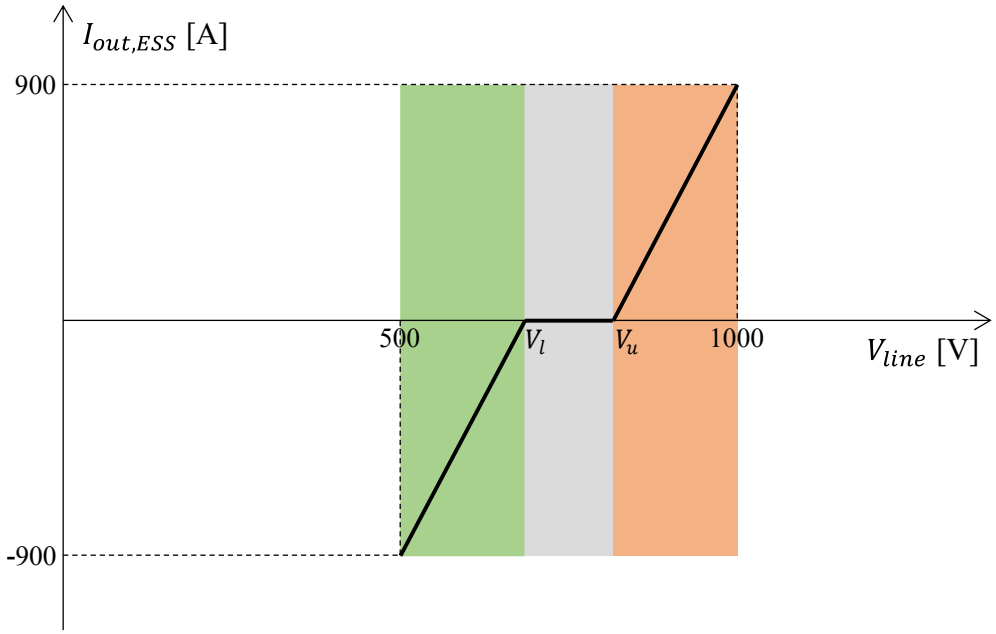

Figure 4-1 Battery control trans-characteristic. Legend: discharging state (green area); idle state (grey area); charging state (red area).

However, the current that the battery can deliver or absorb is not only limited by the maximum current that can flow in the catenary cables, but also by its C-rate. The C-rate is a measure of the intensity at which a battery is discharged in relation to its maximum capacity. As it was mentioned in paragraph 2.2.5, the higher the C-rate, the faster the battery ages and is prone to failures. Therefore, the C-rate is usually limited to *2C* (complete discharge in 30 minutes) where *C* is the maximum capacity of the battery. Depending on the battery maximum capacity and the battery voltage, the

limitation on the C-rate might or might not limit the output current reference of the battery ESS. The limitation imposed by the C-rate is expressed by equation (14).

$$I_{out,ESS} = \pm 2C \frac{V_{bat}}{V_{line}} \tag{14}$$

If the intersection between the C-rate limitation and the battery control trans-characteristic expressed by equation (13) occurs within the voltage range [500 1000] V, the battery control must also ensure that the battery never works at C-rates higher than 2.

The C-rate limitation and the maximum cable current limitation for a given battery capacity and constant battery voltage are plotted in Figure 4-2.

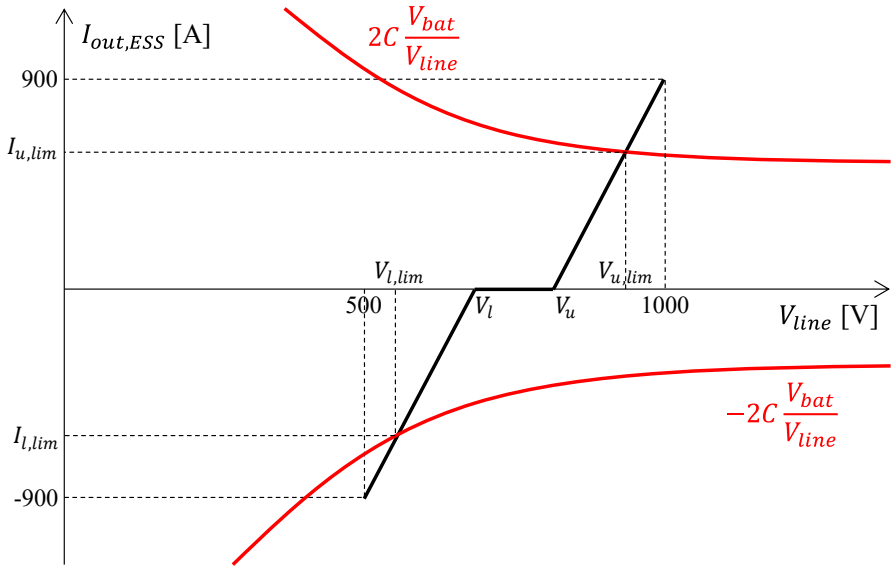

Figure 4-2 Plot of the C-rate limitation curve of a battery of capacity C with constant battery voltage (red) and maximum cable current limitation (black).

The intersections between the black curve (maximum cable current limitation) and the red curves (C-rate limitation at constant battery voltage) represent the lower ($V_{l,lim}$) and upper ($V_{u,lim}$) limits of the catenary voltage for which it is possible to discharge and charge the battery without restrictions, respectively. When the catenary voltage is lower than $V_{l,lim}$ or higher than $V_{u,lim}$ the battery enters in limited discharging or charging state to preserve battery life.

Solving equations (15) and (16), it is possible to determine $V_{l,lim}$ and $V_{u,lim}$ (equation (17) and (18) respectively).

$$A_1(V_{line} - V_l) = -2C \frac{V_{bat}}{V_{line}} \tag{15}$$

$$A_2(V_{line} - V_u) = +2C \frac{V_{bat}}{V_{line}} \tag{16}$$

$$V_{l,lim} = \frac{V_l}{2} + \frac{1}{2}\sqrt{V_l^2 - \frac{8C}{A_1}V_{bat}} \tag{17}$$

$$V_{u,lim} = \frac{V_u}{2} + \frac{1}{2}\sqrt{V_u^2 + \frac{8C}{A_2}V_{bat}} \tag{18}$$

It is worth mentioning that $V_{l,lim}$ is calculated only for the battery capacities that guarantee the positivity of the radicand in equation (17). For higher battery capacities than the one calculated by (19), there is no limitation for the battery discharging because the battery control trans-characteristic does not intersect with the C-rate limitation in the domain of real numbers.

$$C_{limit} \leq \frac{A_1 V_l^2}{8V_{bat}} \tag{19}$$

If the battery maximum capacity is high enough, the C-rate does not introduce any limitation on the reference output current of the battery ESS because $V_{l,lim}$ and $V_{u,lim}$ are outside of the range of interest ([500 1000] V).

The battery control trans-characteristic for a battery storage of capacity *C* that is limited by its C-rate is expressed by equation (20).

$$\begin{cases} I_{out,ESS} = -2C\dfrac{V_{bat}}{V_{line}} & \text{if } 500 \leq V_{line} < V_{l,lim} \quad mode = -2 \\ I_{out,ESS} = A_1(V_{line} - V_l) & \text{if } V_{l,lim} \leq V_{line} < V_l \quad mode = -1 \\ I_{out,ESS} = 0 & \text{if } V_l \leq V_{line} \leq V_u \quad mode = 0 \\ I_{out,ESS} = A_2(V_{line} - V_u) & \text{if } V_u < V_{line} \leq V_{u,lim} \quad mode = 1 \\ I_{out,ESS} = 2C\dfrac{V_{bat}}{V_{line}} & \text{if } V_{u,lim} < V_{line} \leq 1000 \quad mode = 2 \end{cases} \tag{20}$$

In Figure 4-3 it is depicted the battery control trans-characteristic for a battery storage of capacity *C* with constant battery voltage that is limited by its C-rate in the voltage ranges [500 $V_{l,lim}$] V and [$V_{u,lim}$ 1000] V.

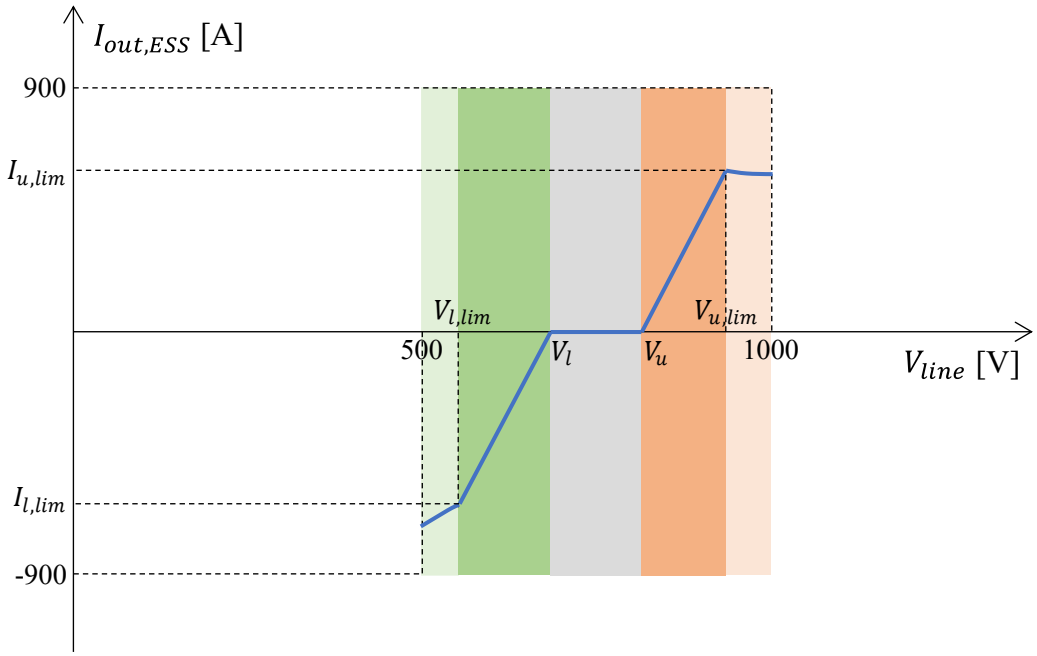

Figure 4-3 Battery control trans-characteristic of battery storage of capacity C and constant battery voltage with C-rate limitation (blue curve). Legend: limited discharging (light green); discharging (green); idle (grey); charging (red); limited charging (light red).

Lastly, the battery control must account for the battery *SOC*. When the battery *SOC* is within the range [10 90] %, the battery operation is solely determined by trans-characteristic (20) or (13), depending on whether the C-rate limits or not the battery operation. If *SOC* is outside the prementioned range, the battery operation must be limited to preserve battery life and slow down calendar and cycle aging [39]. When *SOC* is lower than 10%, the battery discharge must be stopped independently on the catenary voltage level, while when *SOC* is higher than 90 %, it is the battery charge that must be stopped. The battery control trans-characteristics when *SOC* is below 10 % and above 90 % are represented in Figure 4-4 and Figure 4-5 respectively.

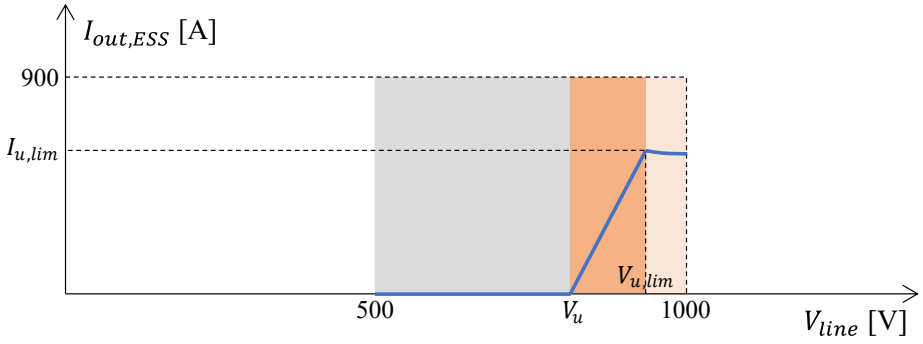

Figure 4-4 Battery control trans-characteristic when SOC is lower than 10%. Legend: idle state (grey); charge state (red); limited charging state (light red).

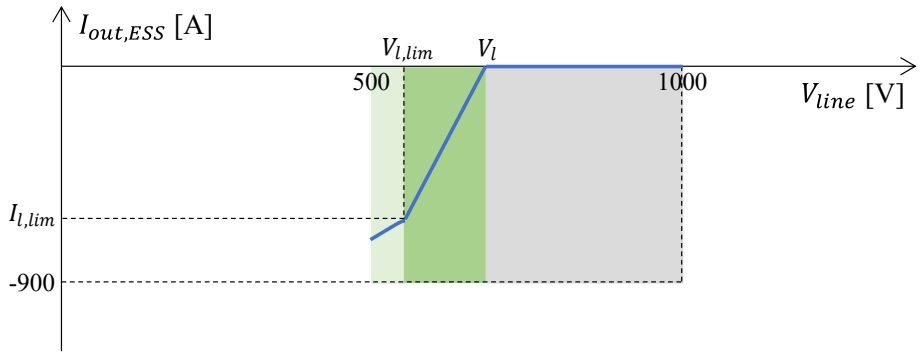

Figure 4-5 Battery control trans-characteristic when SOC is higher than 90%. Legend: idle state (grey); discharge state (green); limited discharging state (light green).

4.2 Simulation results without battery ESS

In paragraph 4.2.1 the voltage profile of FS Marconi-Trento Trieste is analyzed to determine its weak points regarding voltage drops, thus the best locations for battery ESS installation. An analysis of the voltage distribution at the battery connection point is then performed in 4.2.2 to determine the idle range of battery control that allows to have battery discharge when the catenary is overloaded and battery charge during the remaining part of the day.

4.2.1 Location of stationary battery ESS

To determine the best location of the stationary battery ESS, a 24 h simulation of the operation of the considered feeding section is performed. The best locations for battery ESS installation are the ones characterized by a voltage level outside of the admissible voltage range set by regulations ([500 1000] V). Looking at the minimum voltage profile represented in Figure 4-6 (black curve), the locations where the voltage is below 500 V (highlighted in yellow) are all possible candidates for battery installation.

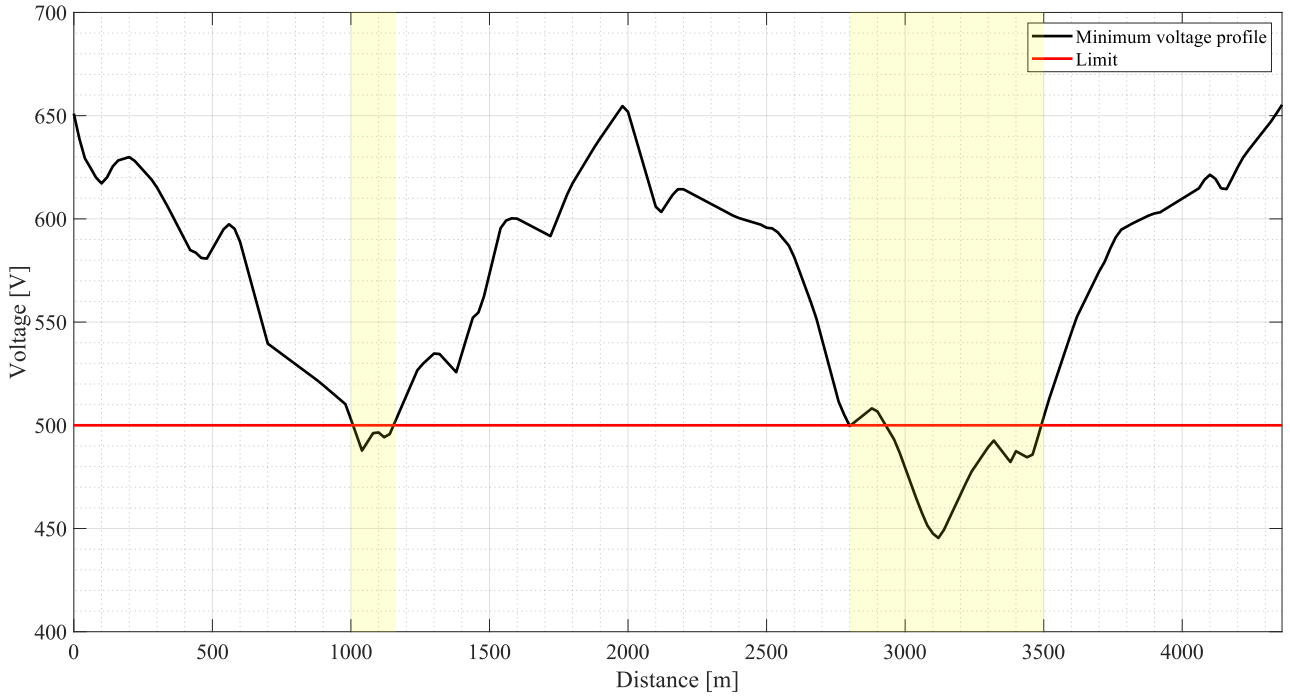

Figure 4-6 Minimum voltage profile along catenary without battery ESS during 24 h simulation.

From Figure 4-6 it can be deduced that it would be best to locate the battery in the ranges [1000 1200] m or [2800 3500] m, which correspond to the middle of the overhead bifilar lines in the outward and return journey respectively. However, the minimum voltage profile along the catenary is not the only factor that affects the choice of battery location: cost of installation and space availability must be considered too. The route of FS Marconi-Trento Trieste mostly takes place inside the medieval town, as it can be seen in Figure 4-7. Because of the limited available space inside the historic center, the ESS should be placed outside of the city walls. Therefore, excluding the parts of the catenary which lay within the city walls, the only remaining possible location for the ESS is at 2800 m, which corresponds to Porta San Vitale.

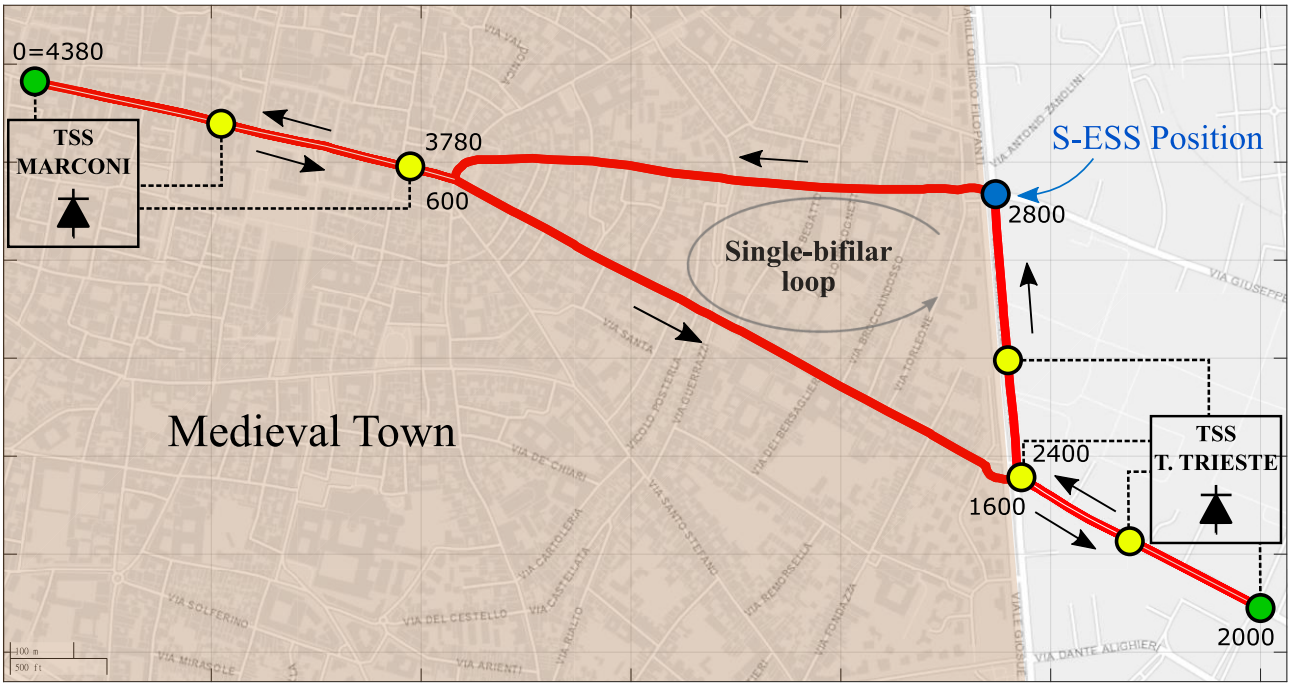

Figure 4-7 Route of FS Marconi-Trento Trieste and chosen location of stationary battery ESS.

4.2.2 Determination of battery control idle range

Once the location of the BESS has been determined, its control must be tuned to have discharge when there is the highest bus traffic (07:00 am-08:00 pm) and charge when the bus traffic is not as severe (08:00 pm-02:00 am) or during the night when buses do not circulate (02:00 am-05:00 am).

The tuning of the battery control is performed by analyzing the voltage distribution at the battery connection point when the battery is not connected. The battery objective is to support the traction substations during peak hours to improve the voltage profile of the catenary and decrease the losses. The battery should discharge in the period between 07:00 am and 08:00 pm because of the higher bus frequency that causes the deepest voltage drops. To make sure that on average the battery discharges in that period, the lower bound of the idle range is set to the mean value of the voltage distribution between 07:00 am and 08:00 pm. The voltage distribution at 2800 m between 07:00 am and 08:00 pm is depicted in Figure 4-8, where the mean value is indicated in black. Therefore, the lower bound of the idle range is set to 710 V.

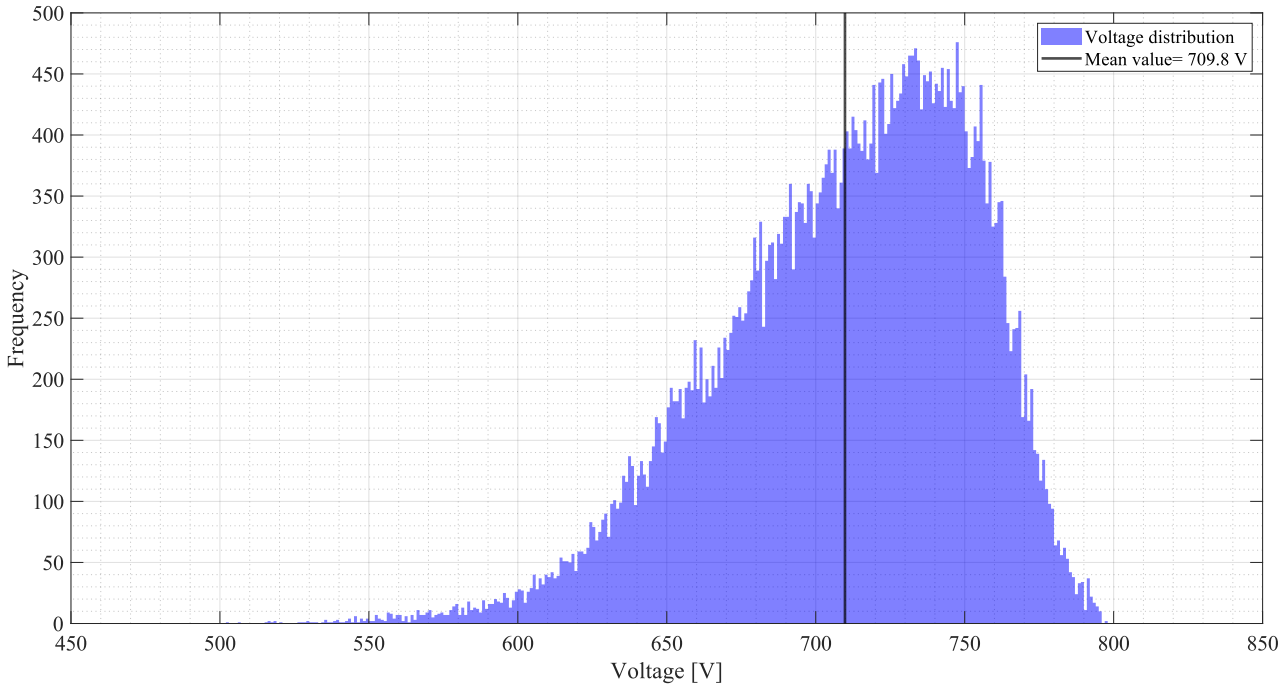

Figure 4-8 Voltage distribution at 2800 m without battery ESS between 07:00 am and 08:00 pm.

The upper bound of the idle range should be set to a voltage value that allows to have charging when the FS is not overloaded. Therefore, the upper bound of the idle range is set to the mean value of the voltage distribution at 2800 m in a 24 h simulation. Setting the upper bound to 740 V means that on average the battery charges half of the time during its daily operation.

4.3 Battery control for FS Marconi-Trento Trieste

Once the lower (V_l) and upper (V_u) bounds of the idle range are set to 710 V and 740 V, respectively, the battery control, expressed in its general form by equation (20), can be reformulated as follows:

$$\begin{cases} I_{out,ESS} = -2C\dfrac{V_{bat}}{V_{line}} & \text{if } 500 \le V_{line} < V_{l,lim} \quad mode = -2 \\ I_{out,ESS} = \dfrac{900}{210}(V_{line} - 710) & \text{if } V_{l,lim} \le V_{line} < 710 \quad mode = -1 \\ I_{out,ESS} = 0 & \text{if } 710 \le V_{line} \le 740 \quad mode = 0 \\ I_{out,ESS} = \dfrac{900}{260}(V_{line} - 740) & \text{if } 740 < V_{line} \le V_{u,lim} \quad mode = 1 \\ I_{out,ESS} = 2C\dfrac{V_{bat}}{V_{line}} & \text{if } V_{u,lim} < V_{line} \le 1000 \quad mode = 2 \end{cases} \tag{21}$$

The expressions of $V_{l,lim}$ and $V_{u,lim}$, which depend on the instantaneous value of the battery voltage and the battery capacity, are given by equations (22) and (23) respectively.

$$V_{l,lim} = 355 + \frac{1}{2}\sqrt{710^2 - \frac{1680}{900}CV_{bat}} \tag{22}$$

$$V_{u,lim} = 370 + \frac{1}{2}\sqrt{740^2 + \frac{2080}{900}CV_{bat}} \tag{23}$$

Therefore, the trans-characteristic of the battery control when battery SOC is within the admissible range ([10 90] %) for different battery capacities is depicted in Figure 4-9. In the simulation V_{bat} is set to the actual output voltage of the battery, which varies with its SOC level, while Figure 4-9 is plotted keeping the battery voltage constant and equal to 400 V for visualization proposes. If the battery capacity is higher than the one expressed by equation (24), the battery control trans-characteristic and the C-rate limitation curve do not intersect in the real domain. Therefore, the battery discharge is not limited by the C-rate.

$$C_{limit} \leq \frac{\frac{900}{210} \cdot 710^2}{8 \cdot 400} = 675 \text{ Ah} \tag{24}$$

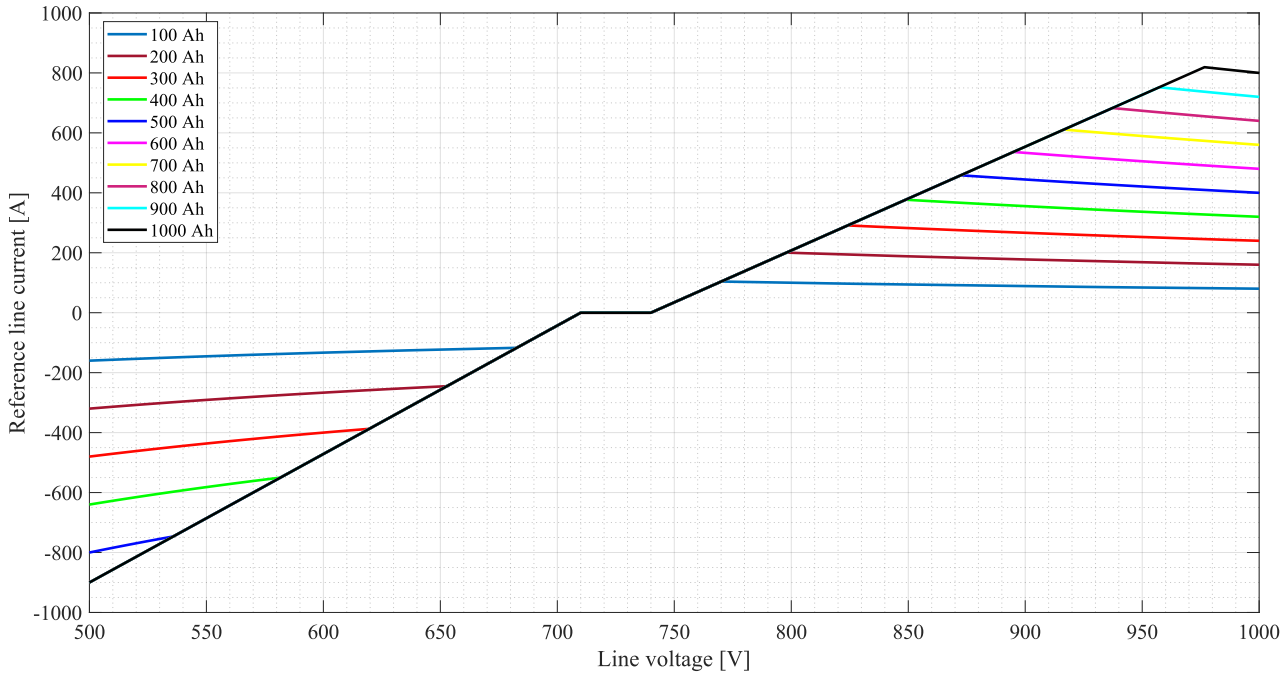

Figure 4-9 Battery control trans-characteristic for FS Marconi-Trento Trieste for different battery capacities and V_{bat} = 400 V when SOC is within 10 % and 90 %.

The trans-characteristics of the battery control when battery SOC is lower than 10 % and higher than 90 % are represented in Figure 4-10 and Figure 4-11 respectively.

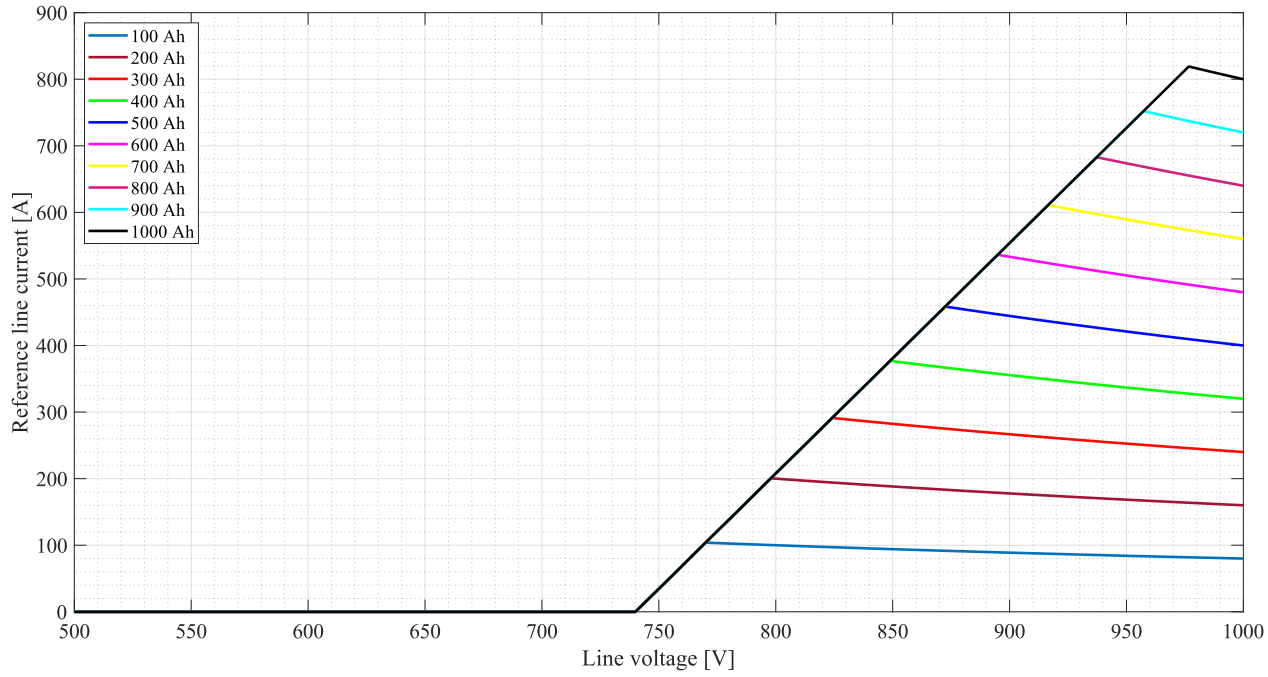

Figure 4-10 Battery control trans-characteristic for FS Marconi Trento Trieste for different battery capacities and V_{bat} = 400 V when SOC is lower than 10 %.

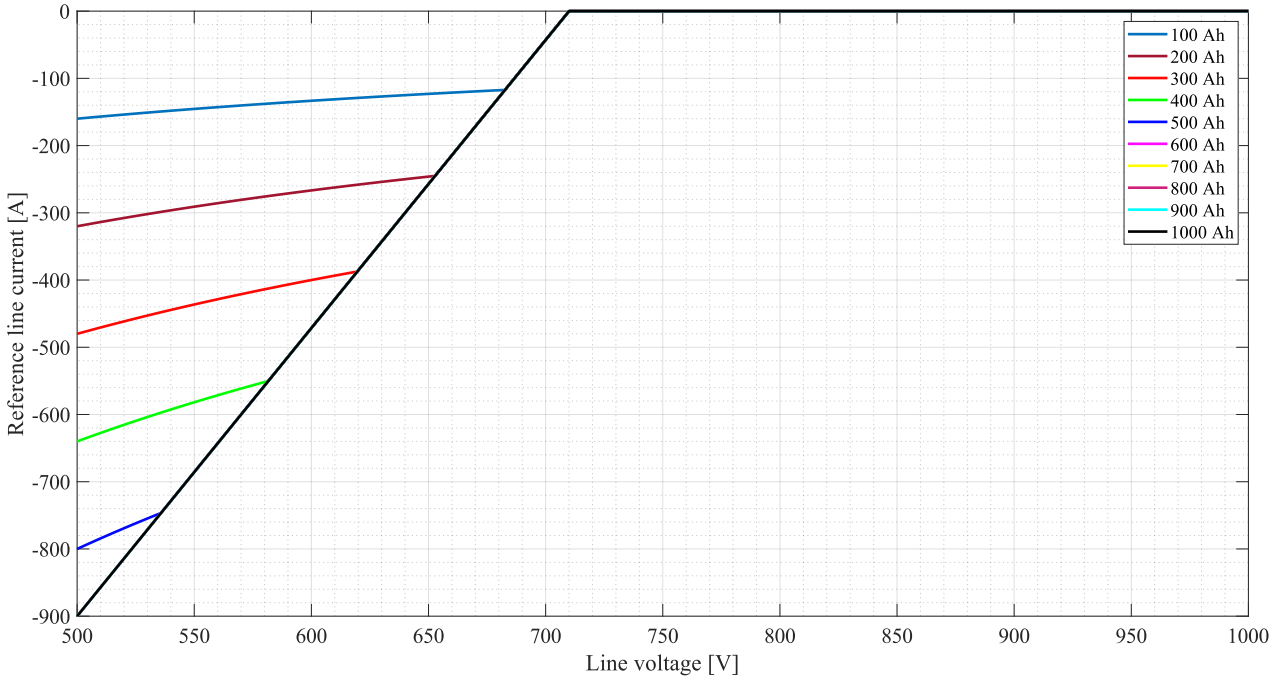

Figure 4-11 Battery control trans-characteristic for FS Marconi-Trento Trieste for different battery capacities and V_{bat} = 400 V when SOC is higher than 90 %.

4.4 Prediction of voltage distribution at the battery installation point

From the knowledge of the voltage distribution at 2800 m it is possible to predict the voltage distribution derived by the installation of a stationary BESS in the same position by intersecting the battery control trans-characteristic with the catenary load curve at each instant of the simulation.

According to the circuit theory, since the catenary is modelled using only resistors, and voltage and current generators it can be represented by its equivalent Thevenin circuit. Therefore, the load curve of the catenary can be easily derived from the equivalent Thevenin circuit (Figure 4-12) of the FS from the battery connection point (2800 m).

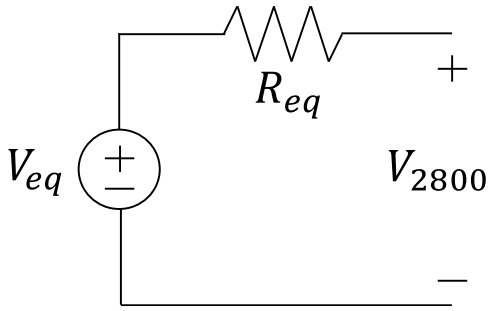

Figure 4-12 Equivalent Thevenin circuit of FS Marconi-Trento Trieste from battery connection point (2800 m).

To calculate the equivalent resistance of the Thevenin circuit (R_{eq}) the current generators, which represent the trolleybuses, are open-circuited, while the voltage generators, which represent the traction substations, are short-circuited. Therefore, the equivalent resistance of the catenary does not depend on the instantaneous number of trolleybuses connected to the FS, but only on the battery connection point. On the contrary, the Thevenin equivalent voltage (V_{eq}) is the open-circuit voltage at the battery connection point, which depends on the instantaneous number of trolleybuses connected to the FS and on their instantaneous current absorptions. The open-circuit voltage at the battery connection point can be easily derived from the simulation of the FS without battery extracting at every instant the voltage value at 2800 m.

The slope of the load curve at every instant of the simulation ($\Delta I/\Delta V$) corresponds to the equivalent Thevenin conductance (G_{eq}=1/R_{eq}). Since the equivalent Thevenin resistance depends only on the point from which the equivalent circuit is evaluated and the catenary resistance does not change in time, the load curve is characterized by a constant slope. It is obvious that the slope of the load curve increases as the battery connection point moves closer to the traction substation. This would explain why the installation of a battery ESS in proximity of the TSSs does not lead to any appreciable voltage improvement.
The Thevenin equivalent voltage generator action is to translate the load curve to the left or to the right according to the bus traffic in the feeding section.

The equivalent Thevenin conductance is derived directly from simulations of the FS without the battery ESS (25): V_{2800} is the voltage at the battery connection point when it is open-circuited

(Figure 4-13), while I_{norton} is evaluated short-circuiting the overhead bifilar line at the battery connection point (Figure 4-14) and measuring the current that flows through it.

$$G_{eq} = \frac{I_{norton}}{V_{2800}} \tag{25}$$

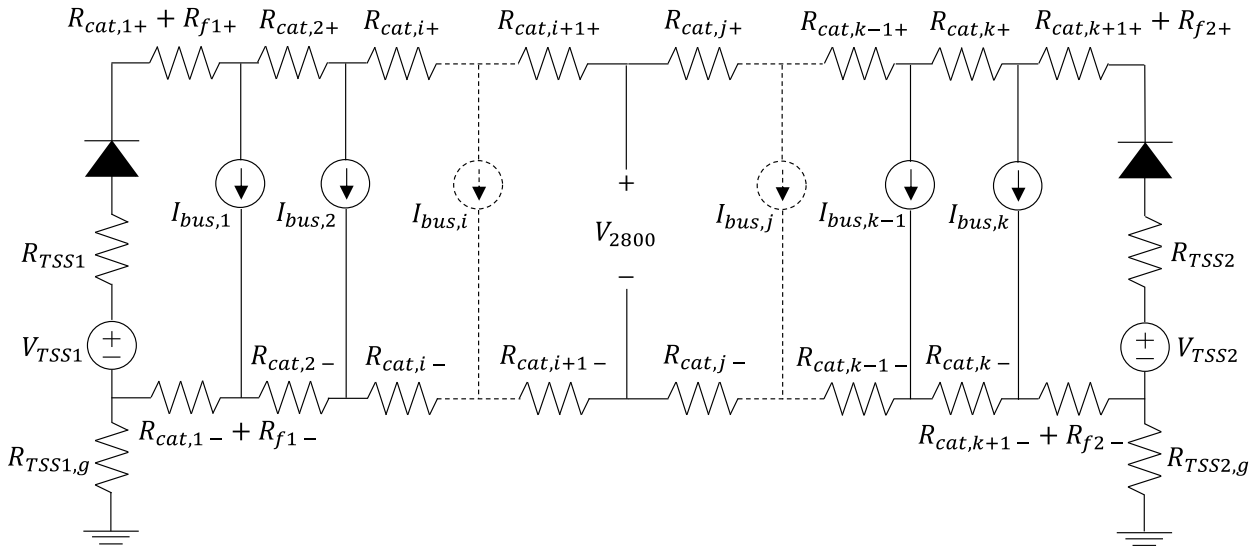

Figure 4-13 Simplified electric scheme of FS Marconi-Trento Trieste for the evaluation of V_{2800}.

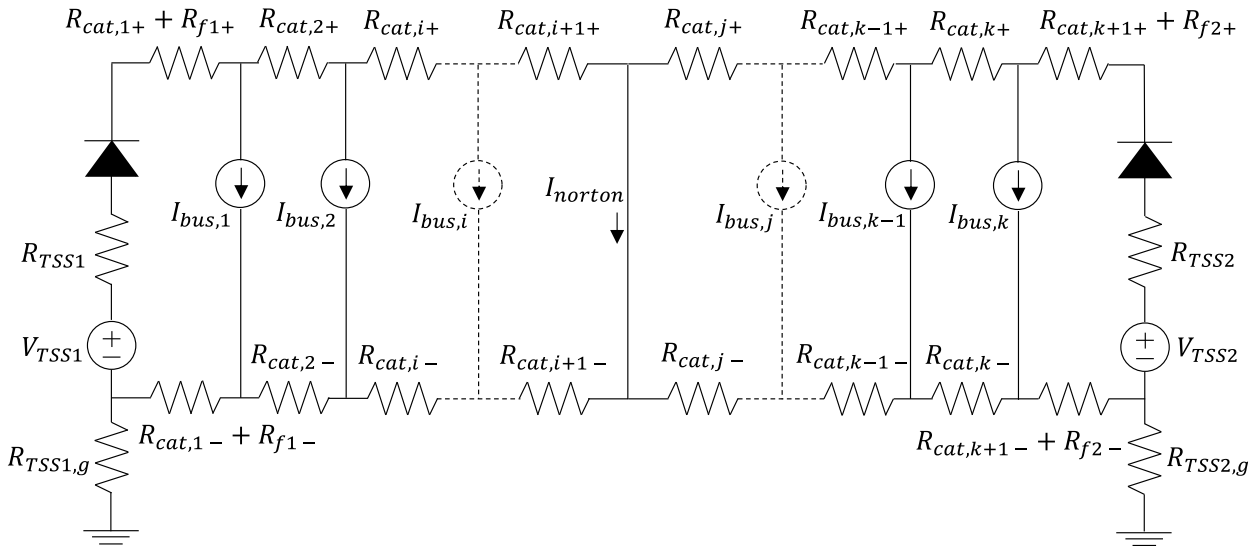

Figure 4-14 Simplified electric scheme of FS Marconi-Trento Trieste for the evaluation of I_{norton}.

Performing the aforementioned simulations, the equivalent conductance of the Thevenin circuit of FS Marconi-Trento Trieste seen from the battery connection point is 5.57 S.

The voltage distribution derived from the installation of a battery ESS of capacity *C* is predicted intersecting at every instant the battery control trans-characteristic, expressed by equation

(21), and the load curve of the catenary at 2800 m, expressed by equation (26), where G_{eq}= 5.57 S and $V_{eq} = V_{2800}$.

$$I_{line} = -G_{eq}(V_{line} - V_{eq}) \quad (26)$$

The prediction is based on the following assumptions:

1. the battery voltage is constant and equal to its nominal value (400 V);
2. the battery control and the catenary operate in sync (no delay between the two);
3. the battery is correctly sized (the SOC level is between 10 % and 90 % for the entire duration of the simulation).

Out of all these assumptions, the third one is probably the most unrealistic because it assumes that all battery capacities can sustain the FS operation and that their SOC level never goes above 90 % or below 10 %. As it is illustrated in paragraph 5, in reality the SOC level would exceed the SOC upper limit if there was no SOC limitation in the battery control and not all battery capacities are correctly sized (SOC level reaches 10 %).

For illustrative purposes, in Figure 4-15 it is depicted the battery control trans-characteristic for different values of battery capacity and the load curve of the FS at 03:00 am, 08:15 am and 09:00 am to show the battery control action.

At 08:15 am the line voltage at 2800 m is 532 V (left red dot), which lays in the battery discharge region of the battery control. The introduction of a battery ESS allows to move the working point toward the idle region, thus reducing the voltage drop. The higher the battery capacity, the better the improvement in the voltage drop. As it is clearly visible in Figure 4-15, the intersection between the load curve and the battery control trans-characteristic for battery capacities 100 Ah, 200 Ah, and 300 Ah occurs in the limited discharging region (output current limited by C-rate), so the working points are different (green dots). For battery capacities above 300 Ah, the working point (blue dot) is the same because the intersection happens in the normal discharging region. If the third assumption were to be true, this would mean that installing a battery ESS with the capacity higher than 400 Ah does not lead to any improvement of the voltage profile, but only to an increase of the cost.

At 09:00 am the line voltage at 2800 m is 730 V (middle red dot), which lays in the battery idle region, thus the introduction of the battery ESS does not affect the voltage level. Indeed, if the line voltage is within the range [710 740] V, the battery is inactive. Therefore, in the idle range the voltage distributions with and without the battery ESS should be the same.

At 03:00 am the line voltage at 2800 m is 799.6 V (right red dot), which lays in the charge region of the battery control. The introduction of a battery ESS leads to the translation of the working point to the left toward the idle region. As it is clearly visible in Figure 4-15, only the intersection between the load curve and the battery control trans-characteristic for the 100 Ah battery occurs in the limited charging region (output current limited by C-rate). Therefore, the 100 Ah battery has a different working point (green dot) with respect to the other battery capacities (blue dot), whose working point lays in the normal charging region. As it was said for the battery discharge, if the third assumption was true, this would mean that any battery capacity above 100 Ah leads to the same voltage improvement.

In general, the battery control action is to move the working point toward the idle region, thus concentrating the voltage values around the idle range (blue arrows).

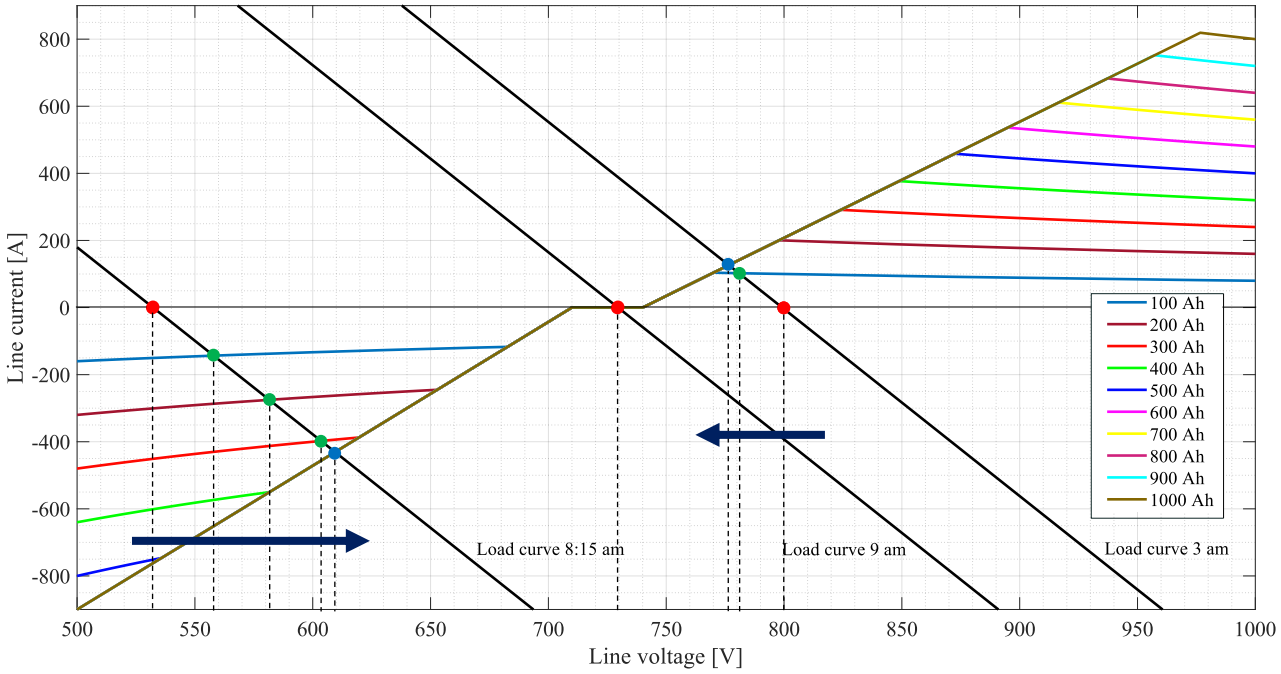

Figure 4-15 Load curves of FS at 2800 m at 03:00 am, 08:15 am, and 09:00 am, and battery control trans-characteristic for different values of the battery capacity.

Summarizing what was said for Figure 4-15, the introduction of the battery ESS should reduce the dispersion of the voltage distribution at battery connection point. If the battery operation is limited by the C-rate, the higher the battery capacity, the lower the voltage dispersion (Figure 4-16), while if it is not limited by the C-rate, any battery capacity leads to the same voltage distribution (Figure 4-17). Obviously, in reality the same voltage distributions can be obtained only in the event that the battery ESS is correctly sized (SOC always between 10 % and 90 %).

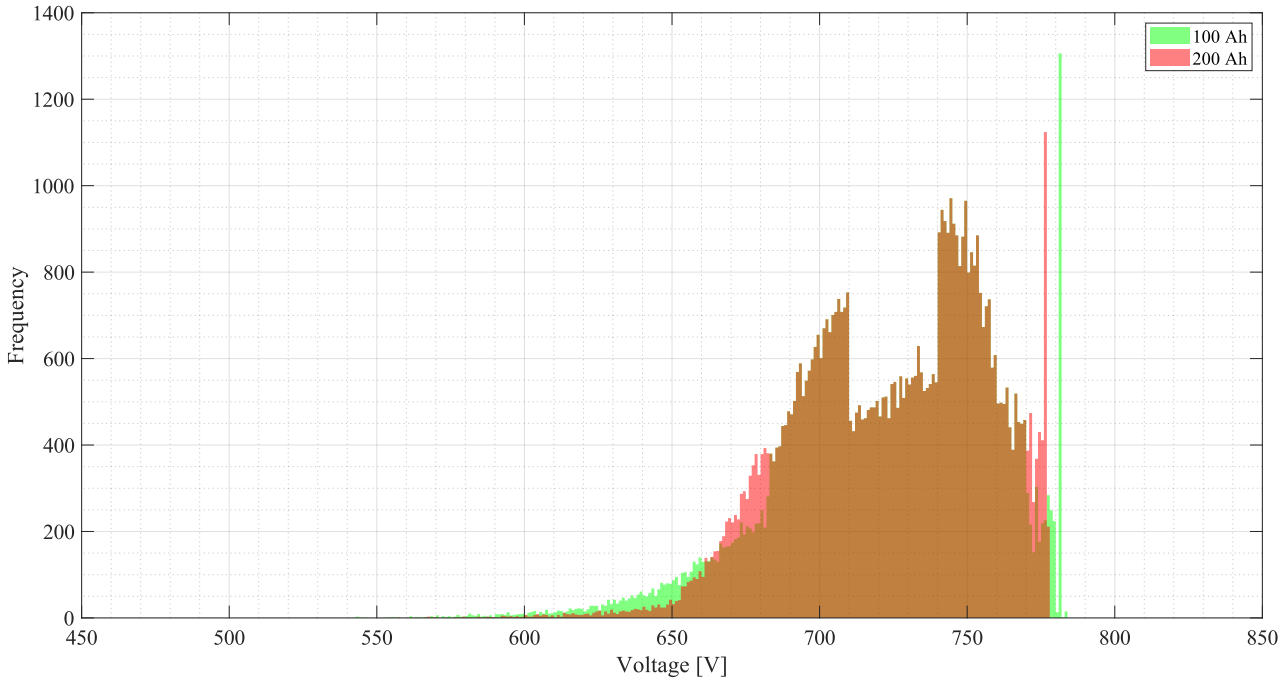

Figure 4-16 Comparison between predictions of voltage distribution at 2800 m with 100 Ah and 200 Ah battery between 06:00 am and midnight.

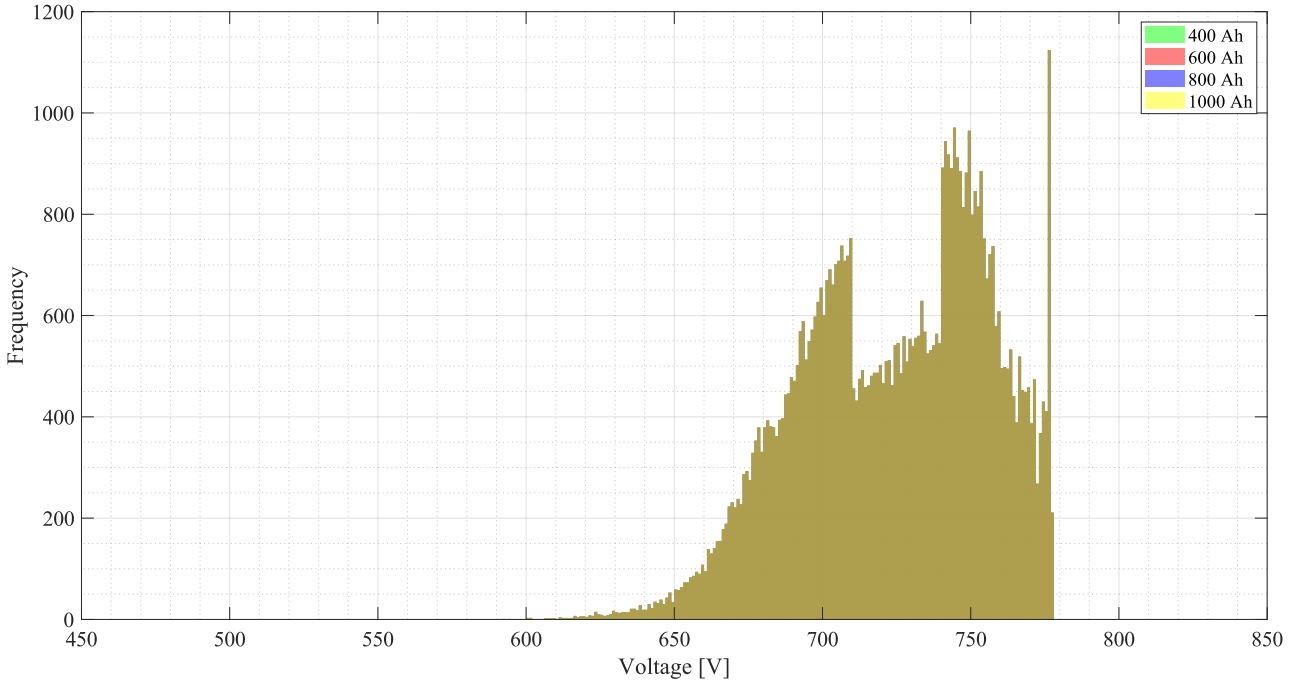

Figure 4-17 Comparison between predictions of voltage distribution at 2800 m with batteries ranging between 400 Ah and 100 Ah between 06:00 am and midnight.

Finally, in Figure 4-18 it is depicted the comparison between the predicted voltage distribution with an 800 Ah battery and the voltage distribution obtained from the simulation without the battery ESS in the interval between 08:00 am and 07:00 pm. As it was expected the voltage distributions in the idle range are the same.

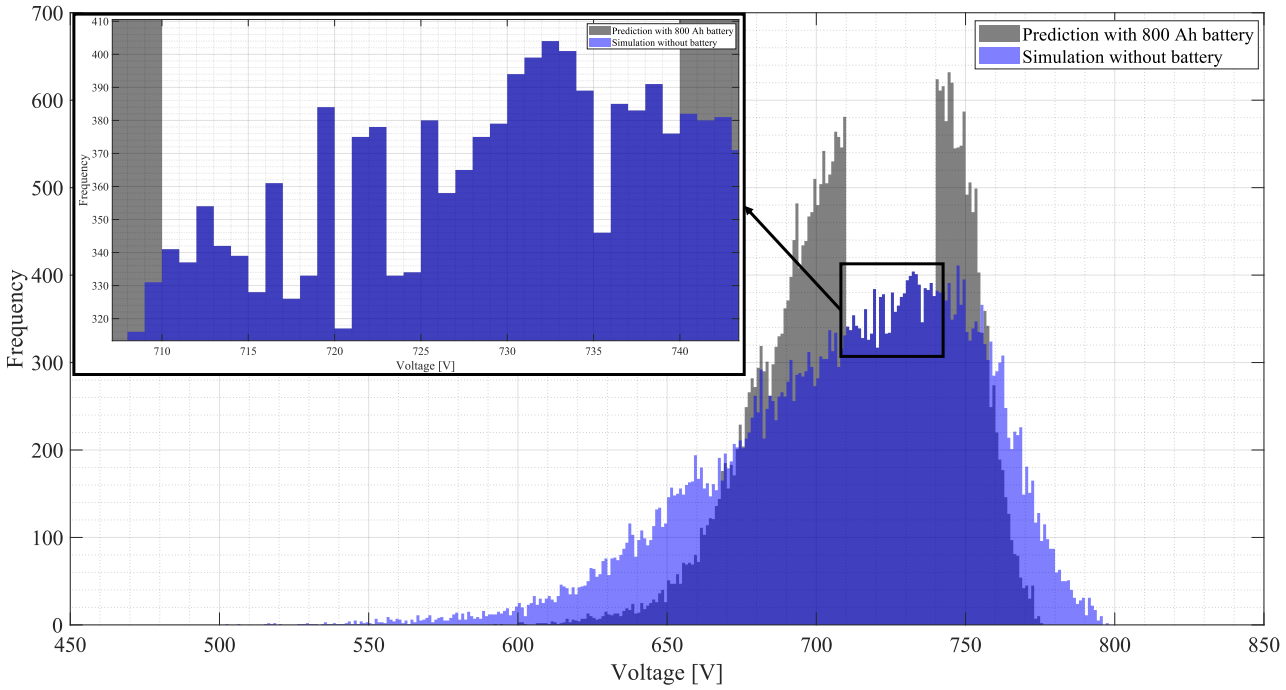

Figure 4-18 Comparison between the predicted voltage distribution with 800 Ah battery and the voltage distribution obtained from the simulation without the battery ESS in the interval between 08:00 am and 07:00 pm.

Being the output voltage of the TSSs set to the average output voltage of the 12-pulse rectifier (800 V) and the current absorption of the IMC trolleybuses always positive (regenerative breaking energy stored in the on-board battery), the catenary voltage is never higher than 800 V. Therefore, the battery control above 800 V remains un-used. To improve the battery control, the knowledge of the load curve could be used for the tuning of the slope of the battery control, which could be chosen according to the desired voltage distribution at battery connection point.

4.5 ESS modelling

The stationary battery energy storage system is composed by a battery storage system and a boost converter, which is used to step up the voltage from the battery (input) to the catenary (output).

The Battery block has been used to model the Lithium-ion battery in Simulink [38]. The temperature and aging (due to cycling) effects on the battery performance are disregarded in the analysis. The parameters of the Li-ion battery, that are independent on the battery capacity, are listed in Table 4-1.

Lithium-ion battery		
Parameter	**Value**	**Unit of measure**
Nominal voltage	400	V
Cut-off voltage	300	V
Fully charged voltage	465.6	V

Table 4-1 Lithium-ion battery parameters.

The boost converter electrical scheme is represented in Figure 4-19. However, it is not necessary to model the converter in such detail to evaluate the impact of the insertion of a stationary battery ESS in trolleybus networks. The implementation in Simulink of switches would indeed slow down the simulation (due to the necessary decrease of the simulation step) without providing any additional information. Therefore, the presence of a boost converter is implemented through a MATLAB function (29) that states the equality of its input and output power (27).

$$I_{in}V_{in} = I_{out}V_{out} \tag{27}$$

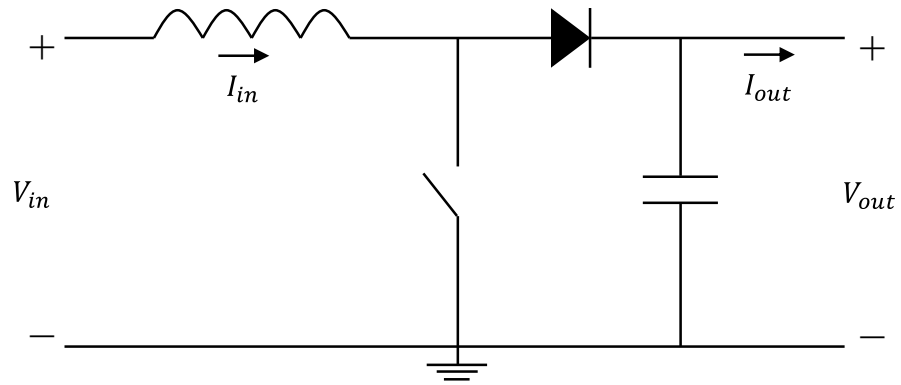

Figure 4-19 Boost converter electrical scheme.

Let's now analyze the model of the battery ESS represented in Figure 4-20:

i. Green circle: battery block;
ii. Yellow rounded square: output of battery block;
iii. Violet circle: controlled current sources that simulate the operation of the boost converter. The output current of the ESS is determined by the battery control (Figure 4-21), while the battery current is determined by the converter control (Figure 4-22);
iv. Light blue rounded squares: measurement blocks of the battery current and voltage, and of the battery ESS output current and voltage;

v. Red rounded square: resistors that simulate the feeders that connect the battery ESS to the catenary negative and positive poles.

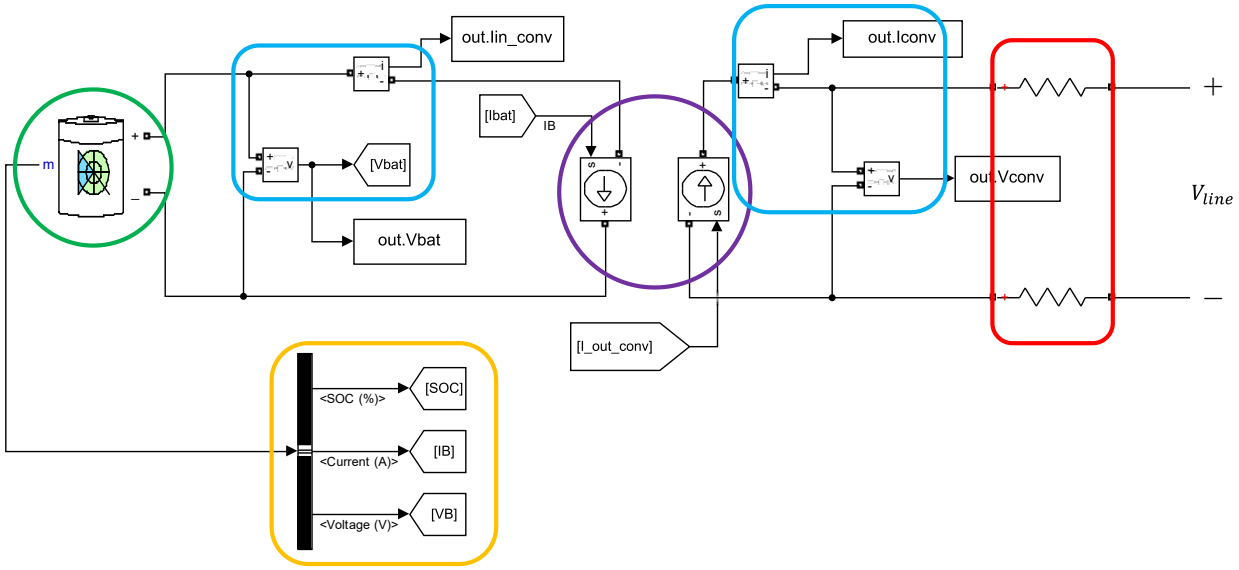

Figure 4-20 Simulink model of battery and converter.

The battery state (charge, discharge or idle) is determined by the battery control (Figure 4-21), which is implement using the MATLAB function, whose expression is given by equation (28).

$$[I_{ref}, mode] = \text{fcn}(V_{lmeas}, SOC, V_{bat}, capacity) \quad (28)$$

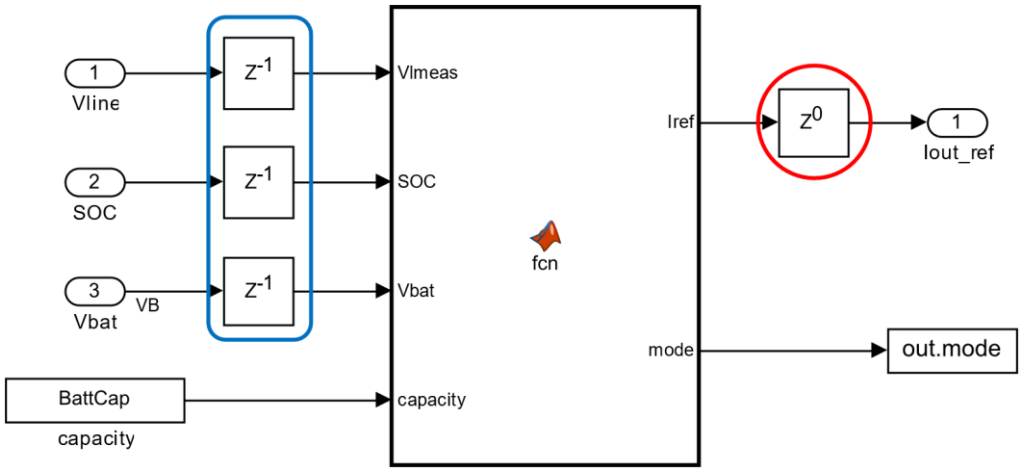

Figure 4-21 Battery control Simulink model.

The inputs of the battery control are the catenary voltage at the battery ESS connection point (V_{lmeas} [V]), the state of charge of the battery (SOC [%]), the battery voltage (V_{bat} [V]), and the maximum capacity of the battery storage ($capacity$ [Ah]), while the outputs of the control are the

reference output current of the battery ESS (I_{ref}[A]), and an indicator of the battery state ($mode$). The $mode$ is 0 when the battery is inactive, 1 and 2 when it is charging, and -1 and -2 when discharging. The difference between $mode$ 1 and 2, and $mode$ -1 and -2 is explained in paragraph 0. The code of MATLAB function (28) is provided in paragraph 4.6 for the considered feeding section.

The battery current is determined by the converter control (Figure 4-22), which is implemented using the MATLAB function, whose expression is given by equation (29).

$$[I_{bat}] = \text{fcn}(I_{out}, V_{line}, V_{bat}) \tag{29}$$

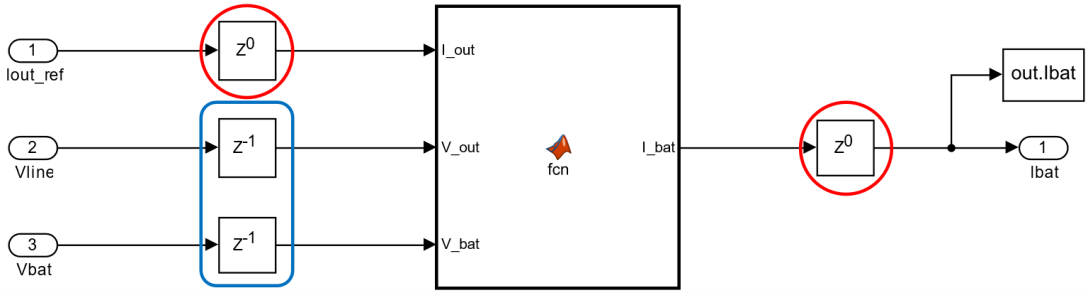

Figure 4-22 Converter control Simulink model.

The inputs of the converter control are the output current of the battery ESS (I_{out} [A]), the catenary voltage at battery ESS connection point (V_{line} [V]), and the battery voltage (V_{bat} [V]). The code of MATLAB function (29) can be found hereafter.

```
function I_bat = fcn(I_out, V_out, V_bat)

I_bat= (I_out*V_out)/V_bat;
```

The battery control and the catenary are supposed to work in real-time, but to break logic loops, the operation of the battery ESS is delayed by 1 simulation step with respect to the trolleybus network operation (bus schedule). The higher the simulation step, the more the simulation results differ from the actual battery operation. The delay is implemented using the delay blocks circled with the blue rounded squares in Figure 4-21 and Figure 4-22. The blocks circled in red in the same figures perform the initialization to zero of the input and output current of the converter, while the delay blocks initialize V_{bat} and V_{line} to their nominal value (400 V and 750 V, respectively), and *SOC* to its initial value.

4.6 Simulink model of FS Marconi-Trento Trieste with battery

In Figure 4-23 it is depicted the Simulink model of feeding section Marconi-Trento Trieste with the battery ESS installed at position 2800. The battery ESS is connected to the catenary through two 20 m long feeders (one per pole) composed by 1 cable of 240 mm^2 section. The resistance of these feeders can be computed applying equation (9) and it is equal to 2.06 mΩ.

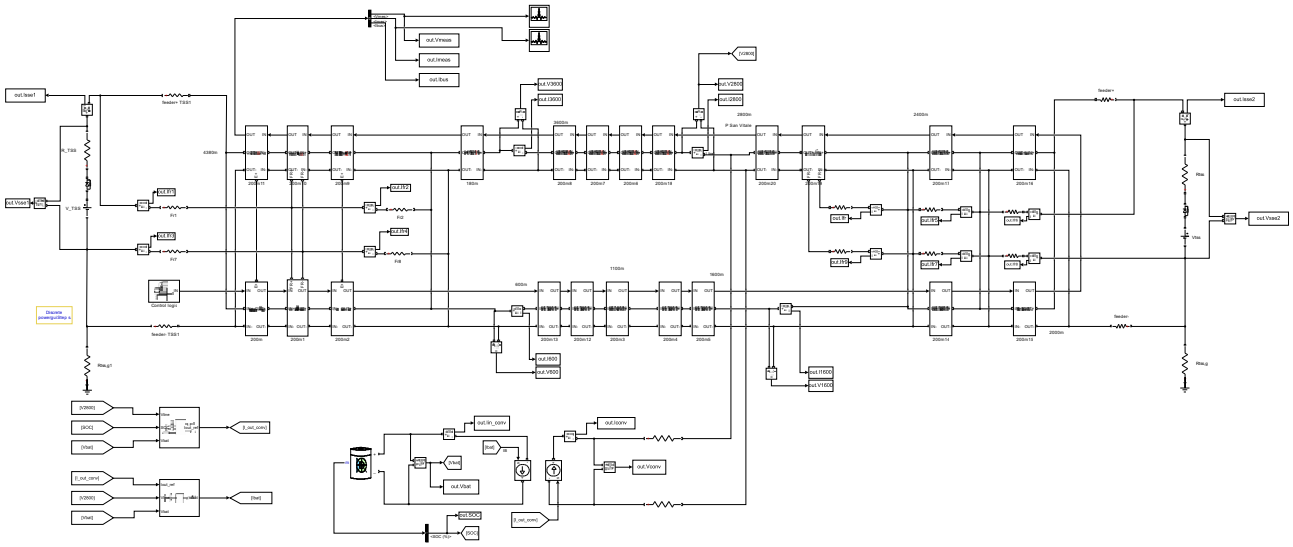

Figure 4-23 Simulink model of FS Marconi-Trento Trieste with battery ESS connected at 2800 m.

The code of MATLAB function (28), which implements the battery control introduced in paragraph 4.1, can be found in the Appendix.

5 Simulation results with battery ESS

The simulation results presented in this chapter are meant to show the impact that the installation of a battery ESS has on the FS operation. Firstly, in paragraph 5.1 the capacity of the BESS is chosen accordingly to the energy demand of the trolleybuses between 07:00 am-08:00 pm. Then, in paragraph 5.2 the voltage distribution at BESS connection point is compared with the voltage distribution obtained in the simulation without battery and with the prediction. Paragraph 5.3 shows the improvement in the voltage profile along the catenary due to the BESS installation at peak hours, while the current profile along the catenary is analyzed in paragraph 5.4. In paragraph 5.5 the correct operation of the C-rate limitation implemented by the battery control is proven. In paragraph 5.6 some information about the energy saved from the installation of the BESS is provided. Finally, paragraph 5.7 lists proposed forthcoming developments.

5.1 Choice of battery capacity

Once the idle range of the battery control has been chosen ([710 740] V), the Simulink model with the battery ESS connected at 2800 m is run to determine which is the suitable size of the battery pack that allows to improve the catenary operation. Figure 5-1 shows the SOC profiles for battery capacities varying between 100 Ah and 1000 Ah in a 24 h simulation (from 00:00 am to 11:59 pm). The initial SOC is initially set to 50 % to be able to observe one entire cycle of charging and discharging. As it is clearly visible in the figure, the battery SOC is kept in the range [10 90] % by the battery control.

As has been mentioned in paragraph 2.3.2, the trolleybus frequency is much higher in the interval between 07:00 am and 08:00 pm, which leads to deeper voltage drops that activate the battery discharge. In the remaing part of the day, the bus traffic is low enough to activate the battery re-charge, that leads to the lowering of the voltage profile with respect to the case without battery ESS. According to the voltage level at BESS connection point, the battery control determines the output current that better improves the overall voltage profile of the catenary.

Looking at the SOC profiles in Figure 5-1, it can be deduced that the highest battery discharging current occur in the periods 07:00 am-10:00 am, 02:00 pm-03:00 pm and, 05:00 pm-08:00 pm when the bus traffic is the highest (end and beginning of working and school day). Indeed, these discharging currents lead to an abrupt decrease of the battery SOC level. Between

08:00 pm and 01:00 am, the bus frequency is low enough to allow the re-charge of the battery, which is completed during night time when the trolleybuses do not travel.

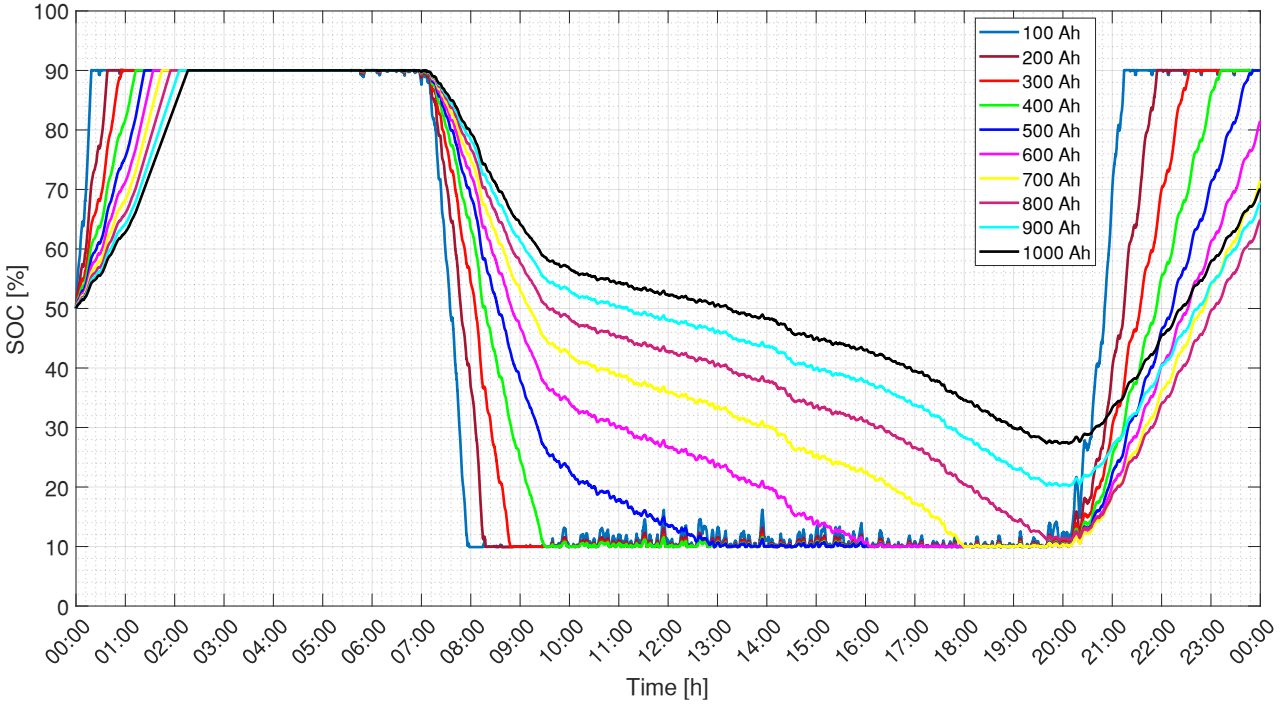

Figure 5-1 SOC profiles for different battery sizes in 24 h simulation.

Looking at the SOC profile curves it is also possible to determine the most suitable battery capacity for the application. It is important to rememeber that once the battery is complitely discharged (10 % SOC level), the battery control keeps it inactive until the bus frequency is low enough to allow its re-charge to preserve the battery integrity. However, while the batteries are inactive, the catenary voltage profile remains as if the battery ESS was never installed (see grey area in Figure 5-2). The only way to sustain the traction substations operation for the whole day is to install a battery ESS of capacity higher than 700 Ah because batteries from 100 Ah to 700 Ah reach 10 % SOC level before 08:00 pm.

The green and red areas in Figure 5-2 highlight the behaviour of the voltage at 2800 m during the discharging and charging process, respectively. As expected, during the battery discharge the voltage level at BESS connection point is higher than when no battery is installed. In the same way, during the re-charge the voltage level is lower because the current circulating in the catenary is higher.

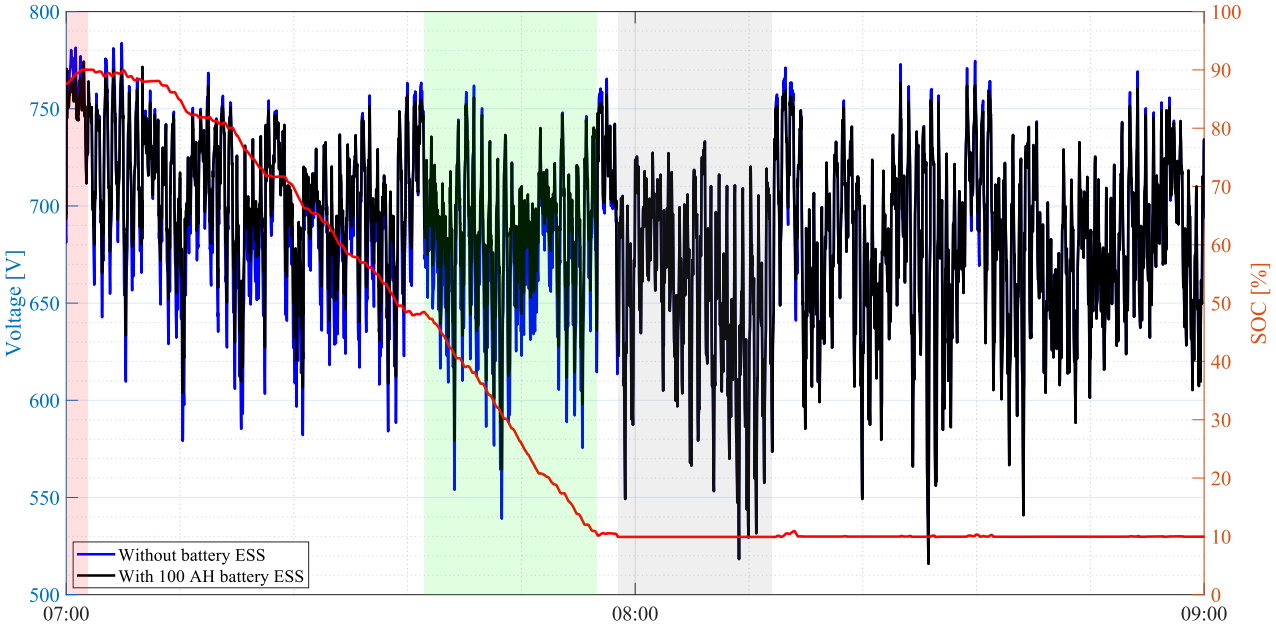

Figure 5-2 Voltage at 2800 m with and without 100 Ah battery ESS and SOC profile between 07:00 am and 09:00 am. Legend: charge mode (red area); discharge mode (green area); idle mode (grey area).

Due to limited space availability the most suitable battery capacity for the application is 800 Ah, which not only occupies a lower volume with respect to higher capacity batteries but is also less expensive. In Figure 5-3 the SOC profiles of 700 Ah, 800 Ah and 900 Ah batteries are illustrated to highlight the under-sizing of the first (SOC reaches 10% at 06:00 pm) and the oversizing of the last (20% SOC at 08:00 pm). In conclusion, the analysis of the impact of the installation of a battery ESS in the FS Marconi-Trento Trieste is done considering a battery capacity of 800 Ah.

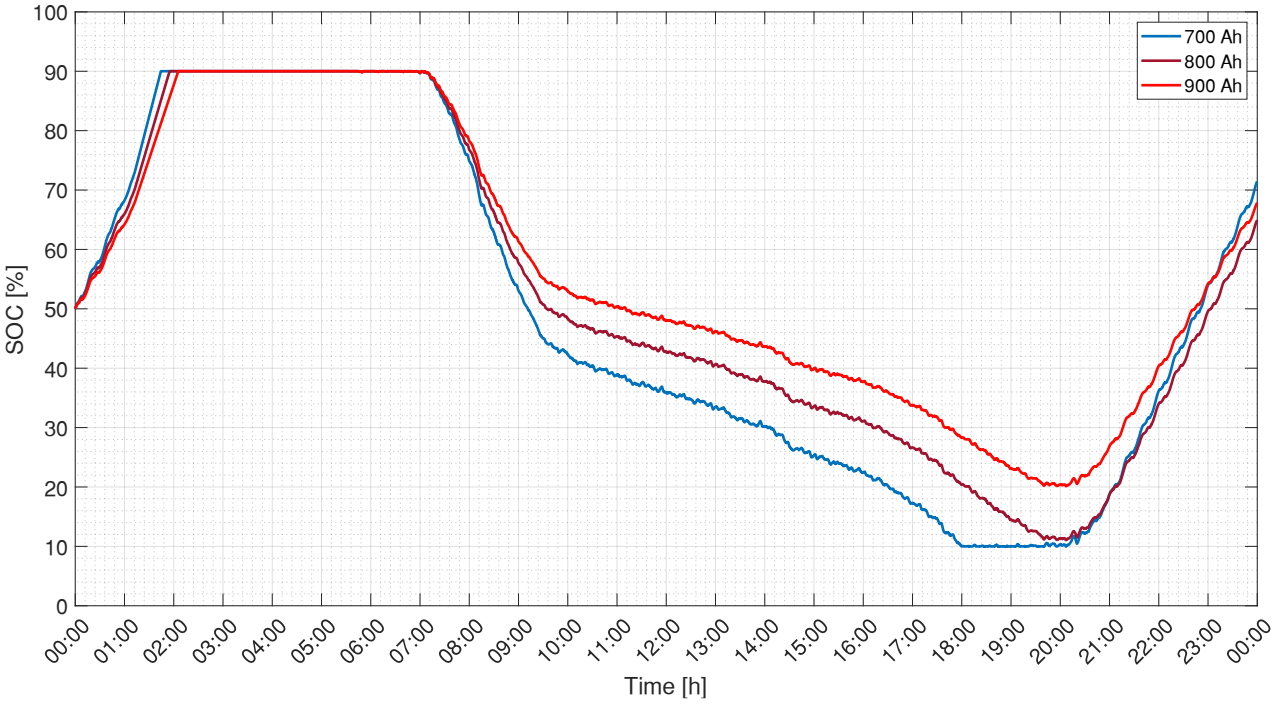

Figure 5-3 SOC profiles of 700 Ah, 800 Ah and 900 Ah batteries in 24 h simulation.

Setting the initial SOC equal to the final SOC (65 %) allows to determine the improvement in terms of grid energy absorption and Joule losses.

5.2 Impact of battery installation on voltage distribution at 2800

In this paragraph, the voltage distributions at battery connection point (2800 m) obtained through the simulations with and without battery are compared. Furthermore, the simulation with the battery ESS is used to validate the analytical results obtained in paragraph 4.4.

Figure 5-4 compares the voltage distributions at 2800 m for the discharging process (07:00 am-08:00 pm) obtained when the battery ESS is connected or not. As expected, the voltage distribution gets narrower when the battery is connected (more concentrated around the idle range), and the mean value is higher (715.5 V with respect to 710 V without the battery). It is possible to demonstrate that the battery control is working by the observation of the voltage distributions in the idle range ([710 740] V). When the voltage level of the catenary is within the idle range of the battery control, the battery is inactive, so the battery does not give any contribution to the voltage profile. Therefore, the voltage distributions with and without battery ESS should overlap in the range [710 740] V. The line plots in Figure 5-4 represent the Kernel probability distributions fitted to the acquired data for the case with (red line) and without (blue line) battery ESS.

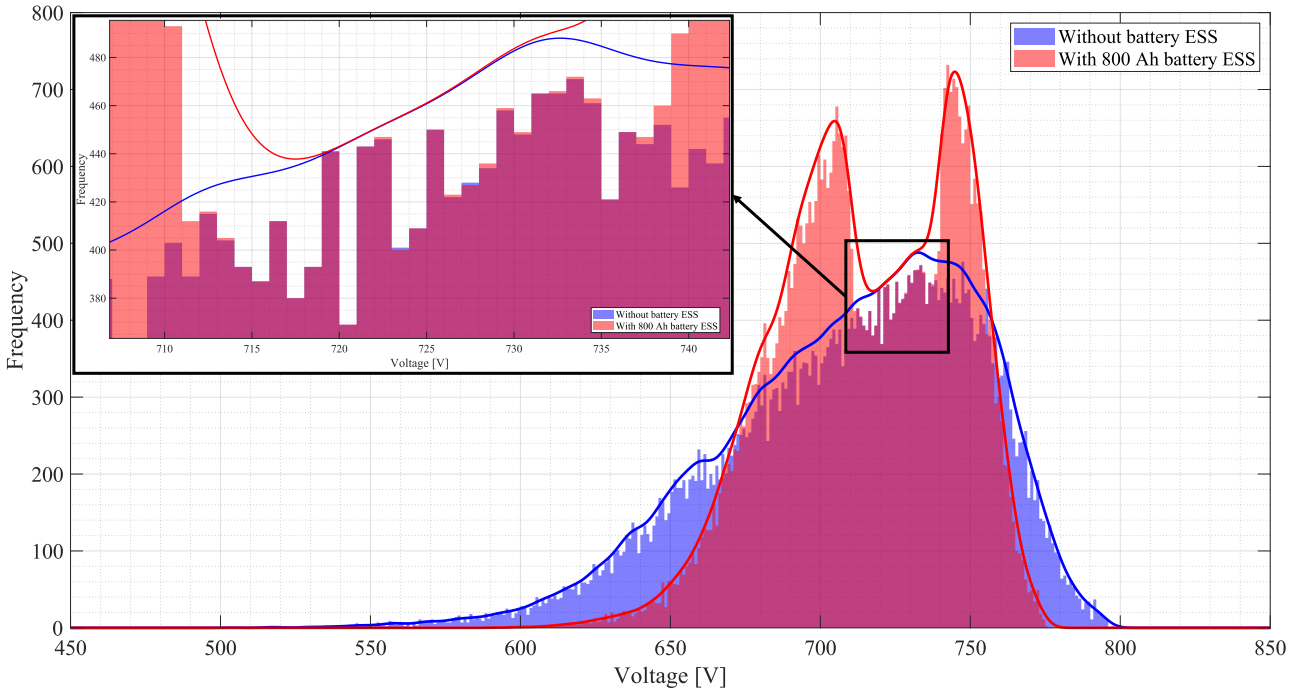

Figure 5-4 Voltage distribution at 2800 m with and without battery ESS between 07:00 am and 08:00 pm.

Looking at the close-up of the idle range in Figure 5-4, it is visible that the histogram bars are almost overlapping and that they differ the most closely to the upper and lower limits of the idle range. This difference can be explained reminiscing that in the simulation the battery control does not work in synchronism with the catenary operation to avoid logic loops. The 1 simulation step delay of the battery control with respect to the catenary is the reason why the two distributions do not perfectly overlap: the battery control determines the battery ESS output current based on the voltage level at 2800 m in the previous instant. The higher the simulation step, the bigger the difference between the voltage levels at two subsequent simulation instants and the greater the error performed by the battery control on the decision of the battery ESS output current. Decreasing the simulation step the difference between the two distributions would become non-existent, but the simulation time would be too high. In Figure 5-5 it is illustrated how decreasing the simulation step from 1 s to 0.1 s decreases the error in the discrepancy between the voltage distributions with and without the BESS in the idle range.

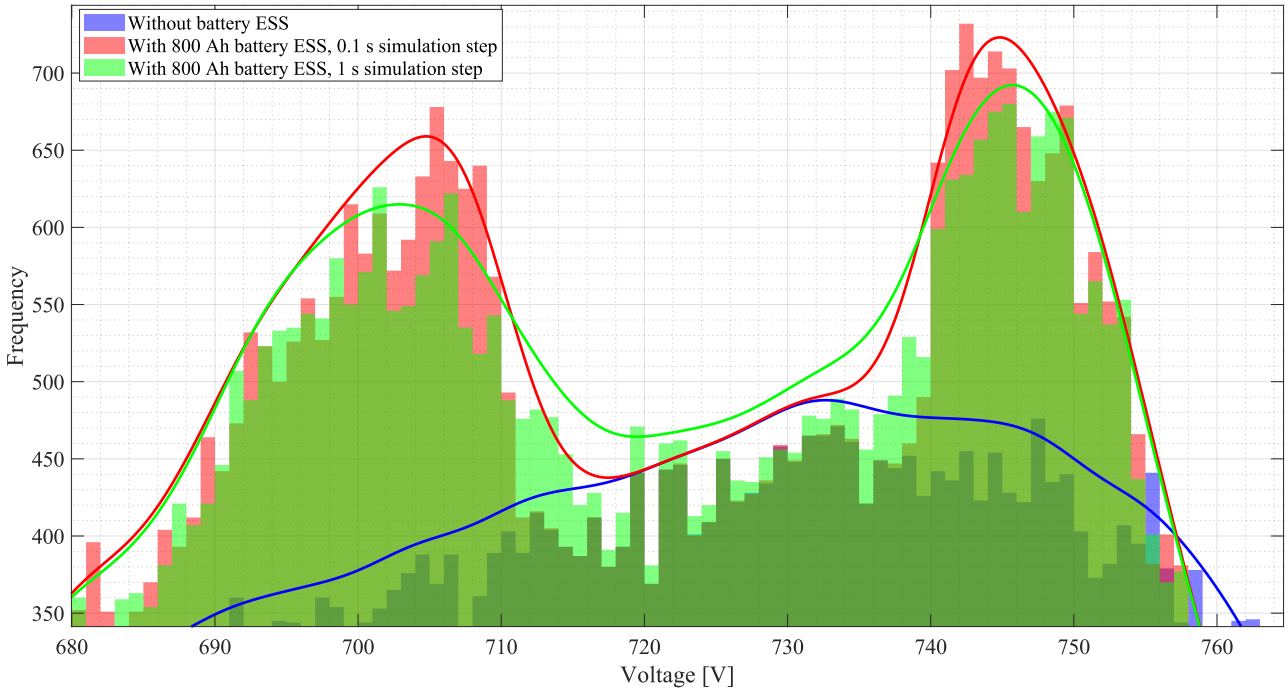

Figure 5-5 Close-up of voltage distributions at 2800 m around idle range in 07:00 am-08:00 pm simulation.

The fact that the battery control bases the decision of the output current on the previous voltage level of the catenary leads to an error also in the distribution close to the idle range: the battery control is not able to correctly identify when the battery should be in idle mode or not. This affirmation can be verified comparing the simulations results obtained with 0.1 s and 1s simulations steps with the prediction of the voltage distribution formulated in paragraph 4.4 where the battery and the catenary are assumed to operate in sync. Figure 5-6 clearly shows how decreasing the simulation step, the probability distributions derived from the simulations' results (green and red lines) get closer to the predicted one (black line). It is safe to assume that if the simulation step tended to zero, then the error would tend to zero too.

It should also be noted that while the prediction assumes that the battery voltage is constant and equal to 400 V, the battery control implemented in the model uses the real battery voltage measured at the battery output. Therefore, part of the reasons of the not perfect overlap can be attributed to the use of the wrong battery voltage level in the building of the prediction.

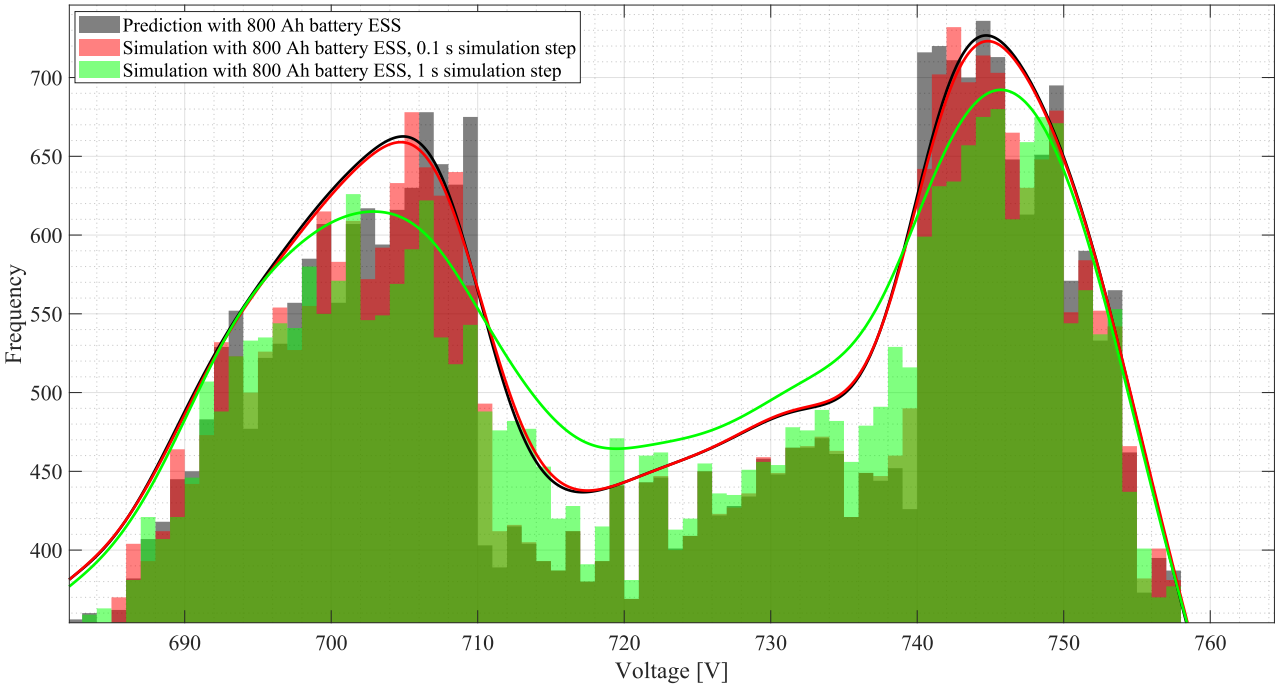

Figure 5-6 Comparison between prediction and simulations with 800 Ah battery ESS (0.1 s and 1 s simulation step) between 07:00 am and 08:00 pm.

Finally, it should be recalled that the prediction is formulated assuming that the battery SOC is always within the range [10 90] %. Looking at Figure 5-2 it is clear that the SOC level of all battery sizes is limited to 90 % between 02:00 am and 07:00 am by the battery control. Therefore, to avoid coming to the wrong conclusions, the comparison between the prediction and the simulations with and without battery ESS should be performed in a range where the assumption is true. Figure 5-7 demonstrates the validity of the prediction. In Figure 5-7 it is also possible to see how the charging of the BESS decreases the voltage level at the connection point. Indeed, while the voltage level at 2800 m without the battery ESS ranges between 550 V and 800 V, the one with the battery ESS does not overcome 780 V.

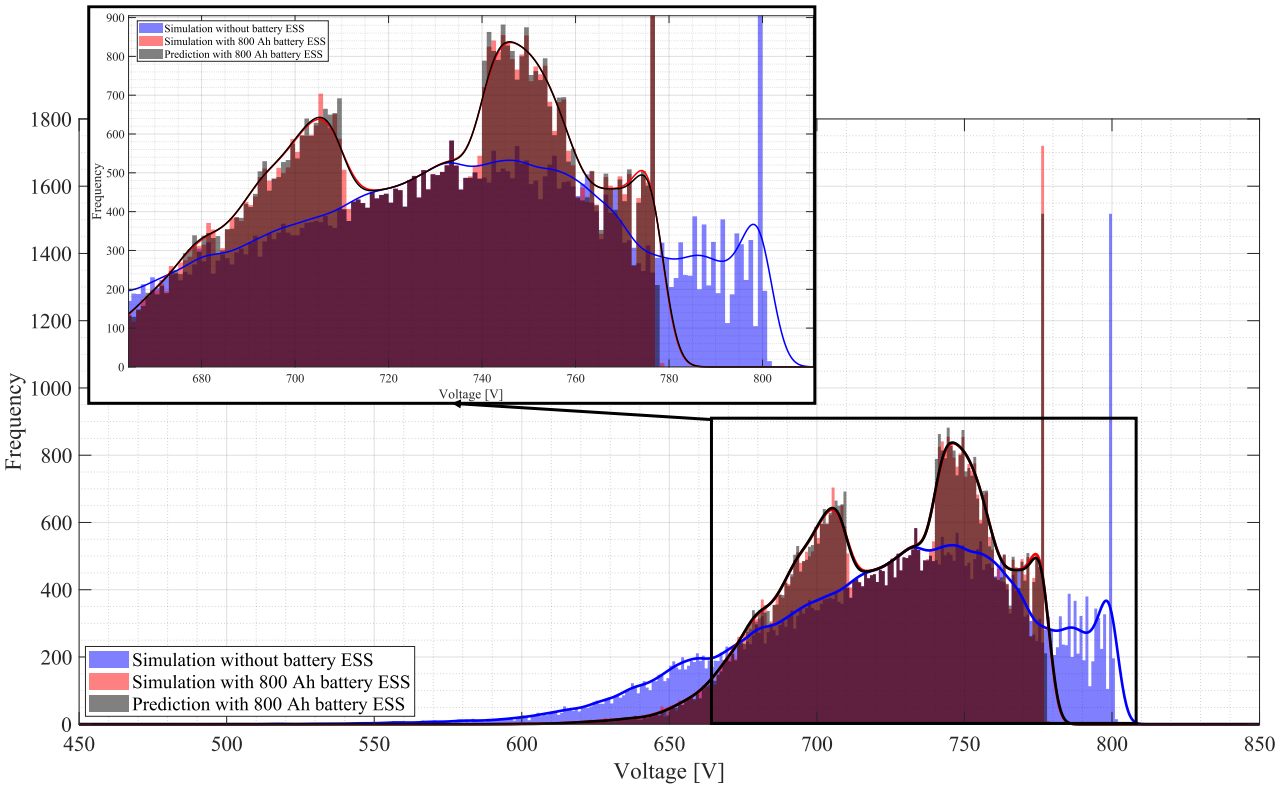

Figure 5-7 Comparison between voltage distributions at 2800 m obtained through prediction and simulations with and without 800 ah battery ESS between 08:00 am and 11:59 pm.

5.3 Impact of battery installation on catenary voltage profile

First of all, it is worth remembering that FS Marconi-Trento Trieste has a total length of 4380 m, and that position 0 and 4380 correspond to TSS Marconi, while position 2000 corresponds to TSS Trento Trieste. The voltage of the FS is acquired every 20 m ("T block" length) with 1 Hz frequency (1 value is saved every 10 simulation steps).

The voltage profiles along the catenary for an entire day simulation, between 07:00 am and 08:00 pm (when BESS discharges) and between 08:00 pm and 02:00 am (when BESS charges) are illustrated in Figure 5-8, Figure 5-9 and Figure 5-10 ,respectively. All blue plots refer to the simulation without battery, while the red ones refer to the simulation with battery. The coloured areas in all these figures represent the 95 % central inter-percentile range of voltage values, that is the voltage interval characterized by a probability between 2.5 % and 97.5 % to occur. In simple terms, the coloured areas represent the voltage values that have a 95 % cumulative probability to occur in the simulated period. The dashed lines represent the minimum and maximum voltage profiles along the catenary, while the solid lines represent the mean voltage profiles.

From Figure 5-8 and Figure 5-9, it is possible to observe that the mean voltage profiles with and without BESS are almost overlapping in a 24 h simulation, while it is higher (0.80% above at the battery connection point) in the scenario with BESS for the 07:00 am-08:00 pm simulation. However, the real advantage of the installation of a battery ESS can be acknowledged looking at the 95 % central inter-percentile range (coloured areas), which represents the dispersion of the results around the mean value at every point (multiples of 20 m) along the catenary. The introduction of the BESS allows to reduce the dispersion of the catenary voltage, thus allowing a future increment of the trolleybus traffic. The width of the 95 % central inter-percentile range during the 24 h simulation and in the 07:00 am-08:00 pm simulation is indeed reduced by 20 % and 30 % at the BESS connection point, respectively. Furthermore, the introduction of the BESS allows to increase the minimum voltage profile making sure that the voltage level is always within the admissible range set by regulations ([500 1000] V) to allow the un-restrained operation of the trolleybuses.

As expected, Figure 5-10 shows that the mean voltage profile of the catenary while the battery charges is lower than the one without the battery ESS (1.3 % below at the battery connection point). The minimum voltage profile without BESS is lower than the one with BESS. This occurrence can be explained looking at the SOC profile in the period between 08:00 pm and 11:59 pm. Even though the battery ESS is mostly charging in this period, the traffic conditions in some moments are such that they activate the battery discharge (SOC level decreases). The minimum voltage profile obtained from the simulation without BESS refers to one of these moments. During the battery discharge the current supplied by the traction substations is lower than in the scenario without battery, thus the voltage drops are reduced. Furthermore, the minimum voltage level at battery connection point (2800 m) obtained after the BESS installation is clearly higher than the one without BESS, as Figure 5-7 demonstrates.

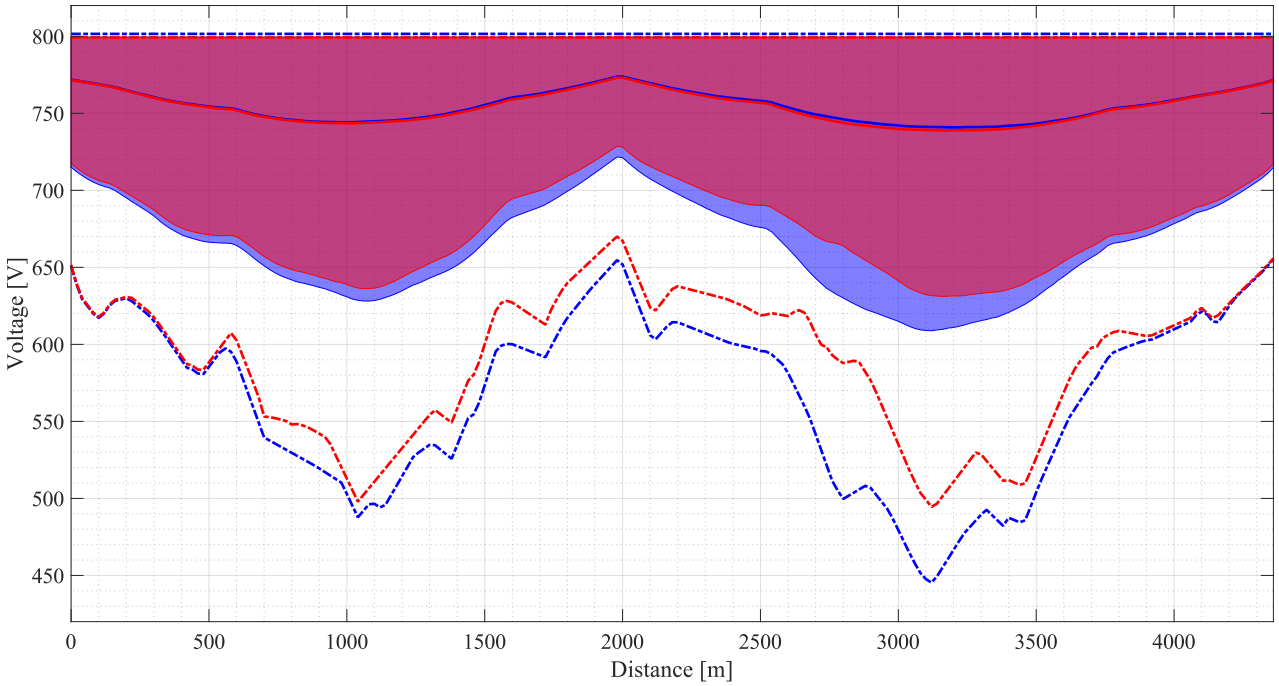

Figure 5-8 Comparison between voltage profiles with (red) and without (blue) 800 Ah BESS along the catenary during 24 h simulation. Legend: Minimum and Maximum voltage profiles (dashed lines); Mean voltage profiles (solid lines); 95 % central inter-percentile range (coloured area).

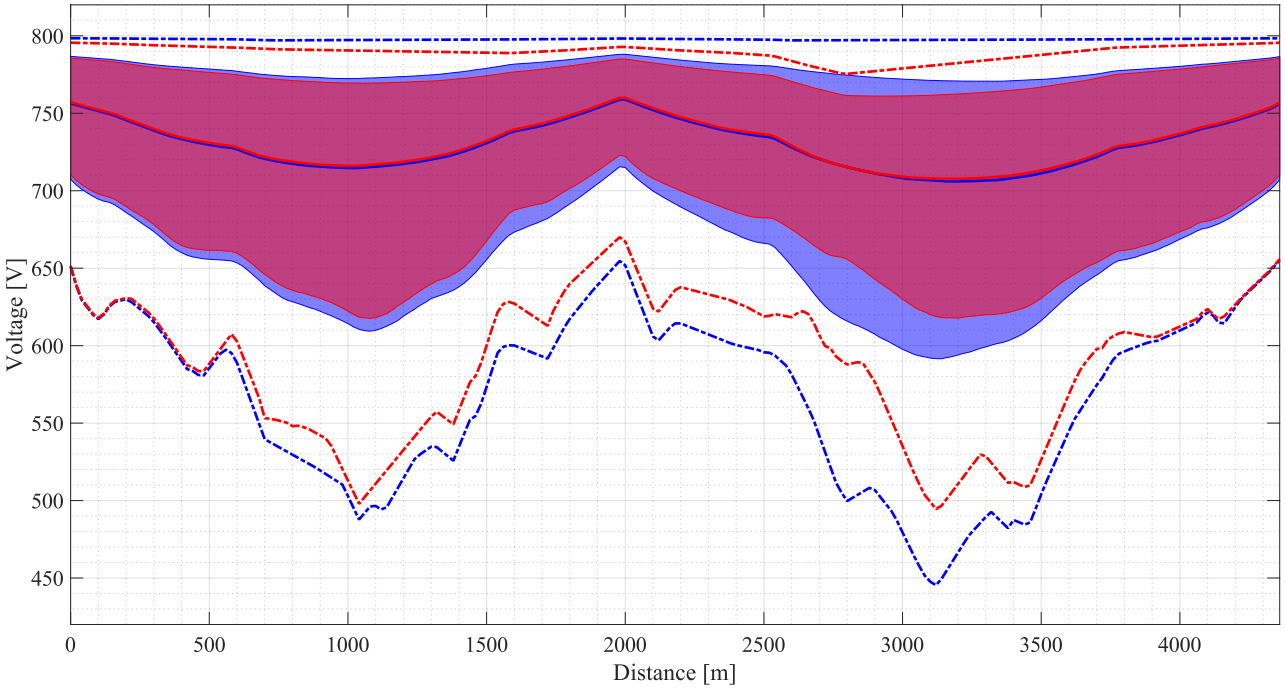

Figure 5-9 Comparison between voltage profiles with (red) and without (blue) 800 Ah BESS along the catenary during 07:00 am-08:00 pm simulation. Legend: Minimum and Maximum voltage profiles (dashed lines); Mean voltage profiles (solid lines); 95 % central inter-percentile range (coloured area).

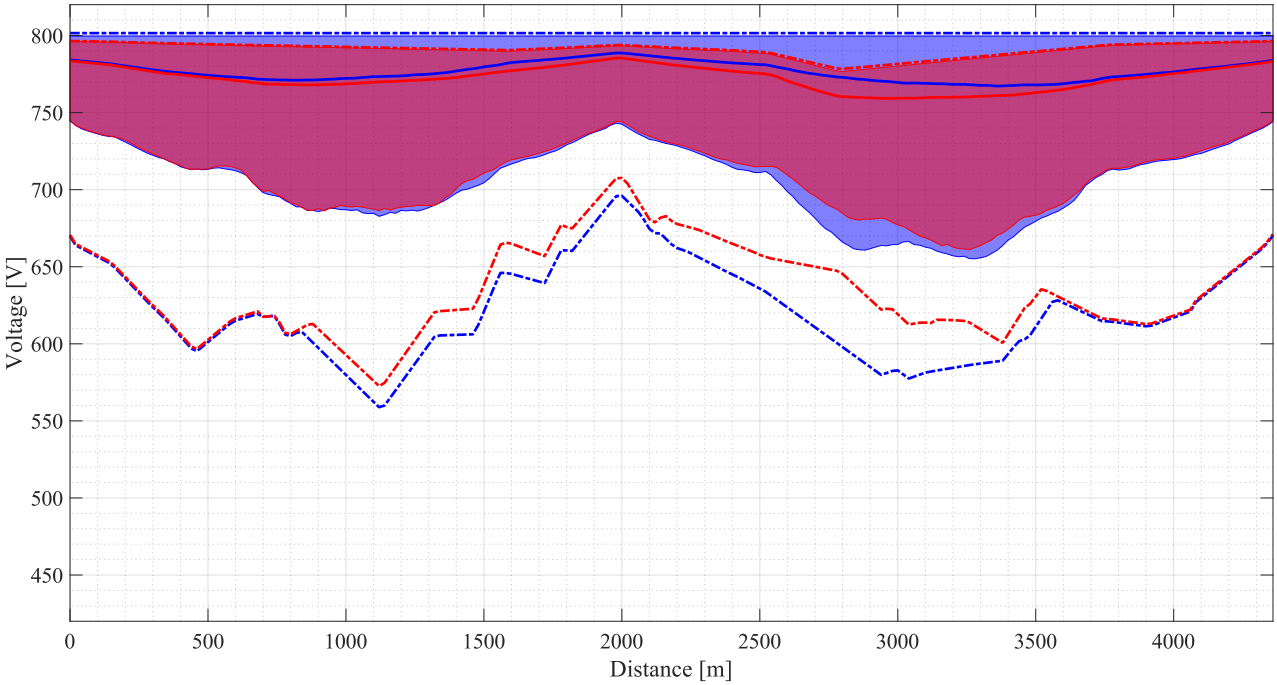

Figure 5-10 Comparison between voltage profiles with (red) and without (blue) 800 Ah BESS along the catenary during 08:00 pm-02:00 am simulation. Legend: Minimum and Maximum voltage profiles (dashed lines); Mean voltage profiles (solid lines); 95 % central inter-percentile range (coloured area).

5.4 Impact of battery installation on catenary current profile

In Figure 5-11 it is illustrated the rms current profile along the catenary from 07:00 am to 08:00 pm in the scenarios with and without the battery ESS. As expected, the battery ESS allows to decrease the current absorption from the TSS feeders (black arrow) and reinforcement feeders (blue arrows for TSS Marconi and green arrows for TSS Trento Trieste). The peaks in the current profile correspond to the feeders and reinforcement feeders connection points. Between the peaks, the current profile decreases due to the current absorption of the trolleybuses. Obviously the most noticeable current reductions happen in the FS segment where the battery ESS is installed (between 2500 m and 3800 m) because the ESS supplies the nearby trolleybuses rather than the TSSs. It is also important to notice that the current is lower than the maximum admissible value set by regulations (450 A) at every point along the catenary.

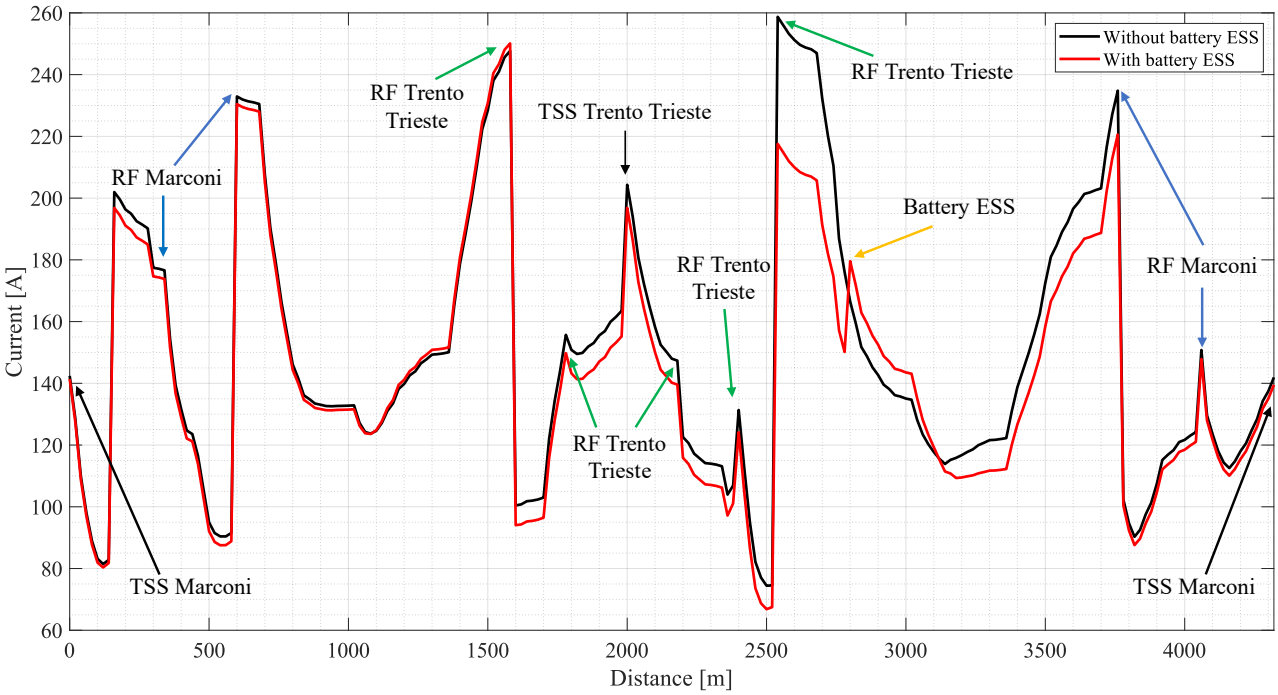

Figure 5-11 Catenary rms current profile between 07:00 am and 08:00 pm with (red) and without (black) 800 Ah BESS.

5.5 Battery current limitation

Even though a 100 Ah battery ESS is undersized, the simulation of the operation of the FS with this battery size is useful to demonstrate that the C-rate limitation implemented by the battery control works. Looking at Figure 5-12 it is indeed possible to see that the battery current never overcomes 200 A.

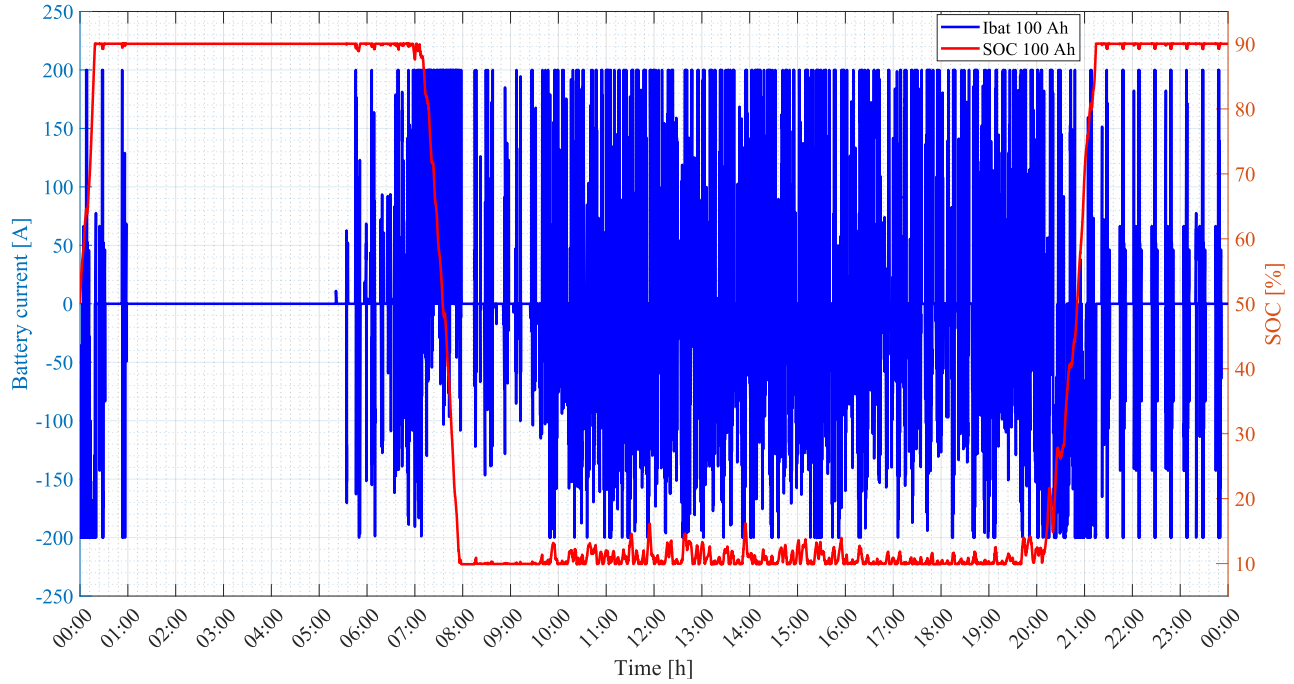

Figure 5-12 Output current of 100 Ah battery and relative SOC level in 24 h simulation.

The maximum discharging current of the 800 Ah BESS is 700 A(Figure 5-13) Therefore, the maximum C-rate at which the chosen battery is exposed to is less than 1C (slower aging with respect to batteries discharged at higher C-rates).

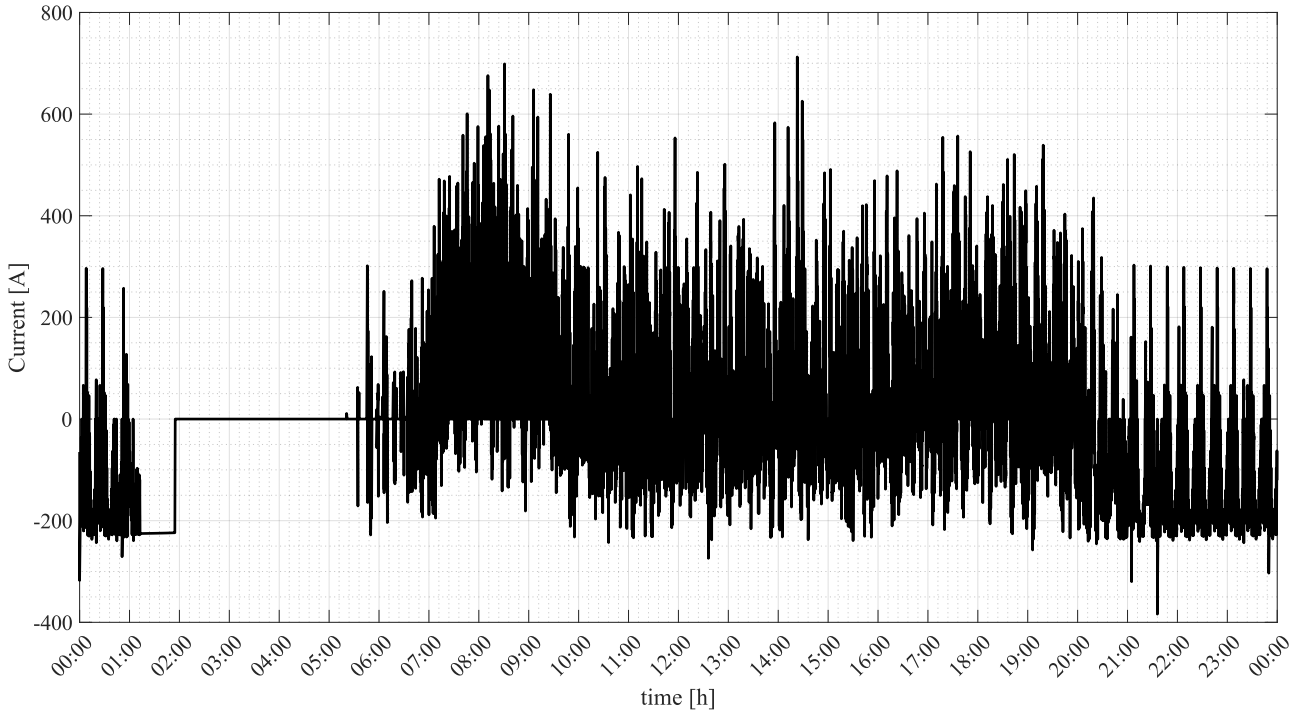

Figure 5-13 Output current of 800 Ah battery during 24 h simulation.

5.6 Energy consumption in 24 h simulation

Finally, it is important to mention the energies absorbed by the trolleybuses and delivered by the traction substations in a 24 h simulation. Setting the initial SOC of the battery ESS equal to the final SOC the energy required from the TSSs to re-charge the battery is accounted for.

For how the trolleybus operation has been simulated, the energy absorbed by the trolleybuses during the daily operation changes accordingly to the voltage profile of the catenary. Being the main objective of this thesis the analysis of the voltage profile of the OCL, the trolleybuses are considered as loads that absorb a certain current profile (blue curve in Figure 2-4). Therefore, their power absorption depends strongly on the voltage profile. The installation of a BESS at position 2800 m of FS Marconi-Trento Trieste allows to decrease the voltage drops during peak hours. Being the current absorption independent on the voltage profile, the power absorption of the trolleybuses increases as the voltage level at the trolleybus poles increases. This condition does not resemble the real trolleybus operation: in reality, as the voltage level at the trolleybus poles increases, its current absorption decreases to keep the power absorption constant. In Table 5-1 it is indeed possible to see an increment of the trolleybuses' energy absorption for the same path and schedule when the BESS is introduced. Therefore, the improvement in terms of losses due to the ESS installation cannot be properly assessed in the simulation. In reality, the losses when the BESS is installed are expected to decrease much more than it is indicated in Table 5-1, where they are calculated as the difference between the energy delivered by the TSSs and the energy absorbed by the trolleybuses.

	TSS energy [kWh]	**Trolleybuses energy [kWh]**	**Losses [kWh]**
Without BESS	14907	13777	1130
With 800 Ah BESS	14908	13854	1053

Table 5-1 TSS, trolleybus energy and losses.

Indeed, due to the BESS installation, the voltage profile of the catenary is raised, as it is demonstrated in paragraph 5.3. If the trolleybuses were to be modelled as constant power loads, the current profile of the catenary would lower because the trolleybus current absorption would decrease. Since the Joule losses are proportional to the square of the current, the lowering of the current would lead to an even bigger decrease of the losses.

5.7 Proposed forthcoming developments

In this paragraph the general ideas about the future possible developments of the proposed model are discussed.

5.7.1 Optimization function to determine the optimal ESS

In this thesis the size and location of the ESS is chosen through simulations. The battery capacity is determined solely looking at the SOC profile making sure that the battery provides a contribution to the trolleybus network operation during peak hours (7 am-8 pm).

In the future, the optimal size of the battery could be obtained solving a constrained optimization problem that takes into consideration all the technical constraints related to the operation of the trolleybus network and of the storage technologies, like it was done in papers [11]-[21], [23], [28]-[32]. The evaluation of the optimal size of the two storage technologies would be a multi-objective problem because it accounts for the improvement of the OCL voltage profile, the added cost of the installation of the ESS, and the savings due to its implementation (Techno-economic analysis).

Furthermore, the feeding section operation due to the installation of different energy storage systems (Supercapacitor, Lithium-ion battery, SC + battery, …) could be analyzed to determine the best possible solution for the application.

5.7.2 Optimization of BESS control

Since the output voltage of the TSSs is set to the average output voltage of the 12-pulse rectifier (800 V) and the current absorption of the IMC trolleybuses is always positive (regenerative breaking energy stored in the on-board battery), the catenary voltage is never higher than 800 V. Therefore, the battery control above 800 V remains un-used. To improve the battery control, the knowledge of the load curve could be used for the tuning of the slope of the battery control in the charging and discharging regions, which could be chosen according to the desired voltage distribution at battery connection point.

5.7.3 Smart trolleybus network

In the future, it is expected a great integration between renewable energy sources (RESs), energy storage systems (ESS), and charging points for electrical vehicles (EVs) and e-Buses.

Due to the current global trend toward greener technologies, the installation of a ESS in the trolleybus network could be a step closer to the development of local energy communities. A battery energy storage system (BESS) indeed could help with the intermittent characteristic of RESs (mainly wind generation and photovoltaic), thus allowing their utilization as green energy sources. Therefore, the future integration of RES, like photovoltaic panels, in the trolleybus network could allow to reduce the pollution created by public transport.

6 Conclusions

The analysis performed in this thesis was carried out in close collaboration with engineers and technicians of TPER, with whom there was a regular interaction for the development of the trolleybus network model such that the real operation of the grid could be emulated.

The analysis of the impact of the installation of a BESS on the operation of FS Marconi-Trento Trieste of the DC trolleybus grid of the city of Bologna was performed considering the current daily schedule and routes of powered bus lines. To perform a more burdensome analysis, all trolleybuses were assumed to be of the IMC type. This assumption, albeit very conservative, allows to study a possible future scenario and verify the catenary operation under high stress conditions.

The developed work proposes a control strategy for a stationary battery energy storage system that considers both the current limitations of the DC bifilar line, due to the cable cross section, and the battery current limitation, given by its C-rate. The correct operation of the control is verified through simulations in Simulink environment, where a model of the FS has been implemented. Said model is able to emulate the daily operation of the FS. To validate the results obtained from the simulations with the battery a prediction is formulated, which is directly derived from the Thevenin equivalent circuit of the FS seen from the BESS connection point.

The results indicate that the installation of a BESS raises the mean and the minimum voltage profiles along the catenary when the trolleybus frequency is the highest (07:00 am-08:00 pm). This result allows to conclude that with the same number of buses circulating in the FS, the current profile, thus the losses, are decreased with respect to the scenario without BESS. The battery control also lowers the voltage dispersion (width of central inter-percentile range) around the mean value at each point along the catenary. Therefore, if the trolleybus frequency were to be increased, it would be more likely that the central inter-percentile range of the voltage profile of FS with BESS would be within the admissible voltage range than in the scenario without. It was also demonstrated that the battery control ensures that the battery does not operate under stress (C-rate lower than *2C*). Finally, the voltage distribution at BESS obtained from simulations validated the prediction.

The battery specifications, such as capacity, pack voltage, and C-rate, and the thresholds for the idle region and slopes of the battery control are not determined through an optimization process, but by an evaluation of the FS operation without battery. The application of an optimization process for the choice and control of the battery ESS can considerably improve the results, opening paths for

future research. Furthermore, the knowledge of the load curve of the FS seen from BESS connection point could be used to determine the slope of the battery control trans-characteristic in the charging and discharging region to obtain the desired voltage distribution.

Appendix

Battery control MATLAB Function

Differently from what has been said up to now, the battery control is implemented using the active sign convention, which defines as positive the electric power flowing out of the battery into the catenary. Therefore, when the catenary voltage is lower than V_l, the battery discharges and its output current is positive, while when the catenary voltage is higher than V_u, the battery charges and its output current is negative.

The script of the battery control MATLAB function can be found hereafter.

```
function [Iref, mode] = fcn(Vlmeas, SOC, Vbat, capacity)

% Initialization of the variables
Iref=0;
mode=0;

% Determination of upper limit of normal charging region
k1 = 740/2 + (sqrt(740^2 + (8*260/900)*Vbat*capacity)/2);
V_u_lim= min(1000, k1);

% Determination of lower limit of normal discharging region
k2 = 710/2+(sqrt(complex(710^2 -(8*210/900)*Vbat*capacity))/2;
if imag(k2) > 0 | imag(k2) <0
    k2=0;
end
V_l_lim= max(500, k2);

if SOC > 10 && SOC < 90

    if Vlmeas >= 710 && Vlmeas <= 740
        % Idle mode
        Iref=0;
        mode=0;
        return
    end

    if Vlmeas > 740
        if Vlmeas <= V_u_lim
            % Normal charging
            Iref = - (900/260)*(Vlmeas - 740);
            mode = 1;
            return
        else if Vlmeas > V_u_lim && Vlmeas <= 1000
                % Limited charging
```

```
                Iref = - (2*capacity* Vbat) / Vlmeas;
                mode = 2;
                return
            end
        end
    end

    if Vlmeas < 710
        if Vlmeas >= V_l_lim
            % Normal discharging
            Iref = - (900/210)*(Vlmeas - 710);
            mode = -1;
            return
        else if Vlmeas < V2
                % Limited discharging
                Iref = +(2*capacity*Vbat)/Vlmeas;
                mode = -2;
                return
            end
        end
    end
end

if SOC >= 90 && Vlmeas < 710
    if Vlmeas >= V_l_lim
        % Normal discharging
        Iref = - (900/210)*(Vlmeas - 710);
        mode = -1;
        return
    else if Vlmeas < V_l_lim
            % Limited discharging
            Iref = +(2*capacity*Vbat)/Vlmeas;
            mode = -2;
            return
        end
    end
else
    if SOC >= 90 && Vlmeas >= 710
        % Idle mode
        Iref=0;
        mode=0;
        return
    end
end

if SOC <= 10 && Vlmeas > 740
    if Vlmeas <= V_u_lim
        % Normal charging
        Iref = - (900/260)*(Vlmeas - 740);
        mode = 1;
```

```
        return
    else if Vlmeas > V_u_lim && Vlmeas <= 1000
            % Limited charging
            Iref = - (2*capacity* Vbat) / Vlmeas;
            mode = 2;
            return
        end
    end
else
    if SOC <= 10 && Vlmeas <= 740
        % Idle mode
        Iref=0;
        mode=0;
        return
    end
end
```

References

[1]. Ratniyomchai, T., Hillmansen, S., & Tricoli, P. (2014). Recent developments and applications of energy storage devices in electrified railways. *IET Electrical Systems in Transportation*, *4*(1), 9-20.

[2]. Bartłomiejczyk, M. (2017). Modern technologies in energy demand reducing of public transport - Practical applications. *2017 Zooming Innovation in Consumer Electronics International Conference: Galvanize Your Creativity, ZINC 2017*, 64–69. https://doi.org/10.1109/ZINC.2017.7968665

[3]. Bartłomiejczyk M. and Mirchevski, S. (2014). Reducing of energy consumption in public transport — Results of experimental exploitation of super capacitor energy bank in Gdynia trolleybus system. *2014 16th International Power Electronics and Motion Control Conference and Exposition*, pp. 94-101, doi: 10.1109/EPEPEMC.2014.6980616.

[4]. Rufer A., Hotellier D. and Barrade, P. (2003). A supercapacitor-based energy-storage substation for voltage-compensation in weak transportation networks. *2003 IEEE Bologna Power Tech Conference Proceedings,*, pp. 8 pp. Vol.3-, doi: 10.1109/PTC.2003.1304470.

[5]. Gao Z., Fang J., Zhang Y., & Sun D. (2014). Control strategy for wayside supercapacitor energy storage system in railway transit network. *Journal of Modern Power Systems and Clean Energy*, *2*(2), 181–190. https://doi.org/10.1007/s40565-014-0060-4

[6]. Lin F., Li X., Zhao Y., and Yang Z. (2016). Control strategies with dynamic threshold adjustment for supercapacitor energy storage system considering the train and substation characteristics in urban rail transit. *Energies*, vol. 9, no. 257, pp. 1–18.

[7]. Iannuzzi, D., Pagano, E., & Tricoli, P. (2013). The use of energy storage systems for supporting the voltage needs of urban and suburban railway contact lines. *Energies*, *6*(4), 1802–1820. https://doi.org/10.3390/en6041802

[8]. Jalali Kashani S. and Farjah E. (2011). Applying neural network and genetic algorithm for optimal placement of ultra-capacitors in metro systems. *2011 IEEE Electrical Power and Energy Conference*, pp. 35-40, doi: 10.1109/EPEC.2011.6070226.

[9]. Calderaro V., Galdi V., Graber G. and Piccolo A. (2013). Siting and sizing of stationary SuperCapacitors in a Metro Network. *AEIT Annual Conference 2013*, pp. 1-5, doi: 10.1109/AEIT.2013.6666809.

[10]. Ciccarelli F., Iannuzzi D., Kondo K., and Fratelli L. (2016). Line-voltage control based on wayside energy storage systems for tramway networks. *IEEE Trans. Power Electron.*, vol. 31, no. 1, pp. 884–899.

[11]. Battistelli L., Fantauzzi M., Iannuzzi D., and Lauria D. (2011). Generalized approach to design supercapacitor-based storage devices integrated into urban mass transit systems. *in Proc. 3rd Int. Conf. Clean Electr. Power (ICCEP)*, Ischia, Italy, pp. 530–534.

[12]. Ratniyomchai T., Hillmansen S., and Tricoli P. (2015). Energy loss minimisation by optimal design of stationary supercapacitors for light railways. *in Proc. Int. Conf. Clean Electr. Power (ICCEP)*, Taormina, Italy, pp. 511–517

[13]. Wang B., Yang Z., Lin F., & Zhao W. (2014). An improved genetic algorithm for optimal stationary energy storage system locating and sizing. *Energies*, *7*(10), 6434–6458. https://doi.org/10.3390/en7106434

[14]. Barrero R., Tackoen X. and Van Mierlo J. (2008). Improving energy efficiency in public transport: Stationary supercapacitor based Energy Storage Systems for a metro network. *2008 IEEE Vehicle Power and Propulsion Conference*, pp. 1-8, doi: 10.1109/VPPC.2008.4677491.

[15]. Battistelli L., Ciccarelli F., Lauria D. and Proto D. (2009). Optimal design of DC electrified railway stationary storage system. *2009 International Conference on Clean Electrical Power*, pp. 739-745, doi: 10.1109/ICCEP.2009.5211971

[16]. Ovalle A., Pouget J., Bacha S., Gerbaud L., Vinot E., Sonier B. (2018). Energy storage sizing methodology for mass-transit direct-current wayside support: Application to French railway company case study, *Applied Energy*, Volume 230, 2018, Pages 1673-1684, ISSN 0306-2619, https://doi.org/10.1016/j.apenergy.2018.09.035.

[17]. Iannuzzi D., Pighetti P. and Tricoli P. (2010). A study on stationary supercapacitor sets for voltage droops compensation of streetcar feeder lines. *Electrical Systems for Aircraft, Railway and Ship Propulsion*, pp. 1-8, doi: 10.1109/ESARS.2010.5665196.

[18]. Ratniyomchai T., Hillmansen S. and Tricoli P. (2014). Optimal capacity and positioning of stationary supercapacitors for light rail vehicle systems. *2014 International Symposium on Power Electronics, Electrical Drives, Automation and Motion*, pp. 807-812, doi: 10.1109/SPEEDAM.2014.6872019.

[19]. Iannuzzi D., Lauria D. & Tricoli P. (2012). Optimal design of stationary supercapacitors storage devices for light electrical transportation systems. *Optim Eng 13***,** 689–704. https://doi.org/10.1007/s11081-011-9160-4

[20]. Jarnut M., Kaniewski J., & Protsiuk V. (2018). Energy storage system for peak-power reduction of traction substation. *2018 Innovative Materials and Technologies in Electrical Engineering (i-MITEL)*, 1–5. https://doi.org/10.1109/IMITEL.2018.8370468

[21]. Graber G., Calderaro V., Galdi V., Piccolo A., Lamedica R., and Ruvio A. (2018). Techno-economic sizing of auxiliary-battery-based substations in DC railway systems. *IEEE Trans. Transport. Electrific*, vol. 4, no. 2, pp. 616–625.

[22]. Lamedica R. *et al*. (2015). Application of battery auxiliary substations in 3kV railway systems. *2015 AEIT International Annual Conference (AEIT)* pp. 1-6, doi: 10.1109/AEIT.2015.7415249

[23]. Capasso A., Lamedica R., Ruvio A., Ceraolo M. and Lutzemberger G. (2016) Modelling and simulation of electric urban transportation systems with energy storage. *2016 IEEE 16th International Conference on Environment and Electrical Engineering (EEEIC)*, pp. 1-5, doi: 10.1109/EEEIC.2016.7555480.

[24]. Farhadi M. and Mohammed O. (2016). Energy Storage Technologies for High-Power Applications. *IEEE Transactions on Industry Applications*, vol. 52, no. 3, pp. 1953-1961, doi: 10.1109/TIA.2015.2511096.

[25]. Xuan L., Kang L. (2020). Energy storage devices in electrified railway systems: A review. *Transportation Safety and Environment*, vol. 2, pp. 183.

[26]. Vazquez S., Lukic S. M., Galvan E., Franquelo L. G., & Carrasco J. M. (2010). Energy storage systems for transport and grid applications. *IEEE Transactions on Industrial Electronics*, *57*(12), 3881–3895. https://doi.org/10.1109/TIE.2010.2076414

[27]. Khodaparastan M., Mohamed A. A., & Brandauer W. (2019). Recuperation of regenerative braking energy in electric rail transit systems. *IEEE Transactions on Intelligent Transportation Systems*, *20*(8), 2831–2847. https://doi.org/10.1109/TITS.2018.2886809

[28]. Lamedica R., Ruvio A., Palagi L., & Mortelliti N. (2020). Optimal siting and sizing of wayside energy storage systems in a D.C. railway line. *Energies*, *13*(23), 1–22. https://doi.org/10.3390/en13236271

[29]. Zhang L., Hu X., Wang Z., Sun F., Deng J. and Dorrell D. G. (2018). Multiobjective Optimal Sizing of Hybrid Energy Storage System for Electric Vehicles. *IEEE Transactions on Vehicular Technology*, vol. 67, no. 2, pp. 1027-1035, doi: 10.1109/TVT.2017.2762368.

[30]. Dutta O. and Mohamed A. (2020). A Comparative Study of Technologies for Wayside Energy Storage in DC Rail Transportation Systems. *2020 IEEE Energy Conversion Congress and Exposition (ECCE)*, pp. 1453-1458, doi: 10.1109/ECCE44975.2020.9236248.

[31]. Ciccarelli F., Iannuzzi D., Lauria D. and Natale P. (2017). Optimal Control of Stationary Lithium-Ion Capacitor-Based Storage Device for Light Electrical Transportation Network. *IEEE Transactions on Transportation Electrification*, vol. 3, no. 3, pp. 618-631, doi: 10.1109/TTE.2017.2739399.

[32]. de la Torre S., Sánchez-Racero A. J., Aguado J. A., Reyes M. and Martínez O. (2015). Optimal Sizing of Energy Storage for Regenerative Braking in Electric Railway Systems. *IEEE Transactions on Power Systems*, vol. 30, no. 3, pp. 1492-1500, doi: 10.1109/TPWRS.2014.2340911.

[33]. European Commission - https://ec.europa.eu/info/index_en

[34]. International Energy Agency - https://www.iea.org/reports/transport-energy-and-co2

[35]. Our World in Data - https://ourworldindata.org/co2-emissions-from-transport

[36]. Statista - https://www.statista.com/statistics/873552/energy-mix-in-italy/

[37]. TPER - https://www.tper.it/

[38]. The Mathworks Inc. - MATLAB & Simulink (R2021a). Battery. Available online: https://it.mathworks.com/help/physmod/sps/powersys/ref/battery.html

[39]. Wikner E., and Torbjörn T. (2018). Extending battery lifetime by avoiding high SOC. *Applied Sciences* 8.10: 1825

[40]. Bartłomiejczy M. (2017). Practical application of in motion charging Trolleybuses service on bus lines," *18th Int. Sci. Conf. Electr. Power Eng. (EPE)*, pp. 1-6.

Acronyms

AC	Alternating Current
BESS	Battery Energy Storage Sysstem
DC	Direct Current
$\boldsymbol{CO_2}$	Carbon Dioxide
EC	European Commission
ECL	European Climate Law
ESS	Energy Storage System
FS	Feeding Section
GHG	Green House Gas
IEA	International Energy Agency
IMC	In-Motion Charging
OCL	Overhead Contact Line
RF	Reinforcement Feeder
RMS	Root Mean Square
RBE	Regenerative Braking Energy
SC	SuperCapacitor
SEI	Surface Electrolyte Interface
SOC	State Of Charge
SoH	State of Health
TPGV	Trasporto Pubblico a Guida Vincolata
TPL	Trasporto Pubblico Locale (local public transport)
TSS	Traction SubStation
WESS	Wayside Energy Storage System

Nomenclature

A	ratio between cable section and 100 mm^2
C	battery capacity [Ah]
C_{limit}	battery capacity above which the battery operation is not limited by its C-rate during discharging [Ah]
G_{eq}	equivalent conductance of Thevenin circuit [S]
I_B	cable design current [A]
$I_{sc\_max}^2\ t$	let-through energy [A^2s]
I_m	mean current of trolleybus [A]
I_{rms}	RMS current of trolleybus [A]
I_s	average starting current of trolleybus [A]
I_{sc_max}	maximum short-circuit current at the beginning of line [A]
I_{sc_min}	minimum short-circuit current at the end of line [A]
$I_{out,ESS}$	output current of BESS [A]
I_Z	cable current rating [A]
L_f	feeder length [m]
k	coupling factor
K	coefficient related to the cable insulation
K^2S^2	specific let-through energy of a cable [A^2S]
L	feeding section length [m]
L_{bus}	length of bus route in FS Marconi-Trento Trieste [m]
$N_{bus/km,i}$	number of trolleybuses per kilometer of bus line *i*
N_{cable}	number of cables in parallel
P_{int}	breaking capacity of the protective device [A]
r	per unit length resistance of a 100 mm^2 cable [Ω/m]
R_{cat}	catenary resistance [Ω]
R_{eq}	equivalent resistance of Thevenin circuit [Ω]
R_f	feeder resistance [Ω]
R_{fr}	reinforcement feeder resistance [Ω]
R_{TSS}	traction substation output resistance [Ω]
$R_{TSS,g}$	traction substation ground resistance [Ω]

S	cable section [mm^2]
t	tripping time of protection device against short-circuits at the beginning of line [s]
V_{2800}	voltage at battery connection point [V]
V_{bat}	battery output voltage [V]
V_{eq}	equivalent voltage of Thevenin circuit [V]
V_l	lower limit of idle region in battery control [V]
$V_{l,lim}$	lower limit of normal discharge mode of battery [V]
V_u	upper limit of idle region in battery control [V]
$V_{u,lim}$	upper limit of normal charge mode of battery [V]
V_{TSS}	traction substation nominal voltage [V]

List of Figures

List of Tables